The effect of peripheral inflammation on *in vivo* functional properties of cortical networks

Dissertation

zur Erlangung des Grades eines
Doktors der Naturwissenschaften

der Mathematisch-Naturwissenschaftlichen Fakultät
und
der Medizinischen Fakultät
der Eberhard-Karls-Universität Tübingen

vorgelegt
von

Karin Dorota Riester
aus Sindelfingen, Deutschland

Mai - 2018

Tag der mündlichen Prüfung:	01.08.2018
Dekan der Math.-Nat. Fakultät:	Prof. Dr. W. Rosenstiel
Dekan der Medizinischen Fakultät:	Prof. Dr. I. B. Autenrieth
1. Berichterstatter:	Prof. Dr. O. Garaschuk
2. Berichterstatter:	Prof. Dr. P. Ruth
Prüfungskommission:	Prof. Dr. O. Garaschuk
	Prof. Dr. P. Ruth
	Dr. M. Kukley
	Prof. Dr. S. Stevanović

Erklärung / Declaration:

Ich erkläre, dass ich die zur Promotion eingereichte Arbeit mit dem Titel:
„The effect of peripheral inflammation on *in vivo* functional properties of cortical networks" selbständig verfasst, nur die angegebenen Quellen und Hilfsmittel benutzt und wörtlich oder inhaltlich übernommene Stellen als solche gekennzeichnet habe. Ich versichere an Eides statt, dass diese Angaben wahr sind und dass ich nichts verschwiegen habe. Mir ist bekannt, dass die falsche Abgabe einer Versicherung an Eides statt mit Freiheitsstrafe bis zu drei Jahren oder mit Geldstrafe bestraft wird.

I hereby declare that I have produced the work entitled "The effect of peripheral inflammation on in vivo functional properties of cortical networks", submitted for the award of a doctorate, on my own (without external help), have used only the sources and aids indicated and have marked passages included from other works, whether verbatim or in content, as such. I swear upon oath that these statements are true and that I have not concealed anything. I am aware that making a false declaration under oath is punishable by a term of imprisonment of up to three years or by a fine.

Tübingen, den ....

Datum / Date Unterschrift / Signature

Abstract

Animals and humans are challenged throughout life by pathogens such as viruses, fungi, parasites or bacteria. The immune system, therefore, has developed effective mechanisms to cope with such infections. It consists of a network of collaborating organs, tissues, cells and proteins to defend the body against harmful influences. The immune system is closely linked with the central nervous system. An inflammatory process in the periphery elicits a mirror inflammatory reaction in the brain, inducing a behavioral response typically referred to as “sickness behavior”, accompanied by significant changes in mood, emotion, and cognition. The molecular mechanisms underlying the complex immune responses are, however, largely unknown.

This work was conducted to investigate how a moderate bacterial inflammation in the periphery affects the *in vivo* functional properties of the cortical network.

To investigate how microglia and neurons react to a peripheral inflammation, we analyzed the properties of these cells in the motor cortex of 4-6 months old mice. We injected the mice intraperitoneally with the bacterial endotoxin lipopolysaccharide (LPS) and compared them to control mice, injected with sterile phosphate buffered saline (PBS).

ELISA analyses of inflammatory cytokines in blood serum and brain samples of LPS-injected mice revealed that the inflammatory signal was transmitted from the periphery to the brain. During the early phase of inflammation, 5 h after LPS injection, we measured in both sample types a strong up-regulation of inflammatory cytokines such as Tumor necrosis factor alpha (TNF-α), Interleukin-1beta (IL-1β), Interleukin-6 (IL-6), CC-chemokine ligand 2 (CCL2) or Interleukin-10 (IL-10). However, this cytokine response was transient and during the late phase of inflammation, 30 h after LPS injection, most of the cytokines returned to control level.

To analyze the functional properties of the main immune cells of the brain, the microglia, we filled the cells with the calcium (Ca^{2+}) -sensor Oregon Green BAPTA-1 (OGB-1) by means of single cell electroporation and measured their spontaneously occurring Ca^{2+}-signals by two-photon Ca^{2+}-imaging.

We discovered that microglia were able to sense the inflammatory stimulus from the periphery and responded with higher incidences of intracellular Ca^{2+}-signals. This hyperactivity of microglia occurred during the early phase of inflammation. Concomitantly with the lowered cytokine levels in the late phase of inflammation, the

microglial Ca^{2+}-signals diminished. Our data revealed that the LPS-induced hyperactivity was dependent on the function of an intracellular immune-complex, the so-called NLRP3 inflammasome. In the brain, the NLRP3 inflammasome is mainly expressed by microglia. It is known as a sensor of cellular stress factors and it is important for the maturation and secretion of the inflammatory cytokines IL-1β and IL-18. We observed that microglia from NLRP3 knock-out mice ($NLRP3^{-/-}$) did not respond with an increased Ca^{2+}-signaling after injection of LPS. Thus, during peripheral inflammation, LPS-induced inflammatory stress factors might activate the NLRP3 inflammasome within the cells and thereby promote the microglial hyperactivity. The influence of the cytokine TNF-α on the microglial hyperactivity was less pronounced. We did not detect a difference between the Ca^{2+}-signals of TNF-α knock-out mice ($TNF\text{-}\alpha^{-/-}$) and WT animals.

In the late phase of inflammation, microglia changed to a more “reactive” state. This state was characterized by morphological and functional alterations of the cells, including increased soma volumes, proliferation, additional expression of inflammatory cytokines (IL-1β), and accelerated cell process movements. Interestingly, all of these “effector functions” are linked to intracellular Ca^{2+}-signals. Therefore, the strong Ca^{2+}-signaling in microglia during inflammation might have triggered the microglial switch from an early “sensor state” to a late “effector state” of the cells.

To investigate the functional properties of cortical neurons, we labeled them with the Ca^{2+}-sensor GCaMP6f and used two-photon imaging to analyze their spontaneous Ca^{2+}-signals. Similar to microglia, neurons were capable to sense the inflammatory stimulus and reacted during the early phase of inflammation with a pronounced hyperactivity. We observed a clear increase of the frequency of Ca^{2+}-transients in different parts of the cortical circuitry. The frequency of Ca^{2+}-transients increased in the somata of cortical neurons from layer 2/3, in presynaptic axons in layer 1 as well as in somata of neurons in layer 5. By using $TNF\text{-}\alpha^{-/-}$ mice, we demonstrated the importance of this proinflammatory cytokine for the LPS-induced neuronal hyperactivity. Neurons in $TNF\text{-}\alpha^{-/-}$ mice did not react with increased Ca^{2+}-signaling after LPS injection.

In contrast to the microglial hyperactivity, we found that the inflammation-induced neuronal hyperactivity was less dependent on the activation of the

NLRP3 inflammasome. Notably, a malfunction of the microglial NLRP3 inflammasome elicited a heightened basal spontaneous Ca^{2+}-signaling in neurons. Further, we discovered that the spontaneous Ca^{2+}-signaling in inhibitory GABAergic neurons is reduced after LPS injection. Hence, the neuronal hyperactivity during inflammation is probably promoted by a reduced activity of GABAergic cells.

Blocking microglial CSF1 receptors caused an almost complete depletion of microglia within the brain. We found that the depletion of microglia resulted in a general reduction of the basal spontaneous Ca^{2+}-signaling of neurons. Strikingly, the absence of microglia did not affect the early inflammation-induced neuronal hyperactivity.

Taken together, a bacterial stimulus from the periphery leads to a pronounced hyperactivity of the cortical network. Microglia and neurons seem to sense the inflammation individually and react with a transient up-regulation of intracellular Ca^{2+}-signals. With this work, we provided insights in the *in vivo* behavior of specific cells types (microglia, GABAergic, and glutamatergic neurons) and structures (presynapse, postsynapse) during the inflammatory process and shed light on the intracellular Ca^{2+}-signaling of these cells/structures during the course of inflammation. We found evidence that the activation of specific cytokines is underlying the altered brain signaling and showed that neurons react to this inflammatory condition in a microglia-independent manner.

Zusammenfassung

Tiere und Menschen sind zeit ihres Lebens mit Krankheitserregern wie Viren, Pilzen, Parasiten oder Bakterien konfrontiert. Ihr Immunsystem hat daher wirksame Mechanismen entwickelt, um mit solchen Infektionen fertig zu werden. Es besteht aus einem Netzwerk von kollaborierenden Organen, Geweben, Zellen und Proteinen, welches den Körper vor schädlichen Einflüssen schützt. Das Immunsystem ist hierbei eng mit dem zentralen Nervensystem verbunden. Ein entzündlicher Prozess in der Peripherie löst im Gehirn eine spiegelbildliche Entzündungsreaktion aus, die wiederum eine Verhaltensantwort in Gang setzt, welche typischerweise als "Krankheit" bezeichnet wird und mit deutlicher Veränderung der Stimmung, Emotion und Kognition einhergeht. Die molekularen Mechanismen, die den komplexen Immunantworten zugrunde liegen, sind jedoch weitgehend unbekannt.

Ziel dieser Arbeit war es zu untersuchen, wie sich eine moderate bakterielle Infektion auf die funktionellen Eigenschaften des kortikalen Netzwerks auswirkt.

Um herauszufinden, wie Mikroglia und Neurone auf eine periphere Entzündung reagieren, haben wir die Eigenschaften dieser Zellen im motorischen Cortex von 4-6 Monate alten Mäusen analysiert. Hierfür injizierten wir Mäusen intraperitoneal das bakterielle Endotoxin Lipopolysaccharid (LPS) und verglichen sie mit Kontrollmäusen, die sterile phosphatgepufferte Kochsalzlösung (PBS) erhielten.

ELISA-Analysen von inflammatorischen Zytokinen in Blutserum und Gehirnproben von LPS-injizierten Mäusen bewiesen eine Übertragung des Entzündungssignals von der Peripherie auf das Gehirn. In der frühen Entzündungsphase, 5 h nach LPS-Injektion, maßen wir sowohl im Serum als auch im Gehirn eine starke Erhöhung inflammatorischer Zytokine, wie z.B. Tumor-Nekrose-Faktor alpha (TNF-α), Interleukin-1beta (IL-1β), Interleukin-6 (IL-6), CC-Chemokin-Ligand 2 (CCL2) oder Interleukin-10 (IL-10). Diese Zytokinantwort war lediglich vorübergehend und in der späten Phase der Entzündung, 30 h nach LPS-Injektion, kehrten die meisten Zytokine zu ihrem Kontrollniveau zurück.

Um die funktionellen Eigenschaften der wichtigsten Immunzellen im Gehirn, der Mikroglia, zu untersuchen, schleusten wir den Calcium (Ca^{2+}) -Sensor Oregon Green BAPTA-1 (OGB-1) mittels Elektroporation in die Zellen ein. Im Anschluss maßen wir spontan auftretende Ca^{2+}-Signale der Mikroglia mittels Zwei-Photonen-Mikroskopie.

Wir fanden heraus, dass Mikroglia den Entzündungsreiz aus der Peripherie wahrnahmen und vermehrt mit intrazellulären Ca^{2+}-Transienten reagierten. Diese Hyperaktivität der Zellen war charakteristisch für die frühe Phase der Entzündung. Bei sinkendem Zytokinspiegel in der späten Phase, verringerte sich auch die Häufigkeit der Ca^{2+}-Signale. Weiterhin konnten wir zeigen, dass die LPS-induzierte Hyperaktivität der Mikroglia von der Funktion des so genannten NLRP3-Inflammasoms abhängt. Das NLRP3-Inflammasom ist ein intrazellulärer Immunkomplex, welcher im Gehirn hauptsächlich von Mikrogliazellen exprimiert wird. Es fungiert als Sensor für zelluläre Stressfaktoren und ist wichtig für die Reifung und Sekretion der inflammatorischen Zytokine IL-1β und IL-18. Wir konnten beobachten, dass Mikroglia in NLRP3 Knock-out-Mäusen ($NLRP3^{-/-}$) keine Verstärkung ihrer Ca^{2+}-Signalgebung nach LPS-Injektion zeigten. Daraus lässt sich schließen, dass eine periphere Entzündung zu einer Ausschüttung von Stressfaktoren führt, die das NLRP3-Inflammasom in den Zellen aktiviert und somit die mikrogliale Hyperaktivität fördert. Der Einfluss des inflammatorischen Zytokins TNF-α auf die mikrogliale Hyperaktivität war hingegen zu vernachlässigen. Im Vergleich zu Kontroll-Tieren konnten wir keine veränderte Ca^{2+}-Signalgebung in TNF-α Knock-out-Mäusen ($TNF\text{-}\alpha^{-/-}$) feststellen. In der späten Entzündungsphase wechselten die Mikroglia in einen „reaktiveren“ Zustand. Dieser wurde von einer Reihe von morphologischen und funktionellen Veränderungen der Zellen begleitet, wie z.B. einem größeren Zellkörpervolumen, Proliferation, zusätzlicher Expression entzündlicher Zytokine (IL-1β) und einer beschleunigten Bewegung der Zellfortsätze. Interessanterweise sind alle diese "Effektor-Funktionen" mit intrazellulären Ca^{2+}-Signalen verknüpft. Folglich könnte die starke Ca^{2+}-Signalgebung den Wechsel der Zellen von ihrem frühen "Sensor-Zustand" zu einem späten "Effektor-Zustand" verursacht haben.

Um die Eigenschaften kortikaler Neurone zu untersuchen, markierten wir Neurone mit dem Ca^{2+}-Sensor GCaMP6f und analysierten ihre spontane Ca^{2+}-Signalgebung mittels Zwei-Photonen-Mikroskopie. Ähnlich wie Mikroglia, waren auch Neurone dazu in der Lage, den Entzündungsreiz aus der Peripherie wahrzunehmen. Auch sie reagierten mit einer ausgeprägten Hyperaktivität in der frühen Entzündungsphase.

Wir beobachteten einen deutlichen Anstieg der Frequenz von Ca^{2+}-Transienten in verschiedenen Teilen des kortikalen Netzwerks. Die Frequenz der Ca^{2+}-Transienten

stieg in den Zellkörpern kortikaler Neurone aus Schicht 2/3, in präsynaptischen Axonen in Schicht 1, sowie in Zellkörpern tiefer gelegener Neurone aus Schicht 5.
Mit Hilfe der TNF-$\alpha^{-/-}$ Mäuse konnten wir die Bedeutung des inflammatorischen Zytokins TNF-α für die LPS-induzierte neuronale Hyperaktivität nachweisen. TNF-$\alpha^{-/-}$ Mäuse zeigten keine Verstärkung der Ca^{2+}-Signalgebung nach LPS-Injektion. Zudem schien im Gegensatz zur Hyperaktivität der Mikroglia, die entzündungsinduzierte neuronale Hyperaktivität weniger abhängig von der Aktivierung des NLRP3-Inflammasoms zu sein. Jedoch führte das Fehlen des NLRP3-Inflammasoms unabhängig von der Entzündung zu einer erhöhten basalen spontanen Ca^{2+}-Signalgebung in Neuronen. Weiterhin entdeckten wir, dass bei hemmenden GABAergen Neuronen die Frequenz spontaner Ca^{2+}-Transienten nach LPS-Injektion reduziert war. Daraus lässt sich schlussfolgern, dass die neuronale Hyperaktivität wahrscheinlich durch eine verminderte Aktivität hemmender GABAerger Zellen verursacht wird. Die Blockade mikroglialer CSF1-Rezeptoren resultierte in einer fast vollständigen Elimination der Mikroglia im Gehirn. Wir fanden heraus, dass das Fehlen von Mikroglia zu einer allgemeinen Erniedrigung der basalen spontanen Ca^{2+}-Signalgebung von Neuronen führte. Bemerkenswert war, dass das Fehlen von Mikroglia keinen Einfluss auf die LPS-induzierte neuronale Hyperaktivität hatte.
Zusammengefasst haben wir herausgefunden, dass ein bakterieller Entzündungsreiz aus der Peripherie zu einer ausgeprägten Hyperaktivität des kortikalen Netzwerks führt. Mikroglia und Neurone scheinen die Entzündung individuell wahrzunehmen und reagieren mit einer vorrübergehenden Erhöhung intrazellulärer Ca^{2+}-Signale.
Diese Arbeit gibt Aufschluss über das *in vivo* Verhalten verschiedener Zelltypen (Mikroglia, GABAerger und glutamaterger Neurone) und Zellstrukturen (Präsynapse, Postsynapse) während eines Entzündungsprozesses im Gehirn und beleuchtet die intrazelluläre Ca^{2+}-Signalgebung dieser Zellen/Strukturen im Verlauf des Entzündungsprozesses. Wir fanden Hinweise darauf, dass die Aktivierung bestimmter inflammatorischer Zytokine der veränderten Ca^{2+}-Signalgebung zugrunde liegt und konnten zeigen, dass Neurone unabhängig von Mikroglia auf diesen Entzündungszustand reagieren.

Acknowledgments

I would like to express my gratitude to all who helped me in one or another way to finish this dissertation.

First of all, thank you Prof. Dr. Olga Garaschuk. You not just enabled me to do this work, but also guided and supported me throughout on this path. I am really happy and grateful that I could make the experience to learn and work in your lab and dive into the fascinating world of neuroscience.

Also, thanks to Dr. Maria Kukley and Prof. Dr. Peter Ruth, for being in my advisory board committee and for helping me with useful advice and comments on my work.

Special thanks go also to Dr. Bianca Brawek, who taught me a lot during this time, and with whom I share the love to the charming little microglia. Thanks for the countless useful and sometimes slightly less useful, but motivating and amusing discussions (surely, there were much more useful ones).

Further, I want to express my gratitude to my colleagues and friends who all together contributed in many different ways to a happy scientific atmosphere.
I am thankful for all the productive talks, your support, our collaborations and shared experiences (including shared breakfasts, excursions, coffee breaks and cakes in the kitchen, with the magical table providing an endless source of calories). Overall, thank you for the good time with many smiles and laughter. This is worth a lot.

Moreover, I want to thank my family, who is always there with love and support, making things that sometimes may seem complicated way easier.

Last but not least, thank you Dr. Bartholomäus Odoj, not just for patiently reading the whole torrent of words, but also for your opinion, your encouragement, love and great support.

List of Figures

List of Tables

List of Abbreviations

AAV	Adeno-associated virus
AD	Alzheimer's disease
ADP	Adenosine 5'-diphosphate
AM	Acetoxymethyl
AMPA	α-amino-3-hydroxy-5-methyl-4-isoxazole-propionat
APs	Action potentials
ATP	Adenosine-5'-triphosphate
BAPTA	1,2-bis(2-aminophenoxy)ethane-*N,N,N′,N′*-tetraacetic acid
BBB	Blood brain barrier
BrdU	Bromodeoxyuridine
BW	Body weight
$[Ca^{2+}]_i$	Intracellular free calcium concentration
CASR	Calcium-sensing receptor
CCL	C-C motif chemokine ligand
CD	Cluster of differentiation
CNS	Central nervous system
CSF-1	Colony stimulating factor-1
CX3CL1	CX3C motif ligand 1 / fractalkine
CX3CR1	CX3C motif receptor 1
CXCL10	C-X-C motif chemokine ligand 10
DNS	Donkey normal serum
E. coli	Escherichia coli
e.g.	Exempli gratia / for example
eGFP	Enhanced green fluorescent protein
ELISA	Enzyme-linked immunosorbent assay
ER	Endoplasmic reticulum
EPSCs	Excitatory postsynaptic currents
GABA	γ-aminobutyric acid
GCaMP6	GECI (based on a fusion of green fluorescent protein (GFP), calmodulin (CaM) and M13 (a peptide sequence from myosin light chain kinase)

GECIs	Genetically encoded Ca^{2+}-indicators
HEPES	4-(2-hydroxyethyl)-1-piperazineethanesulfonic acid
Iba1	Ionized calcium-binding adaptor molecule 1
ICA	Independent component analysis
i.e.	Id est / that is to say
IFN-γ	Interferon-gamma
IL(R)	Interleukin (receptor)
IL-1RAcP	IL-1 receptor accessory protein
i.p.	Intraperitoneal
IP_3K	Phosphatidylinositol-4,5-bisphosphate 3-kinase
IP_3(Rs)	Inositol trisphosphate (receptors)
IQR	Interquartile range
IRAK	IL-1 receptor associated protein kinase
LPS	Lipopolysaccharides
MAPK	Mitogen-activated protein kinase
MCBL	Multi-cell bolus loading
MIP	Maximum intensity projection
MyD88	Myeloid differentiation primary response 88
NA	Numerical aperture
NMDA	N-methyl-D-aspartate
NLRs	NOD-like receptors
NLRP3	NLR family pyrin domain containing 3
OGB-1	Oregon Green BAPTA-1
PAMPs	Pathogen-associated molecular patterns
PBS	Phosphate buffered saline
PFA	Paraformaldehyde
PKC	Protein kinase C
PLC	Phospholipase C
PRRs	Pattern recognition receptors
ROI	Regions of interest
ROS	Reactive oxygen species
s.c.	Subcutaneous
SOC	Store-operated calcium channel

SR-B	Sulforhodamine B
TACE	Matrix metalloproteinase TNF-α-converting enzyme
TNF-α	Tumor necrosis factor-alpha
TNFR	Tumor necrosis factor receptor
TLRs	Toll-like receptors
TREM 2	Triggering receptor expressed on myeloid cells 2
UDP	Uridine 5'-diphosphate
VIAAT	Vesicular inhibitory amino acid transporter
WT	Wild type
ΔF/F	Relative change in fluorescence over time

Table of Contents

1. Introduction

1.1 Anatomical components of cortical networks

The cerebral cortex of mammals is a complex structure that coordinates among other functions the sensory-motor integration and is essential for higher cognitive functions including memory formation, emotion and social behavior (Zeisel et al. 2015; Etkin et al. 2011; Bicks et al. 2015). It is composed of different cell types, such as astrocytes, oligodendrocytes, microglia or neurons. Based on histological examinations and the distinct distribution of the cell types and their connections, the cerebral cortex can be categorized in the allocortex and the isocortex. Both have a characteristically layered horizontal structure. The allocortex, including the hippocampus, the rhinal and olfactory cortices, consists of three distinct layers (Palomero-Gallagher and Zilles 2015; Witter 2012). In the following, I will set the focus on the isocortex, as this work deals with inflammation in this brain structure. The isocortex can be classified in specific functional areas, such as the visual, auditory, somatosensory or motor cortical areas. Typically, seven distinct layers can be distinguished in the isocortex of mice (layer 1, 2/3, 4, 5, 6 and 7). The layers consist of specialized populations of neurons with different morphologies, projection targets, gene expression and functions (Molyneaux et al. 2007).

The most superficial layer 1, also termed “external plexiform” or “molecular layer”, is almost devoid of neurons. It consists mainly of axons from different sources (thalamus, layer 2/3, 5, 6 or 7), some inhibitory neurons and apical dendrites from pyramidal neurons of deeper layers (De Paola et al. 2006; Kirkcaldie 2012).

The layer 2/3 or “supragranular pyramidal layer” is dominated by small pyramidal neurons with strong local and cortico-cortical connections. In the motor cortex, there are prominent interactions with subcortical projection neurons of layer 5. In addition to the pyramidal neurons, this layer is also populated by a diverse group of interneurons, like chandelier or basket cells (Kirkcaldie 2012).

Layer 4, the "granular layer" receives input from the thalamus and is strongly pronounced in the somatosensory areas. It contains so-called spiny stellate cells, as well as apical dendrites from layer 6 pyramidal neurons, providing feedback back to the thalamus (Kirkcaldie 2012). The motor cortex, in contrast, lacks a distinctly visible

layer 4, whereby a laminar zone on the border of layer 3 and 5, was reported to provide similar functions, with excitatory inputs from the thalamus and excitatory outputs to layer 2/3 neurons (Yamawaki et al. 2014).

The cortical layer 5 or the “deep pyramidal layer” consists of relatively large pyramidal neurons projecting to various cortical and subcortical brain regions, like the striatum, midbrain, pontine nuclei, brainstem or spinal cord. It can be further subdivided into layer 5A with the cortico-striatal projections and layer 5B with mainly cortico-spinal projections (Kirkcaldie 2012).

Layer 6 or “polymorphic layer” contains neurons with clearly diverse morphologies. It is mainly considered as output layer with strong reciprocal projections to the thalamus. The neurons from this layer are connected with different cortical areas and are able to modulate the thalamic drive in these regions, making them an important part of the cortico-cortical communication (Kirkcaldie 2012).

Layer 7, the “subgriseal layer” is the deepest cortical layer. It is present in several areas of the mouse cortex and is separated from the layer 6 by stratum, containing only very few cells. The so-called subplate neurons of layer 7 project to layer 1 and across the corpus callosum (Kirkcaldie 2012).

In addition to the layered structure, cortical neurons are often organized in so-called “functional columns”. One column is hereby considered as a group of adjoining cells that are working on the same “functional project” (Mountcastle 1997). The functional structures were described especially for the sensory areas, like the visual, the somatosensory or auditory cortices, whereas in the motor cortex, the organization is less clear and it is difficult to distinguish between columnar functional structures (Hatsopoulos 2010). This work mainly focuses on the motor cortical areas. They are responsible for the orchestration and execution of motor behaviors (Fritsch and Hitzig 2009; Ferrier 1874).

1.2 Systemic inflammation

Microbial pathogens are a common source of morbidity in humans. A bacterial infection leads to classical symptoms of “sickness” as altered body temperature, nausea, loss of appetite, fatigue, decreased motor activity, reduced interest in social interactions and depression. This “sickness behavior” is a reaction of the organism, initiated to efficiently cope with the infection (Dantzer 2009; Perry and Cunningham

2007). Phagocytic cells of the innate immune system, like monocytes or tissue macrophages, are the first line of defense against a peripheral infection. They get activated through pattern recognition receptors (PRRs), which can be classified into membrane-bound and cytoplasmic PRRs. One type of the membrane-bound PRRs are the toll-like receptors (TLRs). So far, in mammals, 13 distinct members of the toll-like receptor family are described (TLR 1-13). They can be found on many different cell types. In the periphery, besides monocytes and macrophages, dendritic cells, neutrophils, and epithelial cells express TLRs. In the brain, they are present on microglia, astrocytes, oligodendrocytes, and neurons (Hanke & Kielian 2011). TLRs are able to recognize different pathogen-associated molecular patterns (PAMPs), such as viral ribonucleic acid, bacterial flagellin, lipoteichoic acid or lipopolysaccharide (LPS) (Albiger et al., 2007). LPS is a bacterial cell wall component of gram-negative bacteria. It interacts specifically with TLR-4. This interaction leads to an oligomerization of TLR-4 and the recruitment of adaptor proteins, inducing pathways that trigger the production of various inflammatory cytokines, such as Interleukin-1α, Interleukin-1β (IL-1β), Tumor necrosis factor-α (TNF-α), C-C motif chemokine ligand 2 (CCL2), Interleukin-6 (IL-6) or Interleukin-10 (IL-10) (Lu, Yeh, and Ohashi 2008; Albiger et al. 2007). The cytokines function hereby as mediators that coordinate the systemic inflammatory response to an infection (Hines et al. 2013; Dantzer 2009). Under physiological conditions, the brain is protected from direct influence of inflammatory mediators by the blood-brain barrier (BBB). Nevertheless, a systemic inflammation in the periphery engenders a mirror inflammatory response in the brain. There are four known pathways, which enable the immune communication from the periphery to the brain (Dantzer 2009) (Figure 1): (1) In the neural pathway, locally produced cytokines activate primary afferent nerves, like the vagal nerve. The vagal afferents, in turn, project to different brain regions that are associated with the induction of “sickness behavior”, for instance, the nucleus tractus solitarius, the brain stem, the hypothalamus or other limbic structures. (2) The second pathway is a humoral pathway, where circulating peripheral cytokines or inflammatory mediators directly access and affect the brain by diffusion at the circumventricular organs (CVO), brain regions that lack a contiguous BBB.

(3) Additionally, many cytokines can be transported over the BBB in an energy-dependent active manner. This process involves specific cytokine transporters in the BBB and represents the third pathway.

(4) In the last pathway, the inflammatory cytokines activate perivascular macrophages and endothelial cells that start to secrete inflammatory mediators by themselves and thereby transmit the signal from the periphery to the central nervous system (CNS).

Taken together, all pathways lead to an inflammation in nervous tissues, termed neuroinflammation, and trigger a central inflammatory response, resulting in the activation of brain immune cells, such as microglia.

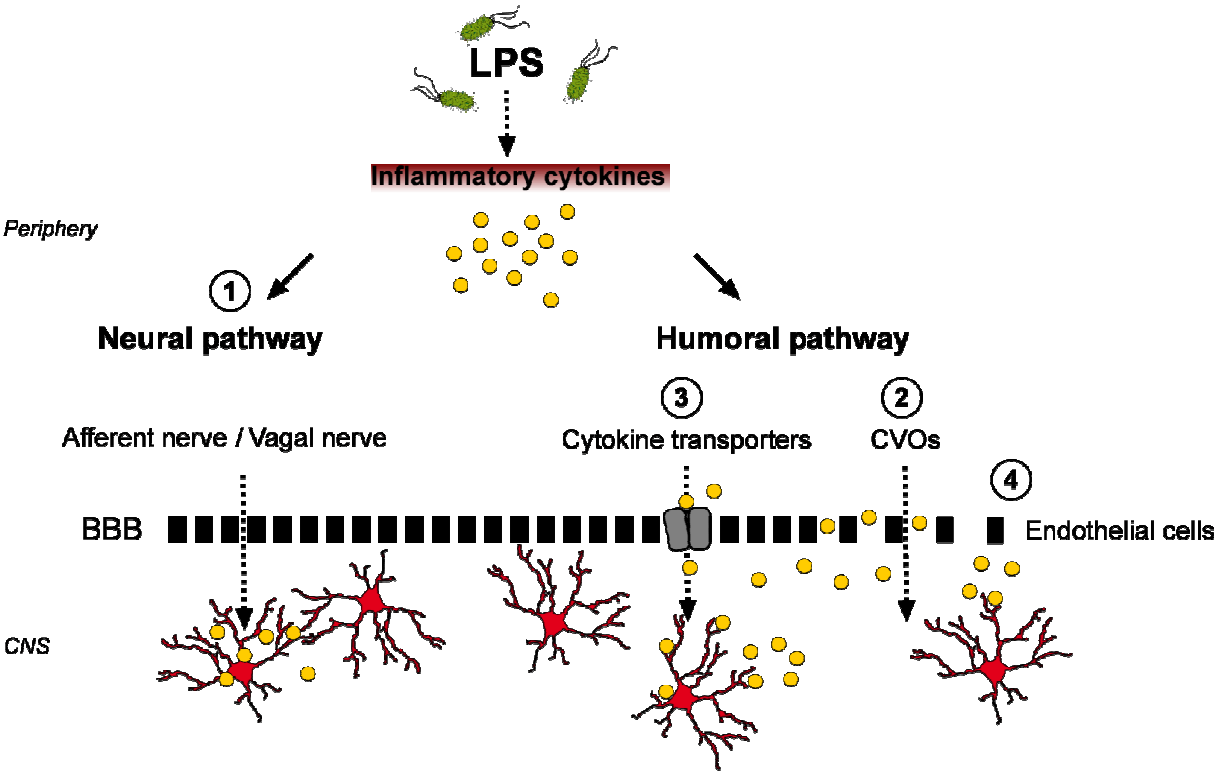

Figure 1 Overview of different pathways from the periphery to the brain

(1) In the neural pathway, locally produced cytokines activate primary afferent nerves, like the vagal nerve that transmit the inflammatory signal to the central nervous system (CNS). **(2)** In the second pathway, a humoral pathway, circulating peripheral cytokines or inflammatory factors directly access and affect the brain by diffusion at the circumventricular organs (CVOs). **(3)** In the third pathway, cytokines can be transported over the blood-brain barrier (BBB) in an energy-dependent active manner by the activation of specific cytokine transporters in the BBB. **(4)** In the fourth pathway, the inflammatory cytokines activate perivascular macrophages and endothelial cells, that start to secrete inflammatory mediators by themselves and thereby transmit the signal from the periphery to the CNS. All pathways transmit the inflammatory signal to the brain and lead to an activation of brain cells like microglia.

1.3 Functional properties of microglia

Microglial cells play a pivotal role in the immune system of the CNS. They are abundantly present within the whole brain and, depending on the region, around 5-12 % of the cells in the mouse brain are microglia (Lawson et al. 1990). They represent a heterogeneous population of innate immune cells with a broad functional diversity. Microglia are essential for the maintenance of the normal brain homeostasis. They have an impact on synapse remodeling (Tremblay, Lowery, and Majewska 2010; Paolicelli et al. 2011) and stand in close interaction with astrocytes and neurons, impacting the activity of the entire network (Wake et al. 2009; Liu, Tang, and Feng 2011). Under healthy physiological conditions, they are characterized by a ramified morphology with small cell bodies and fine processes. They use their highly motile processes, to constantly scan their environment (Davalos et al. 2005; Nimmerjahn, Kirchhoff, and Helmchen 2005). After sensing an inflammatory stimulus, microglia switch from a “resting surveying state” to an “activated effector state”. According to the strength of the stimulus, this activation is associated with an alteration of their morphology from ramified over a hypertrophic to a highly migratory amoeboid state (Kozlowski and Weimer 2012; Kettenmann et al. 2011). The functional significance of the morphological change is not fully understood. However, it is associated with a higher reactivity of microglia, including migration of the cells, the clearance of apoptotic cells and the phagocytosis of pathogens or cell debris (Nimmerjahn, Kirchhoff, and Helmchen 2005; Petersen and Dailey 2004). Upon a local tissue injury or exposure to a “danger signal” like adenosine triphosphate (ATP), usually released by damaged cells, microglia can direct their motile processes towards the harmed cell or even move to the site of the injury. Microglial processes are able to actively shield the healthy tissue, protecting it from secondary damage (Davalos et al. 2005). A characteristic trait of microglia is that they originate from hematopoietic stem cells in the yolk sac and not from bone marrow precursors, like other mononuclear macrophages (Ginhoux et al. 2010). They are believed to have a relatively long lifespan and the feature to proliferate from resident progenitors within the brain. Their proliferation rate is hereby counterbalanced by apoptotic cell death (Askew et al. 2017). In response to an inflammatory insult, microglia can increase their presence by up-regulating the rate of cell division and thereby enabling the innate immune system of the brain to

effectively fight the infection (Fukushima et al. 2015). Calcium (Ca^{2+}) ions are considered to be key regulators of cell proliferation by activating transcription factors and regulating the gene transcription (Berridge, Lipp, and Bootman 2000). As intracellular messenger, Ca^{2+} is involved in several signaling pathways and responsible for the activation of different cellular processes in microglia.

1.3.1 Ca^{2+}-signaling in microglia

Microglia express many surface molecules and receptors enabling them to sense changes in their environment. A binding of inflammatory mediators can activate internal signaling pathways leading to an increased level of cytosolic Ca^{2+} (Kettenmann et al. 2011). Ca^{2+} ions can enter the cell from different sources. Various ionotropic and metabotropic purinergic receptors represent the most prominent sources for an increase of the intracellular Ca^{2+}-concentration ($[Ca^{2+}]_i$) (Eichhoff, Brawek, and Garaschuk 2011; Brawek and Garaschuk 2017; Kettenmann et al. 2011). An activation of ionotropic purinergic P2X receptors, for instance, induces an influx of Ca^{2+} and sodium (Na^+) from the extracellular space and a concomitant efflux of potassium (K^+) through non-selective cationic channels. Another source of Ca^{2+} is the endoplasmic reticulum (ER). An increase in $[Ca^{2+}]_i$ can, for example, be mediated by activation of metabotropic purinergic P2Y receptors, leading to a depletion of the intracellular Ca^{2+}-stores in the ER. The Ca^{2+}-release from the ER stores, in turn, activates so-called store-operated Ca^{2+}-channels (SOC) in the plasma membrane of microglia, initiating a feedback loop with the subsequent further influx of Ca^{2+} from the extracellular space. This feedback loop, in turn, might lead to the refilling of the ER Ca^{2+}-stores (Kettenmann et al. 2011).

1.3.2 Microglial Ca^{2+}-signaling under physiological conditions

Under normal conditions, spontaneous microglial Ca^{2+}-signaling in the somata of ramified microglia of anesthetized mice is a rare event (Eichhoff, Brawek, and Garaschuk 2011; Brawek et al. 2014; Pozner et al. 2015). The significance of Ca^{2+}-signaling in resting microglia is not completely understood, but it is known that somatic spontaneous Ca^{2+}-signaling of microglia does not reflect one to one the activity of the surrounding neurons. This was shown by *in vivo* experiments, measuring microglial Ca^{2+}-transients during disinhibition of the neuronal network by applying the γ-aminobutyric acid ($GABA_A$) receptor blocker bicuculline. Further, it is

known that the more frequently occurring astrocytic Ca^{2+}-waves, present in 70-80 % of all astrocytes are not necessarily accompanied by microglial Ca^{2+}-signals (Eichhoff, Brawek, and Garaschuk 2011). At the same time, many functional properties of microglia are governed by intracellular Ca^{2+}-signals. In addition to mediating cell proliferation, Ca^{2+}-signaling is important for cell migration and phagocytosis (Korvers et al. 2016). Further, a cytosolic Ca^{2+}-increase is linked to gene transcription and release of inflammatory factors such as, for instance, chemokines, reactive oxygen species (ROS) or cytokines like TNF-α and IL-1β (Hoffmann et al. 2003). Microglial Ca^{2+}-signaling thereby represents an important trigger of the central immune response. Hence, spontaneously occurring Ca^{2+}-events might represent a good reflection of the activation state of microglia.

1.3.3 Enhanced microglial Ca^{2+}-signaling during inflammation

The activation of microglia through inflammatory mediators and the effect on their Ca^{2+}-signaling was reported in several *in vitro* experiments. Applying LPS resulted in a chronic elevation of intracellular Ca^{2+}-levels in cultured microglia (Hoffmann et al. 2003; Färber and Kettenmann 2006b). In neonatal cultured microglia, chronic treatment of the cells with LPS was shown to have an impact on the Ca^{2+}-kinetics, with a longer rise and decay time, but no clear effect on the frequency of the Ca^{2+}-transients (Korvers et al. 2016). However, the behavior and morphology of microglia in culture is different than in the intact organism. The cultures derive often from young neonatal brains and immature not yet differentiated microglia (Eichhoff, Brawek, and Garaschuk 2011). Further, the sensitive microglial cells react to the process of cell culturing and the presence of serum factors with a more activated phenotype. It was shown that the isolation of microglia leads to increased levels of cytosolic $[Ca^{2+}]_i$ in the cells and a concomitantly up-regulated expression of microglial activation markers, like the cluster of differentiation 68 (CD68) or IL-1β (Brawek et al. 2017). All these differences prevent a one to one comparison of cultured microglia with microglia in the intact brain under physiological conditions. However, classical attempts to analyze *in vivo* Ca^{2+}-signaling in cells (neurons, astrocytes), like the multi-cell bolus loading technique (MCBL) failed for microglia. MCBL enables the uptake of small-molecule indicator dyes like Oregon Green BAPTA-1 (OGB-1) into the cells. Due to the limited uptake of synthetic Ca^{2+}-dyes in microglia, the data obtained from *in vivo* experiments are rare

(Eichhoff, Brawek, and Garaschuk 2011; Brawek and Garaschuk 2013). One option to investigate Ca^{2+}-signaling under more physiological *in vivo* conditions is, to actively administer Ca^{2+}-sensors into the cells. This can be achieved by means of single cell electroporation (Eichhoff, Brawek, and Garaschuk 2011). Our group could show by using this method that activated microglia in proximity of amyloid beta plaques in a mouse model of Alzheimer`s disease display a significantly higher incidence of Ca^{2+}-transients than resting cells (Brawek et al. 2014). A recently developed mouse line with a genetically encoded Ca^{2+}-sensor in microglia provides another option to investigate Ca^{2+}-dynamics in microglia under *in vivo* conditions (Gee et al. 2014; Pozner et al. 2015).

1.4 Functional properties of cortical neurons

The neuronal network activity in the mouse cortex is highly complex and reflects an elaborate balance between inhibitory and excitatory inputs. Generally, cortical neurons can be divided into two broad classes. The first class (around 80 % of all cells) is represented by excitatory glutamatergic neurons with local as well as long-range projections to their targets. The second class (around 20 % of all cells) is given by inhibitory GABAergic interneurons. They shape the activity of other neurons often through local connections (Molyneaux et al. 2007; Jiang et al. 2015). Even in the absence of external stimuli, neurons are spontaneously active (Shadlen & Newsome 1994; Mazzoni et al. 2007). Upon activation, they fire action potentials (APs). APs are triggered by the opening of voltage-gated ion channels, resulting in an influx of mainly Na^{+}-ions and a subsequent change in the membrane potential. This, in turn, activates voltage-gated Ca^{2+}-channels and leads to a concomitant rapid increase in $[Ca^{2+}]_i$ (Lev-Ram and Grinvald 1987; Berridge, Lipp, and Bootman 2000).

1.4.1 Ca^{2+}-signaling in neurons

At rest, neurons typically have an intracellular free Ca^{2+}-concentration of around 30-100 nM. During neuronal activity, it can rise to 10-100 times higher level (Garaschuk and Konnerth 1997; Berridge, Lipp, and Bootman 2000). Similar as in microglia, the $[Ca^{2+}]_i$ in neurons can be either increased through Ca^{2+}-influx from the external space or through release from the internal stores (ER). A plethora of

different stimuli, like extracellular agonists, inflammatory noxious factors, membrane depolarization or depletion of intracellular stores can lead to the influx of Ca^{2+} into the cell. Responsible for the influx from the extracellular space are Ca^{2+}-permeable channels in the plasma membrane. These include voltage-gated Ca^{2+}-channels, ligand-gated ion channels, like NMDA or AMPA glutamate receptors, as well as the store-operated Ca^{2+}-channels. The Ca^{2+}-release from the ER, in contrast, can be mediated by the activation of special ER membrane receptors, such as the inositol trisphosphate receptors (IP_3Rs) or the ryanodine receptors (Berridge, Lipp, and Bootman 2000; Grienberger and Konnerth 2012). Activation of metabotropic glutamate receptors, for instance, is known to mediate the production of inositol triphosphate (IP_3), which can activate IP_3Rs. The ryanodine receptors react to cytosolic Ca^{2+}-increases, initiating the so-called Ca^{2+}-induced Ca^{2+}-release.

An increase in $[Ca^{2+}]_i$ is generally driven by a strong concentration gradient. After the signaling event, the resting cytosolic $[Ca^{2+}]_i$ needs to be restored. This task is accomplished by a set of specialized Ca^{2+}-pumps. The plasma membrane Ca^{2+}-ATPase and the Na^+/Ca^{2+}-exchangers extrude Ca^{2+} out of the cell, whereby the sarcoendoplasmic reticulum calcium transport ATPase pumps, return Ca^{2+} to the internal stores (Berridge, Lipp, and Bootman 2000).

1.4.2 In vivo Ca^{2+}-imaging in populations of cortical neurons

The neuronal activity and the concomitant changes in $[Ca^{2+}]_i$ can be tracked *in vivo* with the help of fluorescent Ca^{2+}-indicator molecules. In 2003, Stosiek et al. introduced the multi-cell bolus loading technique (MCBL), enabling convenient labeling of a whole population of neurons and astrocytes with small synthetic Ca^{2+}-indicators, like OGB-1. After bolus loading OGB-1 into the brain tissue, it is quickly taken up by the cells and the cell activity can be monitored subsequently. This technique enabled for the first time *in vivo* measurements of the intracellular Ca^{2+}-signaling in neuronal circuits at single-cell resolution and provided insights into the sensory-driven activity pattern of layer 2/3 neurons in the barrel cortex (Stosiek et al. 2003). Thereafter, MCBL was widely used to study neuronal network activity in the intact brain of wild type (WT) animals (Kerr, Greenberg, and Helmchen 2005; Ohki et al. 2005; Sullivan et al. 2005) and in different animal models of disease (Busche et al. 2008; Wenzel et al. 2017). Labeling neuronal networks with OBG-1 by means of MCBL leads to a staining of neuronal somata, as well as the surrounding of

the neurons, which is termed neuropil. The neuropil consists of dendrites, spines, axons, presynaptic boutons, and glial processes (Chklovskii, Schikorski, and Stevens 2002). However, due to a lack of contrast, a clear discrimination between these compartments is not possible. Electroporation provides another option to load neurons with Ca^{2+}-indicators. This technique can either be used to stain cells individually via single cell electroporation (Judkewitz et al. 2009) or stain several cells at once by bulk electroporation (Nagayama et al. 2007).

Over the years the methods of measuring Ca^{2+}-signaling steadily improved and a wide range of different Ca^{2+}-indicators are known today. Because of their distinct properties, in terms of sensitivity, kinetics, excitation or emission spectra, they can be used in various approaches and applications (Olga Garaschuk and Griesbeck 2010; Grienberger and Konnerth 2012). In addition to small synthetic Ca^{2+}-indicators, another option to visualize neuronal Ca^{2+}-signals is the use of genetically encoded Ca^{2+}-indicators (GECIs). GECIs can be transferred into the organism by gene delivery methods like *in utero* electroporation, virus-based gene transfer, or generation of transgenic mouse lines. Nowadays, there is a possibility to take advantage of several different transgenic mouse lines that express GECIs in variable types of tissue (Mank et al. 2008; Tallini et al. 2006; Ji et al. 2004; Zariwala et al. 2012). GCaMP6 is a commonly used GECI. It is a sensitive Ca^{2+}-indicator protein and it was reported to reliably detect single APs in neurons (Chen et al. 2013). With the help of, for example, an adeno-associated virus (AAV) expressing different GCaMP6 variants, specific regions of the neuronal tissue can be effectively labeled. The main advantage of GECIs like GCaMP6, in comparison to synthetic small molecule Ca^{2+}-indicators, is that the indicator expression is quite stable over a longer period of time. This fact enables Ca^{2+}-imaging of individual neurons through a chronic window over weeks. However, as also toxic effects have been reported, the measurements over extended periods of time have to be performed with caution. Cells showing nuclear fluorescence are likely to be unhealthy and might have altered properties, so the imaging of them should be avoided (Steinmetz et al. 2017; Tian et al. 2009). Nevertheless, due to a high contrast and a distinct staining of different cell compartments, with the correct staining paradigm, GCaMP6 can be used to measure Ca^{2+}-signals in the soma, as well as in axonal or dendritic structures of cell populations.

Taken together, Ca^{2+}-imaging provides a good method to capture functional dynamics of neuronal circuits *in vivo.* It can be used to investigate neurons at a single cell or even subcellular level, as well as the whole population of neurons (Stosiek et al. 2003; Prevedel et al. 2016; T. Chen et al. 2013).

1.5 Cytokines

Cytokines are small regulatory proteins, secreted, either by immune cells of the periphery like liver Kupffer cells, monocytes, macrophages, or cells within the CNS. Sources of cytokines in the CNS are invading peripheral immune cells, microvascular endothelial cells, pericytes, the choroid plexus, astrocytes, microglia and neurons (Galic, Riazi, and Pittman 2012). Several hundreds of different cytokines are known, and in addition to mediating interactions between cells and their function in general immune responses, they can act as neuromodulators. They participate, for instance, in neuronal development (Deverman and Patterson 2009; Zhao and Schwartz 1998), regulation of sleep (Krueger et al. 1998) or normal aging (Álvarez-Rodríguez et al. 2012; Vitkovic et al. 2000). The cytokine network is defined by the action of cascades of different pro- and anti-inflammatory cytokines, with positive and negative feedbacks and complex reciprocal interactions (Amiot et al. 1997). Two of the main proinflammatory cytokines are TNF-α and IL-1β, which are described in the chapters below.

1.5.1 Tumor necrosis factor-alpha

TNF-α is constitutively present within the CNS and mainly locally synthesized by glial cells. It is initially produced as a transmembrane protein that can be cleaved into a soluble form by the matrix metalloproteinase TNF-α-converting enzyme (TACE). Both the transmembrane and the soluble form of TNF-α have physiological implications. TNF-α can induce signaling pathways through the activation of the surface receptors Tumor necrosis factor receptor 1 and 2 (TNFR1 and TNFR2) (Zhang and An 2007). Soluble TNF-α acts mainly via TNFR1, which is present on most cell types within the CNS. The transmembrane form of TNF-α, in contrast, has a higher binding affinity to the TNFR2, preferentially expressed by glial and endothelial cells (Santello and Volterra 2012). After binding of TNF-α, several adaptor proteins are recruited, leading to the formation of intracellular protein complexes. These complexes initiate signaling

cascades, resulting in the activation of transcription factors, thereby regulating the expression of specific genes. The effects of TNF-α are pleiotropic. They include influences on cell growth, proliferation, cell migration, apoptosis, necrosis, synaptic scaling, and plasticity, as well as the regulation of the BBB permeability, the induction of inflammation with glial activation or febrile responses (McCoy and Tansey 2008; Santello and Volterra 2012). TNF-α can have protective as well as detrimental effects, depending on the activated receptor type, the duration of its action and its concentration. Under pathological conditions, the initially low levels of TNF-α in the brain can rise rapidly (Santello and Volterra 2012). Especially the soluble form of TNF-α is responsible for inflammatory processes, as demonstrated with knock-in mice expressing mutant TNF-α that is no longer a substrate for TACE cleavage (McCoy and Tansey 2008). During inflammation, there is a general up-regulation of TNF-α and its receptors. TNF-α is hereby thought to orchestrate the production of itself and other cytokines like IL-1β, IL-6, IL-8, CCL2 or IL-10. Blocking the effects of TNF-α in mice, with antibodies against TNF-α, soluble TNF-α receptors, or by using TNF-α knock-out mice, led to significantly reduced cytokine levels and a reduced inflammatory outcome after stimulation with LPS (Amiot et al. 1997).

1.5.2 Interleukin-1 beta

IL-1β represents another major inflammatory cytokine. It holds several physiological functions within the CNS, like the regulation of sleep, food and water intake, temperature regulation, synaptic plasticity and memory formation (Basu, Krady, and Levison 2004; Pinteaux et al. 2002). It is a large hydrophilic protein, which does generally not diffuse across the BBB, but can be secreted endogenously in the CNS by several cell types like astrocytes, oligodendrocytes, neurons, endothelial cells or microglia. Microglia are hereby considered to be the main source of IL-1β (Dantzer 2009; Pinteaux et al. 2002). Under healthy conditions, IL-1β is expressed at relatively low levels, but during pathologies like injuries or systemic infections, the IL-1β levels increase dramatically, inducing inflammation, fever and “sickness behavior” (Pinteaux et al. 2002). As TNF-α, also IL-1β acts in a divergent manner with dichotomic effects, depending on the activated type of receptors, duration of action and concentration. IL-1β activates the Interleukin-1 receptors (IL-1Rs). Two main receptors are known, the IL-1 type-I receptor (IL-1RI) (Sims et al. 1988) and the IL-1 type-II receptor (IL-1RII) (McMahan et al. 1991). IL-1RI can associate with an

IL-1 receptor accessory protein (IL-1RAcP) to activate signaling pathways (Wesche et al. 1997). IL-1Rs are present on almost all cell types in the brain (Pinteaux et al. 2002). IL-1β is initially synthesized as an inactive pro-peptide (Lamkanfi and Dixit 2012). In order to switch to a bioactive mature form, it needs to be post-translationally processed on intracellular protein platforms, known as inflammasomes. In the CNS, inflammasomes are dominantly expressed by microglia and macrophages. Both cell types have a sensor function for danger signals or infectious stimuli (Walsh, Muruve, and Power 2014). In comparison to the toll-like pattern recognition receptors on the surface of the cells, so-called NOD-like receptors (NLRs), located in the cytoplasm of the cells are important to sense intracellular danger signals. An activation of the NLRs can induce the assembly of the inflammasome complex. The complex generally consists of three major parts: a cytosolic pattern-recognition receptor, the enzyme caspase 1 and an adaptor protein facilitating the interaction between the two. One of the main and best-investigated inflammasomes is the NLR family pyrin domain containing 3 inflammasome (NLRP3). NLRP3 can be activated by harmful stimuli, such as amyloid beta, viral, fungal and bacterial components or extracellular ATP. The activation is a two-step process. First, a priming signal like, for example, bacterial LPS is needed, to trigger the transcription of inflammatory cytokine precursors like pro-IL-1β or pro-IL-18. Then, a second trigger, such as ATP, initiates the protein complex formation. This leads to a subsequent activation of the proinflammatory enzyme caspase 1 and the maturation and release of the active forms of IL-1β or IL-18. The release of the pyrogenic cytokine IL-1β into the extracellular space may, for example, induce fever by interacting with temperature-sensitive neurons in the preoptic hypothalamus or modulate the secretion of the corticotrophin-releasing hormone, by influencing neurons of the paraventricular nucleus of the hypothalamus. Corticotrophin-releasing hormone, in turn, can act on the pituitary and regulates the release of corticotrophin and the secretion of glucocorticoids by the adrenal cortex (Whiteside, Quan, and Herkenharn 1999; Gadek-Michalska and Bugajski 2004). The action of cytokines can have a broad impact on the organism. Cytokines have a great spectrum of different activities and always act in the context of other cytokines with opposing or potentiating effects on each other. Overall, they can be considered as junctions

between cells of the immune and neuronal system and represent, among others, one way of the communication between these cells.

1.6 Microglia-neuron interactions

In the recent years, it became more and more clear that microglia play an active role in the development and maintenance of the neuronal circuitry. As highly dynamic cells, they stand in close interaction with neurons. Their fine processes regularly contact neuronal synapses in an activity-dependent manner (Wake et al. 2009; Tremblay, Lowery, and Majewska 2010). Microglia seem to be able to sense neuronal activation, whereby synapses from neurons with higher activity are contacted more frequently. It was shown, that rather small spines are contacted more often and tend to increase under the influence of microglia (Tremblay, Lowery, and Majewska 2010; Eyo and Wu 2013). Microglial cells have the ability to engulf and phagocyte whole synapses. Immune factors of the complement system expressed by synapses and complement receptors on the surface of microglia were shown to mediate phagocytosis and synaptic pruning during development (Stevens et al. 2007; Schafer et al. 2012). Thus, microglia are important for synaptic reorganizations during development as well as in the mature adult brain (Paolicelli et al. 2011; Miyamoto et al. 2013). In addition to the contact-mediated synapse remodeling, microglia have the ability to actively shape the function of neurons by release of modulatory factors. These factors can be prostaglandins, chemokines or cytokines. The cytokine TNF-α, for instance, was implicated in neuronal synaptic scaling and IL-1β was considered to be relevant for long-term potentiation in neurons (Stellwagen and Malenka 2006; Wohleb 2016). All these abilities make microglia essential players of the synaptic network plasticity.

Vice versa, also neurons are important for the development of microglia. Factors released by neurons, like Interleukin-34 (IL-34) or the colony stimulating factor-1 (CSF-1), for example, act on CSF-1 receptors on microglia and participate in the regulation of the development and the viability of microglial cells. A blockade of the CSF-1 receptor results in a robust depletion of microglia within the brain (Elmore et al. 2014; Dagher et al. 2015). Also, neurons can interact with microglia via direct contact-dependent mechanisms or through soluble factors like chemokines, neurotransmitters, and cytokines (Wohleb 2016). Under physiological conditions,

neurons express or release "OFF"-signals, to keep microglia in their surveillance/resting state. Under pathological circumstances, neurons either remove the "OFF"-signals or communicate via "ON"-signals, to actively initiate microglial effector functions (Biber et al. 2007). Chemokines like the CX3C motif ligand 1 (CX3CL1), also known as fractalkine can act as "OFF"-signal. CX3CL1 directly connects neurons with microglia. CX3CL1 is constitutively expressed on neurons and binds the CX3C motif receptor 1 (CX3CR1) expressed on microglia. This bridge between the cells regulates the activity state of microglia. While the ligand is bound to the receptor, microglia remain in their quiescent, ramified state (Wohleb 2016). An improper ligand-receptor connection was shown to alter the responses of microglia to inflammatory and neurotoxic stimuli like LPS and has implications for the survival of the neurons. It is known that CX3CR1 knock-out mice show a stronger morphological activation of microglia and a significantly increased incidence of neuronal cell death (Cardona et al. 2006). Several factors from the immunoglobulin superfamily function as such "OFF"-signals. The CD200 glycoprotein from neurons and the CD200 receptors on microglia represent another direct contact between the cells, mediating the morphological state of microglia. A disrupted CD200/CD200R signaling leads to highly activated microglia and a worsening of neuroinflammatory processes (Masocha 2009; Deckert et al. 2006; Hoek 2000; Meuth et al. 2008). Further, an activation of CD45 receptors expressed by microglia inhibits their activation. After neuronal damage, neurons can release CD22, which activates CD45 receptors (Tan, Town, and Mullan 2000; Mott et al. 2004; Biber et al. 2007). Microglia were also shown to express receptors for neurotransmitters, such as glutamate, GABA, noradrenaline, dopamine or purines. Activation of these receptors *in vitro* was reported to result in changes of the membrane properties of microglia. Moreover, except glutamate, all of these neurotransmitters led to a decreased release of inflammatory mediators, like nitric oxide, TNF-α or IL-1β in response to LPS stimulation. Transforming growth factor-β, expressed in neurons, might represent another neuronal "OFF"-signal to keep microglia quiet. Transforming growth factor-β knock-out mice were characterized by an increased activation of microglia (Brionne et al. 2003; Biber et al. 2007).

On the other hand, instead of down-regulating the activity of microglia, neurons are also capable to release activating "ON"-signals. In presence of danger or harmful stimuli, for example, damaged neurons may release purines like ATP. Such purines can act on microglial purinergic receptors and initiate either inflammatory mediator responses or affect the process motility and phagocytosis of microglia (Koizumi et al. 2007; Wohleb 2016). Upon stimulation, neuronal cultures were shown to release chemokines, such as CX3CL1, C-X-C motif chemokine ligand 10 (CXCL10) or C-C motif chemokine ligand 21 (CCL21) (Limatola et al. 2005; Klein et al. 2005; de Jong 2005). These, in turn, were reported to initiate the migration of microglia. Hence, neurons might actively attract microglial cells in dangerous situations (Biber et al. 2007). In comparison to the "OFF"-signal-neurotransmitters mentioned above, the release of neuronal glutamate can be considered as neuronal "ON"-signal. The stimulation of glutamate receptors on microglia was hereby correlated with the release of proinflammatory TNF-α and concomitant neurotoxic effects (Taylor 2005; Biber et al. 2007). Another "ON"-signal is the triggering receptor expressed on myeloid cells 2 (TREM 2). Released by neurons, it can interact with DNAX-activating protein 12 from microglia and modulate phagocytic functions of these cells. A TREM-2 knock-down leads to disturbed phagocytosis of apoptotic neurons by microglia and to an increased transcription of proinflammatory factors as TNF-α (Takahashi, Rochford, and Neumann 2005; Biber et al. 2007).

1.7 Excitatory effect of peripheral inflammation on neurons

Considering numerous signaling molecules, mediating communication between neurons and microglia, it is not surprising that activation of microglia in response to an immune challenge affects neurons. For example, neuronal cortical slices and hippocampal neuronal cell cultures treated with microglia-conditioned medium were reported to show potentiated NMDA-induced currents (Moriguchi et al. 2003; Hayashi et al. 2006). Additionally, experiments with LPS-injected rats and multi-wire electrode measurements revealed that neurons change their activity pattern after a peripheral infection (Xi and Toth 2000). This activity change was reported to be accompanied by an up-regulation of the transcription factor c-fos, which is expressed when neurons fire APs (Dragunow and Faull 1989). The up-regulation of c-fos was observed in several brain areas, mostly related with the nucleus tractus solitarius, the

paraventricular nucleus, the bed nucleus of the stria terminalis, and the central nucleus of the amygdala. These are brain regions, that lead to activation of the hypothalamic-pituitary-adrenal axis and the autonomic nervous system (Xi and Toth 2000). *In vitro* experiments, using acute mouse brain slices exposed to LPS, revealed increased levels of TNF-α and IL-1β and concomitant facilitation of epileptiform discharges in hippocampal neurons (Gao et al. 2014). Another study, using mouse brain slices, showed that upon stimulation with LPS microglia release ATP. This is followed by a subsequent release of glutamate by astrocytes, ending up in an increased neuronal excitatory transmission (Pascual et al. 2012). Further experiments revealed that LPS-activated microglia actively displaced inhibitory GABAergic synapses in the mouse motor cortex, whereby excitatory synapses did not seem to be affected. This suggests an increased excitation after stimulation with LPS (Chen et al. 2014). Additionally, several electrophysiological recordings from experiments in rodents pointed out that LPS treatment can reduce the threshold for epileptic seizures via cytokine-mediated pathways (Kovács et al. 2014; M. a Galic et al. 2008; Vezzani et al. 2002; Cerri et al. 2016; Rodgers et al. 2009). All these data indicate quite clearly, that the brain is actively involved in the reaction to an inflammatory process. Nevertheless, the underlying mechanisms are not well understood.

1.8 Relevance and aim of the project

Organisms are constantly endangered by infectious stimuli. The role of the intact immune system is to fight those infections, enabling long and healthy life. Apart from the hazard induced by a bacterial infection and the concomitant danger of developing a sepsis, a disturbed balance of inflammatory responses is linked with many severe diseases, like Alzheimer`s disease, multiple sclerosis or Parkinson`s disease.
Thus, it is very important to understand the fundamental mechanisms of the immune responses of an organism. Specifically, to understand how peripheral inflammation affects the brain under *in vivo* conditions. Up to date, such studies are rare and the mechanisms at the cellular and molecular levels are largely elusive.
This project aims to provide a better understanding of the local network function in the *in vivo* cortex during peripheral inflammation.

The specific aims are:

- To provide an *in vivo* characterization of microglial and neuronal signaling during peripheral inflammation

- To decipher the involvement of the specific cell types (microglia, glutamatergic and GABAergic neurons) and structures (presynapses and postsynapses) in different phases of the inflammatory reaction

- To investigate the mechanisms underlying altered brain signaling, in particular, the influence of cytokines and the effect of microglial depletion

2. Material and Methods

2.1 Animals

All experiments were performed with 4-6 months old mice of either sex. The animals were housed under standardized conditions with a 12 h light-dark cycle and free access to water and food. C57BL/6 mice (Charles River, USA) served as wild type (WT) animals in this work. For visualization of microglia, CX3CR1$^{GFP/+}$ transgenic mice (B6.129P-Cx3cr1tm1Litt/J, Jackson Laboratory, USA) or Iba1$^{GFP/+}$ transgenic mice (Tg(Aif1-EGFP)1Kohs, Jackson Laboratory, USA) were used. These mouse lines express enhanced green fluorescent protein (eGFP) under the microglial CX3CR1 promoter (Jung et al. 2000) or the Ionized calcium-binding adaptor molecule 1 (Iba1) promoter (Hirasawa et al. 2005). Ca^{2+}-signals in inhibitory neurons were measured in the offspring of a VIAAT-Cre mouse line (B6.FVB-Tg(Slc32a1-cre)2.1Hzo/FrkJ, Jackson Laboratory, USA) crossed with a GCaMP6 mouse line (B6;129S6-Igs7tm93.1(tetO-GCaMP6f)Hze/J, Jackson Laboratory, USA). The newly generated mouse line (VIAAT-Cre-GCaMP6) expressed the Cre recombinase under control of the vesicular inhibitory amino acid transporter (VIAAT) promoter, which is exclusively active in inhibitory GABAergic neurons. The impact of cytokines was investigated by using Tumor necrosis factor-α (TNF-α$^{-/-}$) and NLR Family Pyrin Domain Containing 3 (NLRP3$^{-/-}$) knock-out mice (B6.129S-Tnftm1Gkl/J and B6.129S6-Nlrp3tm1Bhk/J, Jackson Laboratory, USA). All experimental procedures were in accordance with the institutional animal welfare guidelines and were approved by the state government of Baden-Württemberg, Germany.

2.2 Induction of a peripheral inflammation

For induction of peripheral inflammation, the mice received an intraperitoneal (i.p.) injection of the bacterial endotoxin lipopolysaccharide (LPS) from Escherichia coli (E. coli, serotype O111:B4, Sigma-Aldrich, USA). LPS was diluted in sterile phosphate buffered saline (PBS) and injected at a dose of 1.5 mg/kg body weight (BW). Control animals were injected with an equivalent volume of sterile PBS.

2.3 Enzyme-linked immunosorbent assay (ELISA)

2.3.1 Sample collection and tissue processing

Mice were injected with LPS or PBS as described above (see 2.2). 5 h or 30 h after the injections, the mice were deeply anesthetized with a mixture of ketamine (200 mg/kg BW, Fagron, Netherlands) and xylazine (20 mg/kg BW, Sigma-Aldrich, USA). Blood serum samples were obtained by puncturing the orbital sinus of the mice. The samples were located on ice for 1 h before centrifugation for 15 min at 14 000 x g. After blood collection, the mice were transcardially perfused with sterile PBS and the brain was immediately dissected and snap frozen in 2-methylbutane on dry ice. A Dounce homogenizer (Sigma-Aldrich, USA) was used to homogenize the brain samples in N-PER neuronal protein extraction reagent (1 g brain per 5 ml N-PER reagent, Thermo Fisher Scientific, USA), containing 13.3 % protease inhibitor cocktail (Sigma-Aldrich, USA). Afterward, the brain homogenates were incubated for 10 min on ice, before the cell debris was pelletized by centrifugation (10 000 x g, 10 min at 4 °C). The supernatants were collected and the protein concentration of the homogenates was determined using the Pierce™ BCA Protein Assay Kit (Thermo Fisher Scientific, USA), according to the manufacturer's guide.

2.3.2 ELISA

ELISA Kits (Quantikine ELISA, R & D systems, USA) were used to measure the cytokine levels of IL-1β (Kit sensitivity 4.8 pg/ml), TNF-α (Kit sensitivity 7.21 pg/ml), CCL2 (Kit sensitivity 2 pg/ml), IL-6 (Kit sensitivity 1.8 pg/ml) and IL-10 (Kit sensitivity 5.22 pg/ml). A total volume of 100 µl of the blood serum samples or brain homogenates was used to perform the ELISA analysis, according to the manufacturer's guide. Each sample was hereby tested in duplicate. The chemiluminescent protein signal was measured as optical density with a plate reader (PowerWave XS2, BioTek, USA).

In another group of mice, blood serum samples were collected as described above (see 2.3.1) and the cytokine levels were determined by the company microBIOMix GmbH (Germany) with the Luminex xMAP™-Technology (www.microbiomix.de). The blood serum levels of CCL2, IL-6 and IL-10 were determined by this method.

2.4 Immunohistochemistry

2.4.1 Sample collection and tissue processing

Animals were injected with LPS or PBS as described above (see 2.2). 5 h and 30 h after the injections, the mice were deeply anesthetized with a mixture of ketamine (200 mg/kg BW, Fagron, Netherlands) and xylazine (20 mg/kg BW, Sigma-Aldrich, USA). Afterward, they were transcardially perfused with PBS and 4 % paraformaldehyde (PFA, Roth, Germany). The brains were dissected and fixed overnight, shaking in 4 % PFA at 4 °C. Then, the brains were washed 3 x 10 min with PBS and dehydrated for another 12 h in 25 % sucrose solution (diluted in PBS). The cortices of the brains were cut into four equal parts (frontal left, frontal right, rostral left, and rostral right), separately embedded in TissueTek (Sakura, VWR, USA) and stored at -80 °C until use.

2.4.2. Immunofluorescence staining

2.4.2.1 Iba1 and IL-1β

A cryostat (Leica, Germany) was used to cut the embedded brains into 50 µm thick sagittal slices. All incubations and washing steps were carried out on free-floating sections at room temperature in 24 well plates (Greiner Bio-One, Austria) on a horizontal shaker (Titramax 100, Heidolph, Germany). The cut sections were first washed 3 x 10 min with PBS. To prevent unspecific antibody binding, the slices were incubated for 2 h in blocking solution, containing 10 % donkey normal serum (DNS, Dianova, Jackson Immuno Research, USA) and 1 % Triton X-100 (Sigma-Aldrich, USA) in PBS. Then, the sections were incubated for 60 h with the primary antibody solution. A polyclonal rabbit anti-Iba1 antibody (Wako, USA) was used, in combination with a polyclonal goat anti-IL-1β antibody (R & D Systems, USA). The antibodies were diluted in blocking buffer with 0.04 % NaN_3 at concentrations of 1:3000 for Iba1 and 1:200 for IL-1β. After washing the slices 5 x 10 min with PBS, they were incubated for 3 h with a secondary antibody solution, constantly protected from light. The secondary antibodies were diluted in blocking solution containing 2 % DNS and 1 % Triton X-100 in PBS at concentrations of 1:1000 for donkey anti-goat Alexa Fluor 594 (Iba1-staining) and 1:2000 for donkey anti-rabbit Alexa Fluor 488 (IL-1β-staining) (Invitrogen, USA). Final washing steps with PBS were performed for

4 x 10 min before the slices were mounted on fluorescence-free Superfrost Plus microscope slides (Langenbrinck, Germany) with Prolong Gold Antifade Mounting Medium (Thermo Fisher Scientific, USA).

2.4.2.2 Iba1 and CD68

The embedded brains were cut and processed as described above (see 2.4.2.1). The brain slices were incubated for 1 h in blocking solution, containing 5 % DNS and 1 % Triton X-100 in PBS. Then, the sections were incubated overnight with the primary antibody solution. A polyclonal rabbit anti-Iba1 antibody (Wako, USA) was used in combination with a monoclonal rat anti-CD68 antibody (Bio-Rad, UK). The antibodies were diluted in blocking buffer at concentrations of 1:500 for Iba1 and 1:1000 for CD68. After washing the slices 3 x 10 min with PBS, they were incubated for 2 h with a secondary antibody solution, constantly protected from light. The secondary antibodies were diluted at concentrations of 1:1000 in blocking solution containing 2 % DNS and 1 % Triton X-100 in PBS. Donkey anti-rabbit Alexa Fluor 488 was used for the Iba1-staining and donkey anti-rat Alexa Fluor 594 for the CD68-staining. Final washing steps with PBS were performed for 3 x 10 min before the slices were mounted on fluorescence-free Superfrost Plus microscope slides (Langenbrinck, Germany) with Vectashield Mounting Medium (Vector Laboratories, USA).

2.5 Surgical procedures

2.5.1 Chronic cranial window implantation

The mice were deeply anesthetized with an i.p. injection of fentanyl (0.05 mg/kg BW, Fentadon, Eurovet Animal Health, Netherlands), midazolam (5.0 mg/kg BW, Hameln Pharma Plus, Germany) and medetomidine (0.5 mg/kg BW, Dormilan, Alfavet, Germany). After proving the complete sedation of the animals with a toe-pinch, a hair trimmer was used to remove the fur from the area of surgery. The mice were placed on a warming plate under a dissecting microscope and fixed in a stereotaxic frame. Eye ointment was applied to protect their eyes from drying out. During the entire surgery, the body temperature was monitored with a rectal thermometer (Voltcraft, Conrad, Germany) and maintained between 36-37 °C. To provide a persistent analgesia, the mice received an s.c. injection of 5 mg/kg BW carprofen

(Rymadil, Pfizer, USA). An i.p. injection of 4 mg/kg BW dexamethasone (Sigma-Aldrich, USA) prevented swelling of the brain during the surgery. All surgical instruments were pre-sterilized with a glass bead sterilizer (Fine Science Tools, USA) and cleaned with 70 % ethanol. The skin above the area of surgery was disinfected with a povidone-iodine solution (Braunol, B. Braun, Germany). A local anesthetic (2 % xylocaine, AstraZeneca, UK) was injected s.c., shortly before the skin above the skull was removed with scissors, starting with a horizontal cut and enlarging it laterally to the eyes. After removing the skin and the connective tissue, the skull was dried with compressed air, and a circular glass coverslip with a diameter of 3 mm was placed above the right motor cortex. The glass coverslip was centered at 1.5 mm anterior and 1.5 mm lateral from the bregma. The shape of the glass coverslip was pre-drawn on the bone with a pencil and the cover glass removed. Then, the bone was carefully thinned by using a dental drill (Ultimate 500, NSK, Japan), drilling down a circular shape, corresponding to the pre-drawn area. Between the drilling steps, in regular intervals cold ringer solution (B. Braun, Germany) was applied, to prevent an overheating of the bone. After only a very thin layer of bone was left, a drop of ringer solution was added and the circular drilled bone flap was lifted up with fine tip forceps, cautiously, to keep the dura mater intact. A fresh drop of ringer solution was applied and a sterile 3 mm circular glass coverslip was placed on the brain. With the help of a needle, the glass coverslip was pressed gently onto the brain and glued to the skull with cyanoacrylate glue (UHU, Germany). Once the glue was dry, the whole skull was covered with a thin layer of dental cement (Tetric Evoflow, Ivoclar Vivadent, Liechtenstein), carefully omitting the circular chronic glass window. A custom-made titanium bar was embedded in the dental cement between the ears and fixed with an additional layer of cement. The bar was used for head fixation of the animal under the microscope during the imaging sessions. The cement was hardened by shortly shining ultraviolet light on it. After the cement was solid, the mice were replaced in their home cage and received an s.c. injection of antidote, containing flumazenil (0.5 mg/kg BW, Fresenius, Germany) and atipamezole (2.5 mg/kg BW, Nosedorm, Alfavet, Germany) to antagonize the anesthesia. For the next 3 consecutive days, the mice received s.c. injections of 5 mg/kg BW carprofen. To prevent infections, their drinking water was supplemented with 0.025 % of the antibiotic enrofloxacin (Baytril, Bayer, Germany) for 10 days. To reduce immediate inflammatory effects due

to the surgery, all experimental measurements were performed at the earliest 3-4 weeks after the chronic window implantation.

2.5.2 Acute craniotomy

The mice were deeply anesthetized with 2.5 % isoflurane (CP-Pharma, Germany) in pure oxygen (O_2) and transferred to a warming plate under a dissecting microscope. The body temperature of the mice was constantly maintained between 36-37 °C and the isoflurane concentration was reduced to 0.8-1.5 %. After an s.c. injection of 2 % xylocaine, the skin and the connective tissue above the skull were carefully removed and a custom build recording chamber with a hole in the middle was glued above the motor cortex (1.5 mm anterior and 1.5 mm lateral from the bregma). After the glue was dry, a bone area with a diameter of approximately 3 mm was drilled, until only a thin layer of bone was left. Then, the mouse was fixed in the microscopic setup and the chamber was perfused with an at 37 °C pre-warmed extracellular ringer solution (125 mM NaCl, 4.5 mM KCl, 26 mM $NaHCO_3$, 1.25 mM NaH_2PO_4, 2 mM $CaCl_2$, 1 mM $MgCl_2$, 20 mM glucose, pH 7.4). The ringer solution was constantly bubbled with 95 % O_2 and 5 % CO_2. A thin syringe cannula (30 G) served to cut out a small (< 1 mm^2) craniotomy for the two-photon measurements.

2.6 Single cell electroporation of microglia

An acute craniotomy was performed in $Iba1^{GFP/+}$, TNF-$\alpha^{-/-}$ or $NLRP3^{-/-}$ mice (as described in 2.5.2). Before electroporating microglia in TNF-$\alpha^{-/-}$ or $NLRP3^{-/-}$ mice, the cells were visualized with a tomato lectin staining (Schwendele et al. 2012). For this purpose, 25 µg tomato lectin conjugated with DyLight 594 (Vectorlabs, USA) were dissolved in 1 ml standard pipette solution (150 mM NaCl, 2.5 mM KCl and 10 mM HEPES, pH 7.4). The solution was filtered with a centrifugal filter with a pore diameter of 0.45 µm (Millipore Ultrafree, Merck, USA). Then, a glass pipette with a tip diameter of < 1 µm was filled with the solution and directed into the tissue with a micromanipulator (LN Junior, Luigs & Neumann, Germany), 100 µm below the cortical surface. With an attached pressure injection system (PDES-02D, NPI Electronic, Germany) a short pressure pulse of 30 s with 10-55 kPa was applied. The pipette was retracted and the experiment continued 30 min after the tomato lectin injection. For the single cell electroporation (Eichhoff, Brawek, and Garaschuk 2011),

10 mM Oregon Green 488 BAPTA-1 (OGB-1, Invitrogen, USA) were used in a solution containing 140 mM potassium gluconate, 14 mM KCl, 4 mM NaCl and 10 mM HEPES with a pH of 7.3. The OGB-1 solution (3 µl) was filled into a pipette with a tip diameter of < 1 µm. The pipette was guided to the membrane of an eGFP- or tomato lectin-stained microglia in layer 2/3 of the motor cortex. Then, a negative current of 600 nA was applied for 10 ms, by using a MVCS-02C iontophoresis system (NPI Electronic, Germany). After the electroporation of the cell with OGB-1, the pipette was carefully withdrawn and some minutes later, the Ca^{2+}-signals of the microglia were measured. To prove the viability of the cells, subsequent to the measurements, Ca^{2+}-transients were actively evoked by a short pressure application of 50 µM adenosine 5'-triphosphate (ATP, Sigma-Aldrich, USA) or 100 µM Uridine 5'-diphosphate (UDP, Sigma-Aldrich, USA) in standard pipette solution. The solution was injected in the direct vicinity of the cells.

2.7 Microglial dynamics after local application of ATP

To analyze the dynamics of the microglial process extension in response to a point source of ATP, an acute craniotomy was performed similar to the procedure described above (see 2.5.2). Then, a pipette with a tip diameter of < 1 µm was filled with 7 µl of a solution containing 5 mM ATP dissolved in standard pipette solution. For a better visualization of the pipette, 100 µM Alexa 594 (Invitrogen, USA) was added to the solution. The pipette was directed in the extracellular space of the layer 2/3 motor cortex. A short pressure injection for 50 ms with 30-35 kPa was applied, to ensure an unblocked pipette tip and the microglial process extension was subsequently captured.

2.8 Bulk electroporation of neurons

For functional imaging of somatic Ca^{2+}-signals in deeper cortical layers during inflammation, it was necessary to get a sparse labeling of neurons. Therefore, an acute craniotomy was cut out above the motor cortex (as described in 2.5.2). The Ca^{2+}-sensor Oregon Green 488 BABTA-1 hexapotassium salt (OGB-1, Invitrogen, USA) was dissolved in an intracellular solution containing 175 mM potassium gluconate, 12.5 mM HEPES, 17.5 mM KCl and 5 mM NaCl. A pipette with a tip

diameter < 1 µm was filled with 10 mM of the OGB-1 solution and guided to a depth of 500-600 µm below the cortical surface. To perform the OGB-1 bulk electroporation of neurons, a current with an amplitude of 1 µA, a pulse duration of 25 ms and a frequency of 2 Hz was applied for 10 min (as described before by Nagayama et al., 2007). The Ca^{2+}-imaging of the OGB-1-labeled neurons started 1 h after the labeling procedure, during a time window between 4 and 6 h after injection of LPS or PBS.

2.9 Virus injections

For functional imaging of cortical Ca^{2+}-signals, neurons of mice were labeled with the genetically encoded fluorescent Ca^{2+}-indicator GCaMP6f. After performing a craniotomy (as described in 2.5.1), the neurons were transduced with a neuron-specific viral construct enabling expression of the Ca^{2+}-sensor GCaMP6f under control of the synapsin-promoter (AAV1.Syn.GCamp6f.WPRE.SV40 serotype 1, Penn Vector Core, USA). The viral construct was diluted 1:10 in sterile ringer solution (B. Braun, Germany) and shortly resuspended in an ultrasonic bath. Then, 1 µl of the virus solution was pipetted on a piece of parafilm (Bemis, USA) and sucked into a thin glass pipette (tip diameter of < 15 µm) with a syringe. The pipette was attached to a stereotaxic device, so that the virus-containing pipette could be directed to the craniotomy and placed on a blood vessel-free area of the brain.

2.9.1 Virally-induced GCaMP6f-expression in layer 2/3 neurons

To label neurons of layer 2/3, the pipette was vertically inserted to a depth of 600 µm and the virus solution was slowly injected into the brain tissue (< 0.2 µl in 3 min). Then, the pipette was retracted to a depth of 300 µm and an additional volume of 0.1 µl of the virus solution was injected. After retracting the pipette completely from the brain, a fresh drop of ringer solution was applied and the chronic window implanted (see 2.5.1). This injection protocol led to a broadly stained area of neurons in layer 2/3 of the motor cortex.

2.9.2 GCaMP6f-labeling of axons from the motor cortex

To label ascending axons from neurons of layer 5 in the motor cortex, the pipette was inserted into the brain with an angle of 45 °. Then, a smaller volume of virus solution was slowly injected (< 0.1 µl in 5 min) at a depth of 500-600 µm below the cortical

surface. After injection, the pipette was carefully removed and the chronic cranial window implanted (see 2.5.1).

2.9.3 GCaMP6f-labeling of axons from the somatosensory cortex

To label axons of neurons originating in the somatosensory cortex, a craniotomy above the motor cortex was performed as described above and the chronic cranial window implanted, without adding dental cement. Then, a small hole (0.5 mm^2) was drilled above the somatosensory cortex (-1.5 mm anterior and 3.5 mm lateral of the bregma). The pipette containing the GCaMP6f viral solution was inserted vertically into the opening and carefully injected (< 0.2 µl in 3 min) at a depth of 600 µm below the cortical surface. An additional volume of the virus solution was injected at depth of 300 µm (< 0.1 µl in 2 min). After removing the pipette, the skull was covered with dental cement and the chronic window implantation finalized as described in 2.5.1.

2.10 Two-photon imaging procedures and data analysis

A custom build two-photon laser scanning setup based on a mode-locked Ti:sapphire laser (Mai Tai, Spectra Physics, USA), generating pulsed light with a wavelength ranging between 710-990 nm was used. The laser scanning system (Olympus Fluoview, Olympus, Japan) was connected to an upright microscope (BX51WI, Olympus, Japan) and all images were acquired with a 40 x water-immersion objective (0.8 NA, Nikon, Japan). If not otherwise indicated, a dichroic mirror separated the emission light at 580 nm wavelength. To excite microglial eGFP a 900 nm wavelength was used. For simultaneous imaging of eGFP-labeled microglia and sulforhodamine B (SR-B)-labeled blood vessels, an excitation wavelength of 870 nm was used. DyLight 594, Alexa Fluor 488 or Alexa Fluor 594 were visualized with an excitation wavelength of 800 nm. GCaMP6f was excited at the wavelength of 920 nm (see overview of experimental settings in Table 1).

Table 1 Overview of experimental imaging settings

	Experiment	Dye	Dimensions	Excitation	Size	Depth	Zoom	Steps	Kalman	Time	Frames
A	Immunofluorescence	Alexa Fluor 488 or 594	x-y-z	800 nm	512x512 pixels	25 µm	2.5x	1 µm	3	-	1 frame/s
B	Microglial morphology	eGFP, SR-B	x-y-z	870 nm	512x512 pixels	150 µm	2.5x	1 µm	2	-	1 frame/s
C	Microglial Ca^{2+} -signals	OGB-1	x-y-t	800 nm	360x256 pixels	-	4.0x	-	-	15 min	1 frame/s
		eGFP	x-y-z	900 nm	512x512 pixels	~30 µm	4.0x	1 µm	2	-	1 frame/s
		DyLight 594	x-y-z	800 nm	512x512 pixels	~30 µm	4.0x	1 µm	2	-	1 frame/s
D	Microglial process extension	eGFP, Alexa Fluor 594	x-y-z-t	900 nm	512x512 pixels	20 µm	4.0x	2 µm	2	15 min	1 frame/s
			x-y-z	900 nm	512x512 pixels	20 µm	2.5x	2 µm	2	-	1 frame/s
E	Neuronal Ca^{2+}-signals	GCaMP6	x-y-t	920 nm	512x200 pixels	-	4.0x	-	-	5 min	10 frames/s
			x-y-z	920 nm	512x512 pixels	10 µm	2.5x	1 µm	2	-	1 frame/s
F	Microglial depletion	eGFP, SR-B	x-y-z	870 nm	512x512 pixels	200 µm	2.0x	2 µm	2	-	1 frame/s
		GCaMP6	x-y-t	920 nm	512x200 pixels	-	4.0x	-	-	5 min	10 frames/s
			x-y-z	920 nm	512x512 pixels	10 µm	2.5x	1 µm	2	-	1 frame/s
G	Neuronal Ca^{2+}-signals	OGB-1	x-y-t	800 nm	512x200 pixels	-	4.0x	-	-	5 min	10 frames/s
			x-y-z	800 nm	512x512 pixels	10 µm	2.5x	1 µm	2	-	1 frame/s

The data were analyzed and quantified with software from ElisaAnalysis (http://www.elisaanalysis.com/), ImageJ (http://imagej.nih.gov/ij/), Fiji (http://fiji.sc/Fiji), Igor Pro 6.22A (http://www.wavemetrics.com), Matlab R2015b (https://de.mathworks.com), GraphPad Prism 7 (https://www.graphpad.com) and Microsoft Excel 2007 (https://www.microsoft.com). If not indicated otherwise, the data are reported as median ± interquartile range (IQR).

2.10.1 ELISA analysis

Protein analysis was performed with the help of the online-software ElisaAnalysis.com (Leading Technology Group, Australia). The mean optical density from two sample duplicates was used to calculate the cytokine concentrations of the specific sample. The concentrations were calculated by generating a cytokine calibration curve with a 4-parameter logistic curve fitting. For brain samples, the obtained concentrations were normalized to the total protein concentration, determined before by the BCA assays. The concentrations were expressed as pg/ml for blood serum samples or pg/mg protein for brain homogenates. Outliers were identified with the Grubb`s test for outliers and excluded.

2.10.2 Imaging and analysis of immunofluorescence staining

For imaging, the immunofluorescence staining, the microscopic slides with the brain sections were located under the two-photon microscope and the fluorophores excited with 800 nm. The emitted light was hereby separated with a dichroic mirror

at 570 nm. A 470/100 nm band-pass filter, as well as a 586 long-pass filter, were used. All images were acquired as z-stack images (x-y-z) of 25 µm depth. For further imaging settings, see Table 1A.

The volume of microglial somata was calculated based on Iba1 immunofluorescence using the ImageJ “3 D object counter” macro. A threshold value was adjusted such that the microglial soma volumes were fully detected by the macro. The threshold was hereby kept the same for each mouse. Depending on the intensity of the images, it was determined as 3-6 times the standard deviation of the mean gray values plus the mean gray value of the images.

The CD68 immunofluorescence signal in Iba1-positive microglia was evaluated with the help of the “GECIquant" macro in ImageJ. After subtraction of the background signal, the Iba1-stained cells were detected as regions of interest (ROIs) with the "ROI detection" module. Cells on borders of the z-stacks, without the full cell soma morphology, were excluded from the analysis. To evaluate the intensity of the CD68-staining, the mean gray value per each ROI area was measured.

To determine the fraction of IL-1β-positive cells, the "cell counter" macro in ImageJ was used to count IL-1β-positive cells and the overall number of microglia. Microglia were considered IL-1β-positive if after background subtraction the antibody staining against IL-1β showed a clear cell morphology of the microglial shape. Cells on borders without the full cell soma morphology were discarded.

2.10.3 In vivo imaging and analysis of microglial morphology

Mice with an implanted chronic cranial window were anesthetized with an initial dose of 2.5 % isoflurane in pure O_2, placed on a warming plate and head-fixed with the titanium bar in the microscopic setup. The body temperature of mice was constantly kept at 36-37 °C and their respiratory rate was kept between 90-120 breaths per minute. This was achieved by regulating the concentration of supplied isoflurane between 0.8-1.5 %. To stain the blood vessels before an imaging session, the mice received an i.p. injection of 1 mM sulforhodamine B (SR-B) (Sigma-Aldrich, USA), diluted in sterile PBS at a dose of 10 µg/kg BW. The morphological changes of microglia during peripheral inflammation were assessed over time by imaging z-stacks of the motor cortex at a depth of 50-200 µm below the cortical surface (find imaging settings in Table 1B). The same stacks were measured before and at different time points after the LPS or PBS injections (see Figure 2).

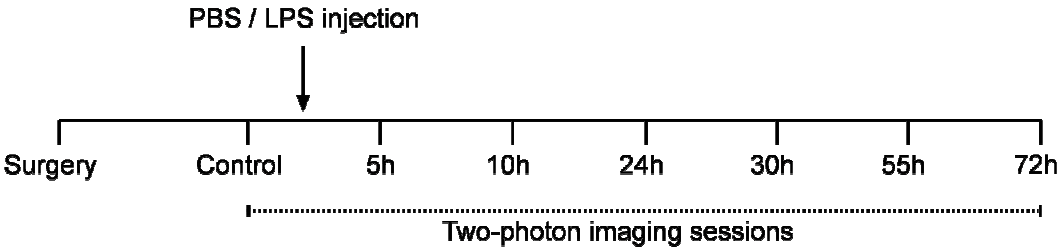

Figure 2 *In vivo* imaging protocol for longitudinal imaging

The numbers of microglial cells in the imaged z-stacks were counted with the help of the "cell counter" macro in ImageJ, whereby cells on borders without the full cell soma were not included. The microglial cell soma volumes and distances between the cells were analyzed with the ImageJ "3 D object counter" macro. To do so, a threshold value was adjusted such that the microglial soma volumes are fully detected by the macro. The threshold was kept the same for the specific z-stacks, imaged at the different time points. Depending on the intensity of the images, it was set at 3-6 times the standard deviation of the mean gray values of the images plus the mean gray value of the images. The distance between the cells was measured between the soma centers.

2.10.4 In vivo Ca^{2+}-imaging and analysis of microglia

Spontaneous Ca^{2+}-signaling of OGB-1-electroporated microglia was measured in acute experiments 5 h or 30 h after the LPS or PBS injections (see Figure 3). Thereby, the Ca^{2+}-signals were captured for 15 min by time-lapse imaging (x-y-t). Afterward, z-stack images of the electroporated cells were captured (see Table 1C for further settings).

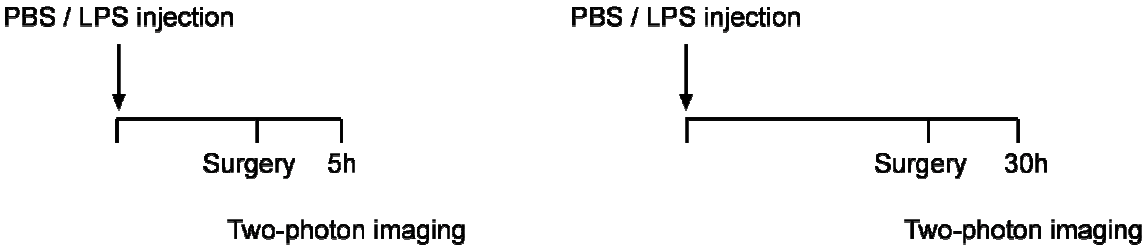

Figure 3 *In vivo* imaging protocol for acute experiments

For the analysis of the spontaneous Ca^{2+}-transients, microglial somata were manually selected as ROIs in ImageJ. Then, the mean intensity values of the ROIs were measured over time. The intensity results were transferred to the Igor Pro software and the relative change in fluorescence ($\Delta F/F$) was calculated after background subtraction with a custom-written macro. The fractions of active cells, showing at least one Ca^{2+}-transient during the 15-min-long recording period were determined. Cells, which did not respond with a Ca^{2+}-transient to the subsequent application of ATP or UDP were excluded.

2.10.5 In vivo imaging and analysis of microglial process extension

To measure the microglial process extension towards an ATP-containing pipette, mice were injected with PBS or LPS. 5 h or 30 h after the injections, the microglial process dynamics were captured with 4D-stacks (x-y-z-t) for a total time of 15 min (see imaging protocol in Figure 3). Afterward, z-stacks of the cells were imaged (find more details in Table 1D).

The microglial process velocity towards the pipette was quantified with the “MTrackJ” macro in ImageJ. The movements of clearly visible eGFP-labeled microglial processes were tracked and the corresponding mean velocities per mouse were analyzed.

2.10.6 In vivo Ca^{2+}-imaging and analysis of layer 2/3 neurons

Mice with implanted chronic cranial windows were anesthetized and fixed in the imaging setup as described above (see 2.10.3). Spontaneous Ca^{2+}-transients in the GCaMP6f-labeled layer 2/3 neurons were captured by time-lapse measurements (x-y-t). After this, z-stack images of the cells were collected (see details in Table 1E). An initial control measurement was performed before injecting the mice with either LPS or PBS. Subsequent Ca^{2+}-imaging of the same neurons was performed at different time points after the injection (see Figure 2).

A custom-written Igor Pro macro was used to analyze the spontaneous Ca^{2+}-transients in the neuronal somata and in the corresponding neuropil region. For evaluation of the somatic signals, the ROIs containing GCaMP6f-labeled neuronal cell bodies were selected manually. To measure the Ca^{2+}-signals in the neuropil, another ROI covering the surrounding of the neurons was included. Big blood vessels and neuronal dendrites were excluded from this neuropil ROI. Afterward, the mean

fluorescent intensities of all ROIs were measured in ImageJ, background subtracted and transformed into ΔF/F form. A change in the ΔF/F signal was counted as a Ca^{2+}-transient if its peak amplitude exceeded values of 3 times the standard deviation of the baseline noise.

To obtain additional information about the exact origin of the Ca^{2+}-signals in our data, a custom-written Matlab algorithm for an independent component analysis (ICA) was used (for a detailed description, see Hyvärinen et al. 2001). This method extracted statistically independent components, by decomposing the Ca^{2+}-transients of each ROI into a set of independent signals. This technique allowed to separate asynchronously occurring somatic Ca^{2+}-signals from the neuropil signal but eliminated all somatic Ca^{2+}-transients occurring synchronously with Ca^{2+}-signals in the neuropil. As a relatively high percentage of non-active cells were detected by this technique, the 75th percentiles per mouse were used instead of the median frequency to test for statistical significance.

2.10.7 In vivo Ca^{2+}-imaging and analysis of layer 2/3 neurons after microglial depletion

Mice with a chronic cranial window and GCaMP6f-labeled neurons were transferred to the imaging setup and the neuronal signaling was measured as described above (2.10.6). After the end of each measurement, the blood vessels were stained with SR-B (as described in 2.10.3) and z-stack images of the microglia at 0-200 µm depth were obtained (see settings in Table 1F). After the initial control measurements, the mice were fed with 1200 mg/kg BW of the CSF1R inhibitor PLX 5622, formulated in standard chow (Plexxikon Inc., USA). This treatment led to a nearly complete depletion of microglia in the brain. After 7 days, the neuronal Ca^{2+}-signaling was measured before and 5 h after the PBS or LPS injection (see imaging protocol in Figure 4). To estimate the degree of microglial depletion, the blood vessels of the mice were stained with SR-B and the z-stacks were reimaged.

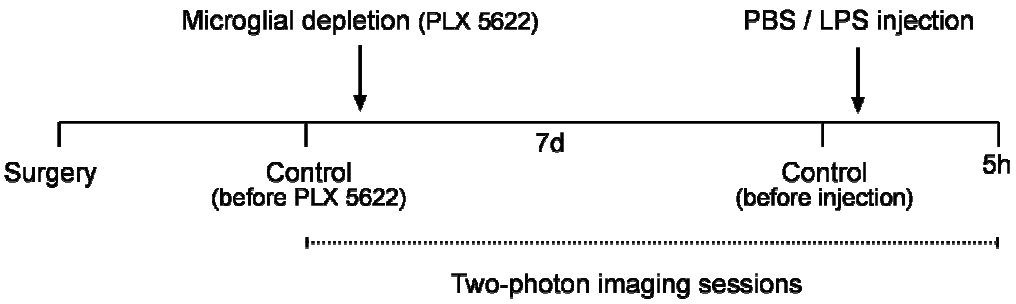

Figure 4 *In vivo* imaging protocol for microglial depletion experiments

The spontaneous neuronal signaling was analyzed as described above (2.10.6). To evaluate the depletion of microglial cells, we counted the eGFP-labeled microglia per field of view (0-200 µm below the cortical surface, within a volume of 0.0062 mm^3) before and after feeding the mice with PLX 5622, with the help of the "cell counter" macro in ImageJ.

2.10.8 In vivo Ca^{2+}-imaging and analysis of cortical axons in layer 1

Mice with a chronic cranial window and GCaMP6f-labeled axons were anesthetized and transferred to the imaging setup. Spontaneous Ca^{2+}-signals from axons in layer 1 of the motor cortex were measured before injecting either LPS or PBS and 5 h after the injections (see Figure 5). Time-lapse images (x-y-t) of the axons were acquired and z-stacks of the axons were obtained similarly as for the neuronal somata imaging (for settings, see Table 1E).

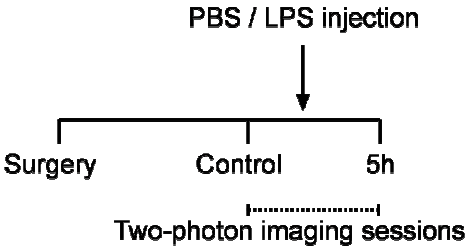

Figure 5 *In vivo* imaging protocol for axonal imaging and imaging of inhibitory neurons

The analysis of axonal spontaneous Ca^{2+}-transients was performed as for the neuronal somata. After manually selecting the ROIs (GCaMP6f-labeled axons), the mean fluorescent intensities of the axons were measured in ImageJ and

background-subtracted fluorescence changes (ΔF/F) were calculated in Igor Pro. A change in ΔF/F was counted as Ca^{2+}-transient when its peak amplitude exceeded 5 times the standard deviation of the baseline noise.

2.10.9 In vivo Ca^{2+}-imaging and analysis of layer 5 neurons

Ca^{2+}-imaging of OGB-1-labeled deep cortical layer 5 neurons was performed in mice with an acute craniotomy above the motor cortex, 4-6 h after the mice received either an LPS or PBS injection (see Figure 6). Time-lapse and z-stack images were acquired similar as described above (see 2.10.6 and Table 1G).

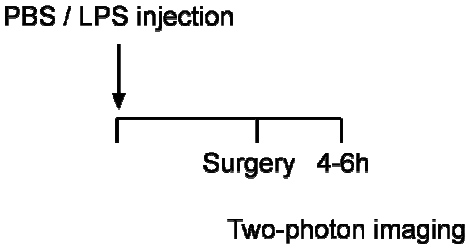

Figure 6 *In vivo* imaging protocol for layer 5 neuronal imaging

For evaluation of the spontaneous neuronal Ca^{2+}-signaling in layer 5, the mean fluorescent intensities of the Ca^{2+}-transients were measured in ImageJ and the fluorescence changes (ΔF/F) after background subtraction were calculated in Igor Pro as described above (see 2.10.6). The signal was counted as a Ca^{2+}-transient if its peak amplitude exceeded values of 3 times the standard deviation of the baseline noise. Note, that strongly labeled cells located in close proximity of the electroporation site were excluded from the analysis.

2.10.10 In vivo Ca^{2+}-imaging and analysis of inhibitory neurons

The Ca^{2+}-imaging of inhibitory neurons was performed in mice with a chronic cranial window above the motor cortex. The mice received either an LPS or PBS injection and the GCaMP6-labeled neurons were measured before and 5 h after the injections (see imaging protocol in Figure 5). Time-lapse images and z-stacks were acquired similar as described in 2.10.6 and shown in Table 1E.

For the analysis of the spontaneous Ca^{2+}-transients in inhibitory neurons see 2.10.6. If the peak amplitude exceeded 6 times the standard deviation of the baseline noise, the signal was counted as Ca^{2+}-transient.

2.11 Statistical analysis

The statistical analysis of the data was performed with the GraphPad Prism 7 software (GraphPad, USA) or Matlab R2015b software (MathWorks, USA). Multiple comparisons of repeated measurements were tested with repeated measures ANOVAs (Friedman's test) and the post hoc Dunn’s multiple comparisons test. The Wilcoxon signed-rank test or a Paired t-test was used in order to compare two repeated measurements. For independent measurements, the Kruskal-Wallis test with a post hoc Dunn’s multiple comparisons test was used. Two independent datasets were compared with the Mann-Whitney U or the Kolmogorov-Smirnov test. For categorical data, the Fisher`s exact test was applied. The Grubb's test served to identify significant outliers. A statistical significance was accepted for p-values ≤ 0.05 (two-tailed, if not otherwise indicated).

3. Results

3.1. Characterization of the lipopolysaccharide-induced peripheral inflammation

3.1.1 Lipopolysaccharide induces slight but significant weight loss in mice

Injecting the bacterial cell wall component lipopolysaccharide (LPS) is commonly used as a model of inflammation and leads to classical symptoms of sickness (Hoogland et al. 2015). In our experimental model of inflammation, mice were injected intraperitoneally with a single LPS dose of 1.5 mg/kg body weight. The injections resulted in a moderate sickness behavior of the animals, consistent with the literature data (Terrando et al. 2010; Czapski et al. 2007; Dénes, Ferenczi, and Kovács 2011; Kozlowski and Weimer 2012; Henry et al. 2008). We evaluated the changes in the body weight of the mice 5 h (early phase of inflammation) and 30 h (late phase of inflammation) after LPS injection. Control animals were injected with similar volumes of sterile phosphate buffered saline (PBS). The body weight of the mice was clearly reduced after induction of inflammation. Figure 7Figure 7 illustrates the normalized body weight of the animals at different time points after the injections. In comparison to their weight before, the LPS-injected animals showed already 5 h after LPS injection a small but significant decrease of their weight, with a median value of 95.62 ± 3.30 % ($p= 0.004$, Wilcoxon signed-rank test). The body weight 30 h after the LPS injections decreased further to a median value of 87.88 ± 10.74 % ($p= 0.004$, Wilcoxon signed-rank test). In contrast, the body weight of the PBS-injected animals remained constant, with a median value of 99.02 ± 1.48 % 5 h after PBS injection ($p= 0.078$, Wilcoxon signed-rank test) and 98.46 ± 3.67 % 30 h after PBS ($p= 0.461$, Wilcoxon signed-rank test).

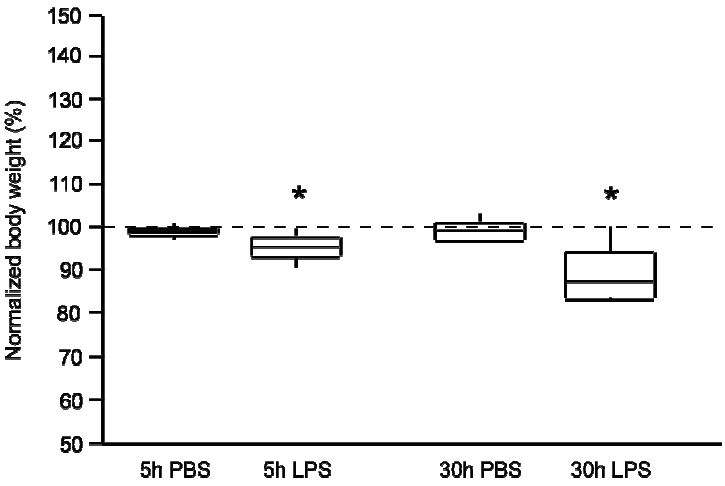

Figure 7 Slight but significant decrease of body weight in mice after induction of peripheral inflammation

Injection of 1.5 mg/kg BW LPS from E. coli (Serotype O111:B4) induced weight loss in 4-6 months old WT mice. Box plots showing the medians (per mouse) of normalized mouse body weight after PBS or LPS injection. LPS resulted in a slight but significant decrease of the mouse body weight 5 h after the injection (n= 10 mice, p= 0.004, Wilcoxon signed-rank test) and a further decrease 30 h after the LPS injection (n= 10 mice, p= 0.004, Wilcoxon signed-rank test). Similar volume injections of PBS showed no effect on the mouse body weight (5 h PBS: n= 10 mice, p= 0.078, Wilcoxon signed-rank test; 30 h PBS: n= 9 mice, p= 0.461, Wilcoxon signed-rank test).

3.1.2 Cytokine profile during a peripheral inflammation

Changes in cytokine levels in response to systemic inflammation with LPS were described in previous studies, but results were quite variable (Hoogland et al. 2015; Nava Catorce and Gevorkian 2016). To understand the inflammatory reaction in our experimental model, we evaluated the profiles of different inflammatory cytokines during the early and the late phase after induction of inflammation. The mice received an injection of either PBS or LPS and the cytokine concentrations in blood sera and brain samples were analyzed by means of ELISA.

3.1.2.1 Inflammation increases blood serum cytokine levels

There was a clear increase of the inflammatory cytokines IL-1β, TNF-α, IL-6, CCL2 and IL-10 in the blood serum 5 h after LPS injection when compared to PBS-injected controls (see Figure 8A and an overview of the concentrations in Table 2). 30 h after the LPS injection, all blood serum cytokine levels were lower. The levels of IL-1β and TNF-α reached a similar concentration as in the corresponding PBS-injected control animals. Only IL-6, CCL2 and IL-10 remained obviously higher compared to PBS controls.

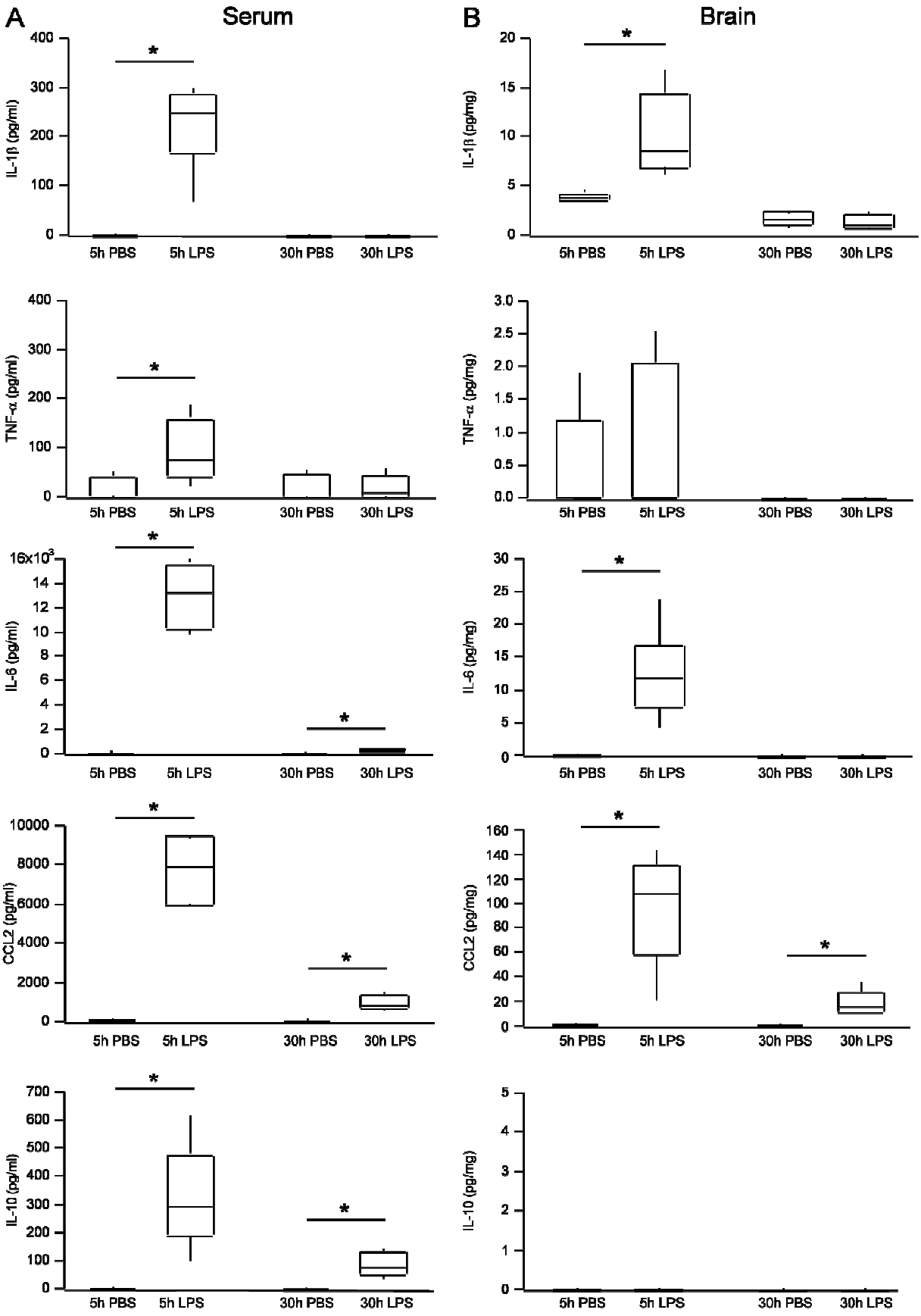
A
Serum
B
Brain
IL-1β (pg/ml)
IL-1β (pg/mg)
TNF-α (pg/ml)
TNF-α (pg/mg)
IL-6 (pg/ml)
IL-6 (pg/mg)
CCL2 (pg/ml)
CCL2 (pg/mg)
IL-10 (pg/ml)
IL-10 (pg/mg)
16x10³
5h PBS
5h LPS
30h PBS
30h LPS
*

Figure 8 Increase of cytokine concentrations during peripheral inflammation

(A) Box plots illustrating the levels (medians per mouse) of inflammatory cytokines measured by ELISA in blood serum samples of 4-6 months old WT mice. Note, a significant increase of all cytokines (IL-1β, TNF-α, IL-6, CCL2 and IL-10) in the blood serum 5 h after LPS injection. 30 h after LPS injection, only IL-6, CCL2, and IL-10 were significantly elevated. **(B)** Box plots illustrating the levels of inflammatory cytokines (medians per mouse) in cortical brain samples 5 h after LPS injection. There was a significant increase of IL-1β, IL-6 and CCL2, whereas the levels of TNF-α and IL-10 remained unchanged compared to PBS-injected controls. 30 h after the LPS injection only the level of CCL2 was significantly higher. The brain levels of IL-1β, TNF-α and IL-10 remained comparable to the PBS-injected controls. All significances were tested by Mann-Whitney test and accepted for p≤ 0.05. For exact p-values and numbers of experimental animals, see Table 2 and Table 3. (The experiments were performed with the help of Elizabeta Zirdum. Blood serum levels of CCL2, IL-6 and IL-10 were determined by the company microBIOMix GmbH).

Table 2 Summary of the blood serum cytokine concentrations

Cytokine concentrations (median ± IQR) in blood sera 5 h and 30 h after PBS or LPS injection.

Serum (pg/ml)	*5h PBS*	*N°*	*5h LPS*	*N°*	*p-value*	*30h PBS*	*N°*	*30h LPS*	*N°*	*p-value*
IL-1β	0 ± 0	6	248.59 ± 61.28	6	0.002 *	0 ± 0	5	0 ± 0	5	-
TNF-α	0 ± 27.92	5	76.23 ± 80.01	6	0.028 *	0 ± 37.09	5	8.759 ± 28.14	6	> 0.999
IL-6	14.75 ± 50.82	5	13250 ± 4500	5	0.036 *	0 ± 0	5	227 ± 178	5	0.008 *
CCL2	75.75 ± 10.6	5	7850 ± 1762.5	3	0.008 *	28.2 ± 18.8	5	792.5 ± 408.5	5	0.008 *
IL-10	0 ± 0	5	293.5 ± 60.5	5	0.008 *	0 ± 0	5	78.9 ± 55.95	5	0.008 *

All comparisons between the data sets were performed with Mann-Whitney test, *p≤ 0.05.
N°= number of experimental animals.

3.1.2.2 Inflammation increases brain cytokine levels

Similar to the blood serum samples, the cytokine concentrations in the brain increased during the early phase of inflammation (see Figure 8B and Table 3). 5 h after LPS injection, the brain levels of IL-1β, IL-6 and CCL2 were significantly higher compared to PBS-injected controls. The concentrations of TNF-α and IL-10 did not reach level of statistical significance and were probably too close to the detection limit. During the late phase of inflammation, most of the brain cytokine concentrations returned to their control levels. Only CCL2 remained elevated 30 h after LPS injection compared to 30 h after PBS injection.

Table 3 Summary of the brain cytokine concentrations

Cytokine concentrations (median ± IQR) in brain lysates 5 h and 30 h after PBS or LPS injection.

Brain (pg/mg)	*5h PBS*	*N°*	*5h LPS*	*N°*	*p-value*	*30h PBS*	*N°*	*30h LPS*	*N°*	*p-value*
IL-1β	3.82 ± 0.6	8	10.5 ± 4.77	8	0.001 *	2.28 ± 1.02	8	2.09 ± 5.65	8	> 0.999
TNF-α	0 ± 1.17	15	0 ± 2.02	15	0.302	0 ± 0	8	0 ± 0	10	-
IL-6	0 ± 0	10	11.78 ± 6.87	10	0.001 *	0 ± 0	10	0 ± 0	10	-
CCL2	1.29 ± 0.11	5	108.08 ± 22.02	5	0.008 *	1.01 ± 0.14	5	16.41 ± 5.39	5	0.008 *
IL-10	0 ± 0	5	0 ± 0	5	-	0 ± 0	5	0 ± 0	5	-

All comparisons between the data sets were performed with Mann-Whitney test, *p≤ 0.05.

N°= number of experimental animals.

Taken together, the ELISA analyses revealed a clear increase of different inflammatory cytokines in the blood serum and in the brain. This increase was observed mainly during the early phase of inflammation, 5 h after LPS injection.

3.2 Functional properties of microglia during a peripheral inflammation

Microglia are essential for the maintenance of normal brain homeostasis. Inflammatory stimuli cause microglia to switch to a reactive state. This switch is accompanied by cell changes, like an altered morphology (Kozlowski and Weimer 2012). The results described below show the reactions of microglia to a peripheral inflammation.

3.2.1 Inflammation changes microglial morphology

To investigate the *in vivo* reaction of microglia over time in response to the peripheral inflammatory stimulus, microglia from CX3CR1$^{GFP/+}$ mice were imaged longitudinally through a chronic cranial window. The mice were anesthetized and the same brain areas were repeatedly imaged over a total period of 72 h.

The induction of a peripheral inflammation with LPS resulted in obvious morphological changes of the cells, like retracted processes and altered soma size (compare Figure 9A PBS with Figure 9B LPS).

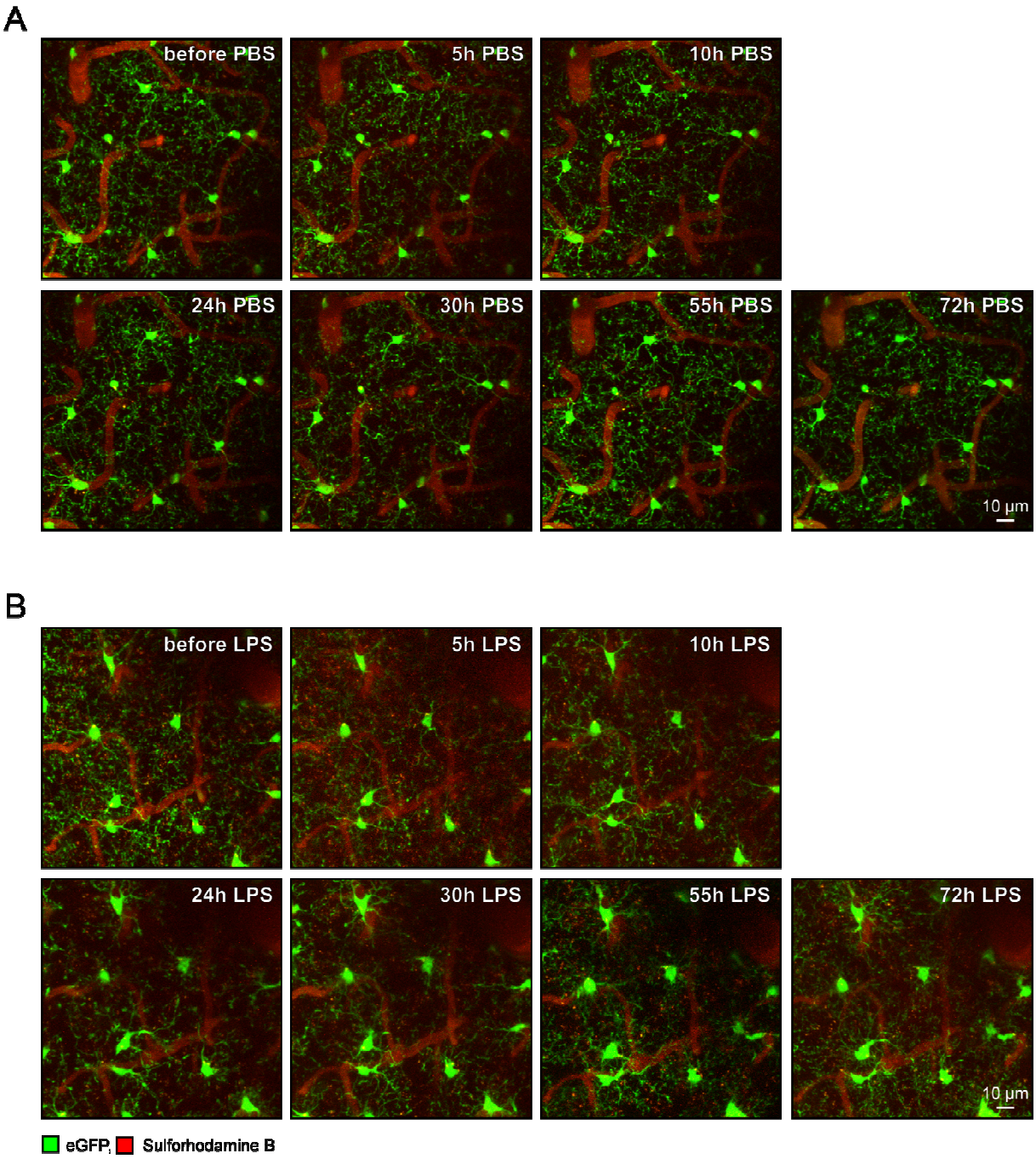

Figure 9 *In vivo* imaging of the microglial morphology over time during peripheral inflammation

Maximum intensity projection (MIP) images (50-100 µm below the cortical surface) from the motor cortex of 5 months old CX3CR1$^{GFP/+}$ mice. Microglial eGFP is visualized in green and blood vessels (in red) are stained by i.p. injections of sulforhodamine B **(A)** Microglial morphology during control condition and at different time points after PBS injection. **(B)** Microglial morphology before and at different time points after LPS injection.

To evaluate the changes of microglia over time, the microglial soma volumes were determined at each time point and normalized to the initial control measurement (Figure 10). Figure 10A shows the normalized microglial soma volume at different time points after PBS injection. PBS-injected animals showed no visible alteration in soma volumes compared to their control measurement, tested with repeated measures ANOVA ($p= 0.229$, Friedman`s test). The comparison of the soma volumes before and 30 h after PBS injection in cumulative histograms supported this conclusion (Figure 10C). In contrast, a repeated measures ANOVA in the LPS-injected animals revealed significant volume changes in microglia after LPS injection if compared to control measurement (Figure 10B, $p= 0.003$, Friedman`s test), but no significance after the post-hoc Dunn's multiple comparisons test ($p> 0.05$). Nevertheless, 30-55 h after LPS injection, there was a clear trend towards an increased cell body volume. This result was supported by the cumulative histograms in Figure 10D, showing the comparison of the soma volumes before and 30 h after LPS injection. During the initial phase of inflammation 5-10 h after LPS injection, we observed a tendency to a soma volume decrease in microglia. This, however, might be an analysis artifact caused by a regularly observed reduction of cell visibility at these time points.

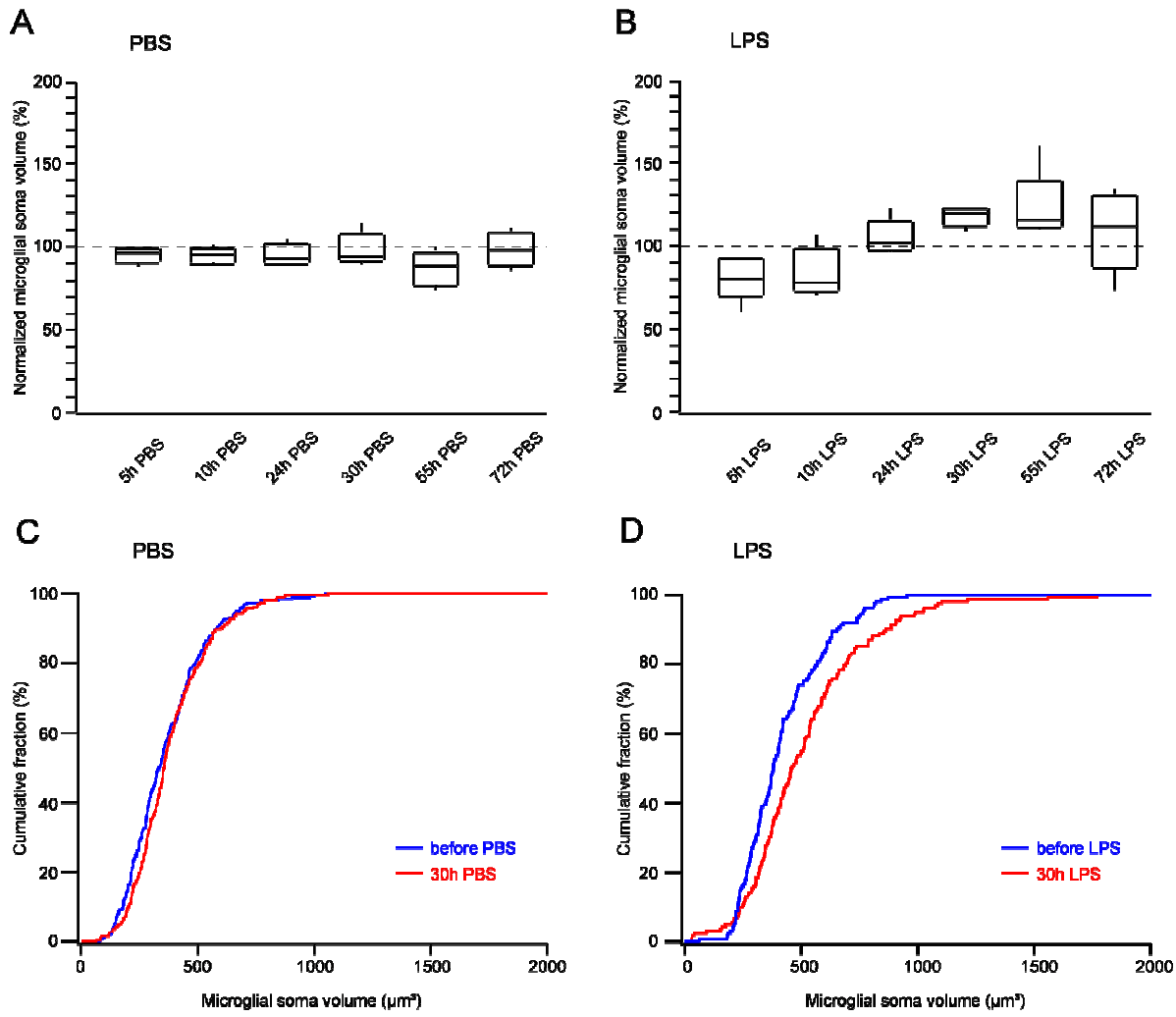

Figure 10 Trend towards increased microglial soma volumes during peripheral inflammation *in vivo*

Quantification of the soma volumes of microglia in the motor cortex of 4-6 months old CX3CR1$^{GFP/+}$ mice (n= 2-6 areas per mouse in 5 mice per group). **(A)** and **(B)** Box plots illustrating the medians (per mouse) of normalized microglial soma volumes plotted as a function of time after PBS (A) or LPS (B) injection. In PBS-injected mice, there was no significant change of the soma volumes after testing with repeated measures ANOVA (p= 0.229, Friedman`s test). LPS injection resulted in a significant volume change of microglia (p= 0.003, Friedman`s test), whereas the post-hoc Dunn's multiple comparisons test revealed no statistical significance (p> 0.05). **(C)** and **(D)** Cumulative histograms of microglial soma volumes before and 30 h after either PBS (C) or LPS (D) injection. Note, no visible changes after PBS injection, however, clearly increased soma volumes 30 h after LPS injection.

In addition to the evaluation of the time course of the morphological changes *in vivo*, we analyzed the morphology of microglia in brain slices *in vitro*. To this end, 4-6 months old WT mice were injected either with PBS or LPS and decapitated 5 h or 30 h after the injections. Then, the brains were fixed and slices of the brains stained with the microglia-specific Iba1 antibody. Figure 11A shows examples of Iba1-stained

microglia from brains fixed 5 h and 30 h after the PBS and LPS injections. In accordance with the *in vivo* results, microglial morphologies in brains fixed 30 h after LPS injection were clearly different compared to brains fixed 30 h after PBS injection. The box plots in Figure 11B display the microglial soma volume change 5 h and 30 h after PBS or LPS injection. The analysis revealed a significant change of the soma volumes ($p= 0.006$, Kruskal-Wallis test). The post-hoc Dunn's multiple comparisons test indicated no significant increase of the volumes 5 h after LPS injection compared to 5 h after PBS injection and 30 h after LPS compared to 30 h after PBS ($p> 0.05$). However, in comparison to the early phase, the soma volumes changed during the late phase significantly (5 h PBS versus 30 h LPS, $p< 0.05$ and 5 h LPS versus 30 h LPS, $p< 0.05$, Dunn's multiple comparisons test). Cumulative histograms of the cell volumes either 5 h (C) or 30 h (D) after PBS and LPS injection are shown in Figure 11C and D. As indicated in the figure, we encountered a significant increase of the cell volumes 30 h after LPS injection (30 h PBS versus 30 h LPS, $p< 0.001$, Kolmogorov-Smirnov test).

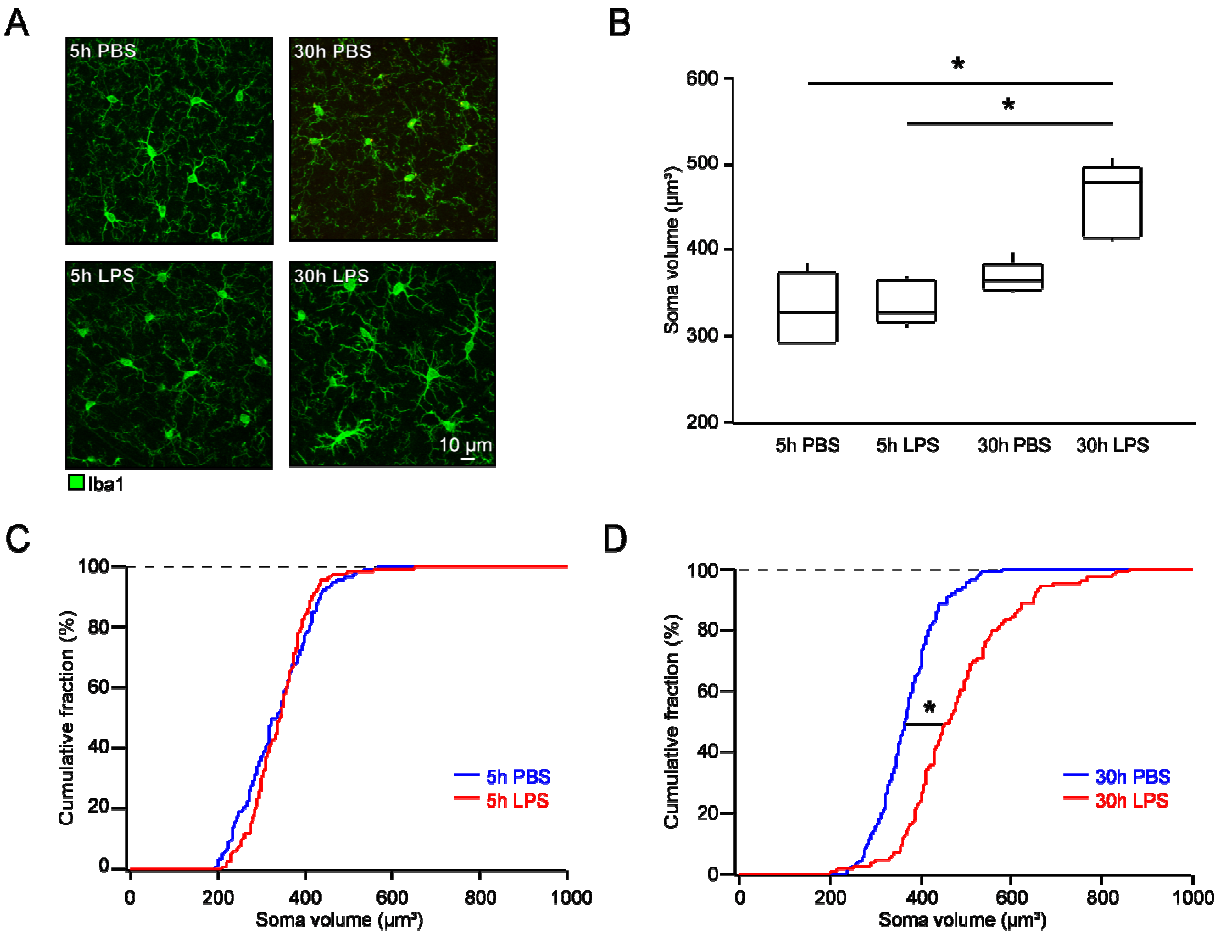

Figure 11 *In vitro* analyses reveal a significant increase in the microglial soma volumes during peripheral inflammation

Immunohistochemical analyses of microglial soma volumes in fixed cortical slices obtained from 4-6 months old WT mice at different time points after PBS or LPS injection. **(A)** Representative MIP images (25 µm depth) of Iba1-stained microglia 5 h and 30 h after PBS or LPS injection. **(B)** Box plots showing the medians (per mouse) of microglial soma volumes 5 h and 30 h after PBS or LPS injection (n= 6-10 areas per mouse in 5 mice per group). Note, a significant difference in the microglial soma volumes between the groups (p= 0.006, Kruskal-Wallis test). There was a significant volume increase 30 h after the LPS injection when compared to 5 h after PBS or LPS injection (p< 0.05, Dunn's multiple comparisons test). Comparison of the volumes between the early time points (5 h PBS and 5 h LPS) and between the late time points (30 h PBS and 30 h LPS) revealed no significant changes (p> 0.05 Dunn's multiple comparisons test). **(C)** and **(D)** Cumulative histograms of microglial soma volumes in brains fixed 5 h (C) or 30 h (D) after PBS and LPS injection. Note, a significant soma volume increase in microglia 30 h after LPS injection when compared to 30 h after PBS injection (p< 0.001, Kolmogorov-Smirnov test), but not 5 h after LPS injection when compared to 5 h PBS control (p= 0.198, Kolmogorov-Smirnov test).

3.2.2 Inflammation affects microglial proliferation

Under normal, healthy conditions, each microglial cell occupies an individual brain domain, with a mean soma-to-soma distance of 40 µm. With 0.05 %-0.69 % of dividing cells per day, the proliferation rate of "resting" microglia is low (Askew et al. 2017). However, pathological circumstances can induce proliferation of the cells. A typical cell cycle length of dividing cells takes around 24-32 h. Accordingly, during the first 24 h after proliferation, two sister microglial cells are located close to each other (Askew et al. 2017). Thus, the distance between the two cells can serve as an indicator of the proliferative state of microglia, whereby cells in close proximity to each other are likely to have recently passed the process of cell division.

To investigate the microglial proliferation during inflammation, we counted the number of cell doublets (cells with a soma-to-soma distance < 20 µm) per volume of imaged brain area at different time points after PBS and LPS injection.

Figure 12A shows a representative image of two microglial cell doublets (indicated by arrowheads). The box plots in Figure 12B and C illustrate the normalized microglial doublet numbers at different time points after PBS or LPS injection (normalized to the initial control measurement). Whereas the doublet numbers under PBS remained constant (Figure 12B, p= 0.299, Friedman`s test), there was an obvious increase under LPS, which, however, did not reach statistical significance (Figure 12C,

p= 0.065, Friedman`s test). This might be due to the high variability of the doublet numbers in the individual mice. Nevertheless, this indicates an at least moderate increase of microglial proliferation. In accordance with the trend towards increased cell doublets after LPS injection, there was a significant change in the density of microglia after LPS injection (Figure 12E, p= 0.020, Friedman`s test). 55 h after LPS injection, there seemed to be a trend towards increased numbers, however, it did not reach statistical significance (p> 0.05, Dunn`s multiple comparisons test). In contrast, testing the microglial density in the PBS-injected mice resulted in no significant change of the microglial density (Figure 12D, p= 0.070, Friedman`s test).

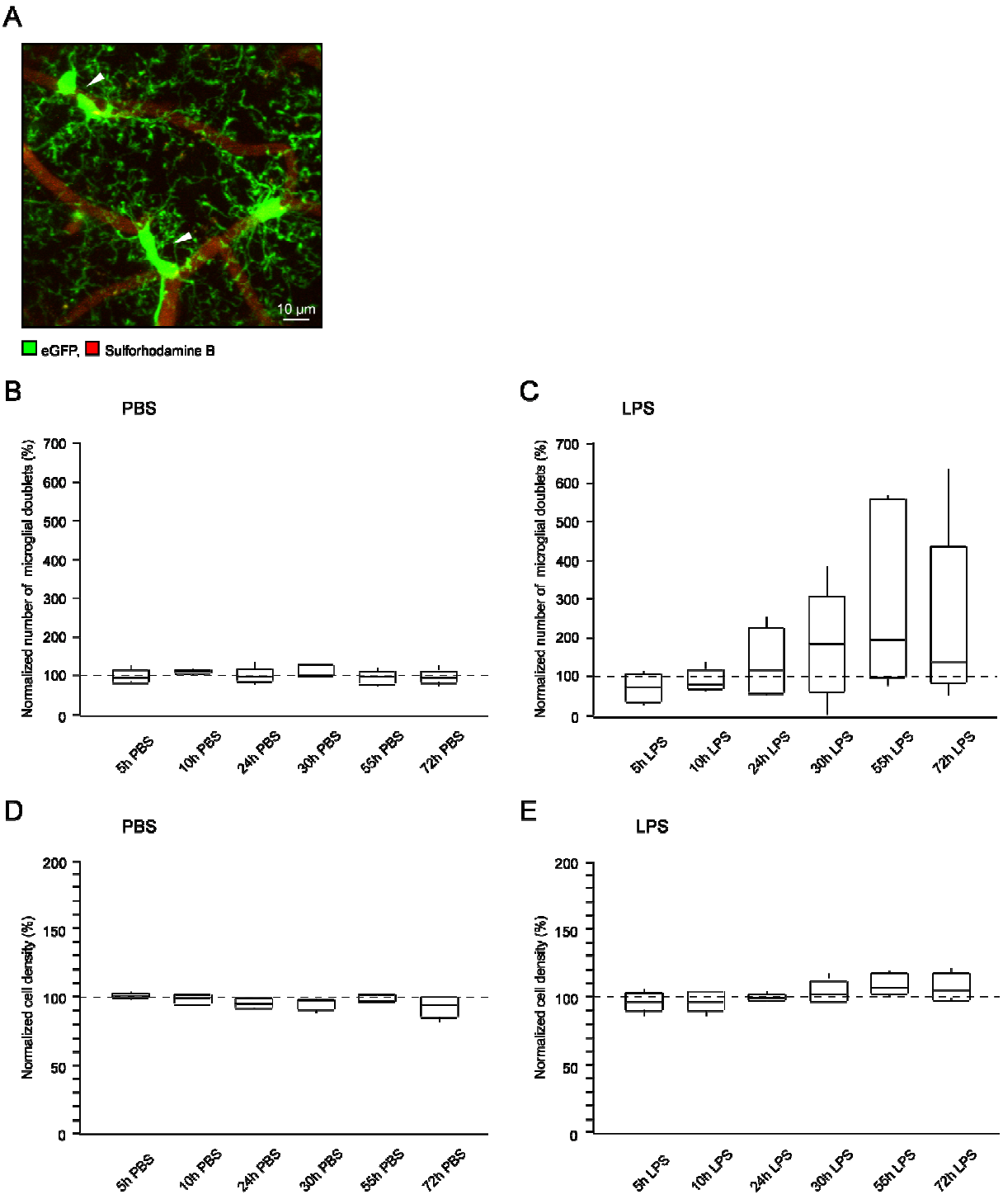

Figure 12 Trend towards increased microglial proliferation during peripheral inflammation

Quantifications of the number of microglial doublets and cell densities in the motor cortex of 4-6 months old CX3CR1$^{GFP/+}$ mice (n= 2-6 areas per mouse in 5 mice per group). **(A)** Representative MIP image (60-110 µm below the cortical surface) of two microglial cell doublets (indicated by white arrowheads). **(B)** and **(C)** Box plots illustrating the medians (per mouse) of normalized microglial soma volumes plotted as a function of time after PBS (B) or LPS (C) injection. Number of doublets at the given time points were normalized to the number of doublets before PBS or LPS injection. There was no significant change in the number of microglial doublets after PBS injection (p= 0.299, Friedman`s test). However, note, a clear trend towards increased doublet numbers after

LPS injection (p= 0.065, Friedman`s test). **(D)** and **(E)** Box plots showing the medians (per mouse) of normalized microglial cell density plotted against the time after PBS (D) and LPS (E) injection. Densities at the given time points were normalized to the cell density before PBS or LPS injection. There was no change in microglial density after injection of PBS (p= 0.070, Friedman`s test). LPS injection resulted in a significant change of microglial cell density (p= 0.029, Friedman`s test), however, with no significant effect after the post-hoc Dunn`s multiple comparisons test (p> 0.05).

In summary, we observed changes in the morphology of microglia with an increase in the cell somata, a clear trend towards an increased microglial proliferation rate and a higher overall cell density. These changes occurred mainly during the late phase of the peripheral inflammation, starting from 30-55 h after the LPS injection.

3.2.3 Inflammation leads to microglial hyperactivity

Apart from morphological changes, microglia can react to pathological conditions with a change in their Ca^{2+}-signaling (Brawek and Garaschuk 2013). The following set of experiments was performed to investigate, if and how the microglial Ca^{2+}-signaling is altered during peripheral inflammation. After electroporation of the cells with the Ca^{2+}-sensitive dye Oregon Green BAPTA-1(OGB-1), we determined the fraction of active microglia, showing spontaneous Ca^{2+}-transients in the course of a 15 min long recording period. We measured cells under control conditions (5 h after PBS injection) as well as during the early (5 h after LPS injection) and the late phase (30 h after LPS injection) of inflammation.

Figure 13 shows a representative electroporated microglia (A) with its corresponding spontaneous Ca^{2+}-transients (B). Peripheral inflammation induced a clear increase of the Ca^{2+}-signaling in microglia. In PBS-injected control mice, only a small fraction of 14 % of cells showed spontaneous Ca^{2+}-transients. In contrast, 5 h after LPS injection, the incidence of Ca^{2+}-transients increased significantly and reached a fraction of 79 % of active cells (Figure 13C, 5 h PBS versus 5 h LPS, p= 0.001, Fisher`s exact test). 30 h after LPS injection, the fraction of active cells was 43 %, thus, reaching an intermediate level between the active cell fractions 5 h after PBS (14 %) and 5 h after LPS (79 %) (Figure 13C, 5 h PBS versus 30 h LPS, p= 0.111 and 5 h LPS versus 30 h LPS, p= 0.120, Fisher`s exact test).

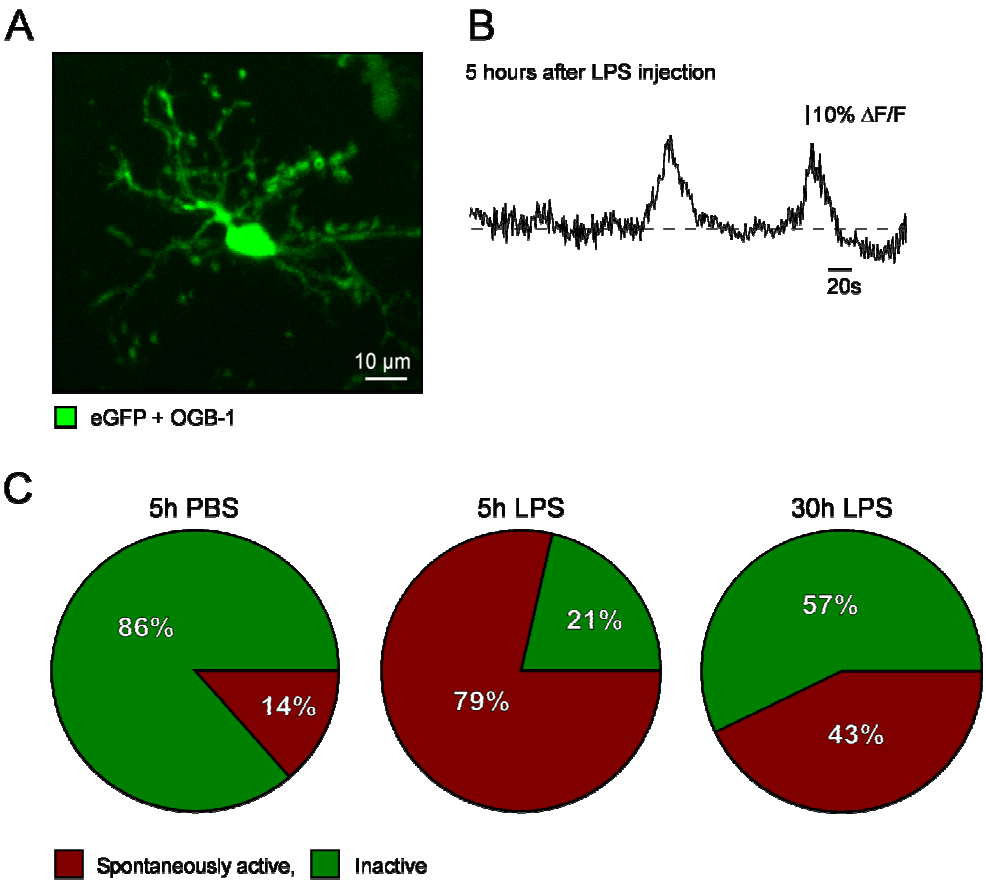

Figure 13 Increase in microglial Ca^{2+}-signaling during peripheral inflammation

(A) MIP image (112-139 µm below the cortical surface) of a microglia in the motor cortex of a 5 months old $Iba1^{GFP/+}$ mouse, filled with the Ca^{2+}-sensitive dye OGB-1 by means of single cell electroporation. **(B)** Spontaneous Ca^{2+}-transients recorded from the cell shown in (A). ΔF/F represents the normalized change in fluorescence. **(C)** Pie charts illustrating the fraction of spontaneously active (red) and inactive (green) microglia after PBS injection and at different time points after LPS injection. The fractions of active/inactive cells were measured in 5 mice per group: with n= 22 cells for 5 h PBS, n= 14 cells for 5 h LPS and n= 14 cells for 30 h LPS. Note, a significant difference in the fractions of active/inactive cells 5 h after LPS injection compared to that 5 h after PBS injection (p= 0.001, Fisher's exact test), with a higher fraction of active cells. Comparing the fractions 30 h after LPS injection with the fraction 5 h after PBS or LPS injection revealed no significant difference (30 h LPS vs. 5 h PBS: p = 0.120; 30 h LPS vs. 5 h LPS: p = 0.111; Fisher's exact test). (This set of experiments was performed by Dr. Bianca Brawek).

3.2.4 Cytokine profiles of $NLRP3^{-/-}$ and $TNF\text{-}\alpha^{-/-}$ mice during a peripheral inflammation

To decipher mechanisms that contribute to the increase of the spontaneous Ca^{2+}-signaling during inflammation, we investigated the role of the proinflammatory cytokines IL-1β and TNF-α. To this end, we took advantage of NLRP3 ($NLRP3^{-/-}$) and TNF-α ($TNF\text{-}\alpha^{-/-}$) knock-out mice.

First, we evaluated the changes in cytokine profiles of these mice in response to either PBS or LPS injections. We determined the cytokine profiles in the blood serum and in the brain via ELISA and observed in both knock-out stains (NLRP3$^{-/-}$ and TNF-α$^{-/-}$) a similar time course of the cytokine expression during inflammation as in WT animals. The concentration of inflammatory cytokines was high during the early phase of inflammation and lower during the late phase (time course data not shown).

3.2.4.1 Cytokine profile of NLRP3$^{-/-}$ mice during the early phase of peripheral inflammation

Next, we directly compared the cytokine expression of NLRP3$^{-/-}$ mice with the respective data obtained in WT animals 5 h after LPS injection (see Figure 14 and an overview of the concentrations in Table 4).

Compared to WT mice, the NLRP3$^{-/-}$ mice showed significantly reduced levels of IL-1β in the blood serum ($p= 0.01$, Mann-Whitney test). Further, we observed a clear trend towards lower IL-1β levels in the brain homogenates of these mice ($p= 0.065$, Mann Whitney test) (Figure 14A, Table 4). Interestingly, compared to WT animals the NLRP3$^{-/-}$ mice showed significantly increased blood serum levels of TNF-α protein ($p= 0.03$, Mann-Whitney test) (Figure 14B, Table 4). However, the brain levels of TNF-α were not detectable in NLRP3$^{-/-}$ mice and comparably low in WT animals ($p= 0.123$, Mann-Whitney test). The brain levels of IL-6 were significantly lower in the NLRP3$^{-/-}$ mice ($p= 0.008$, Mann-Whitney test). The brain levels of CCL2 showed a visible tendency to lower levels ($p= 0.31$, Mann-Whitney test), but this tendency remained below statistical significance when compared to WT animals (Figure 14B, Table 4). The cytokine IL-10 could neither be detected in brains of NLRP3$^{-/-}$ mice, nor in brains of WT mice (plot not shown, see Table 4).

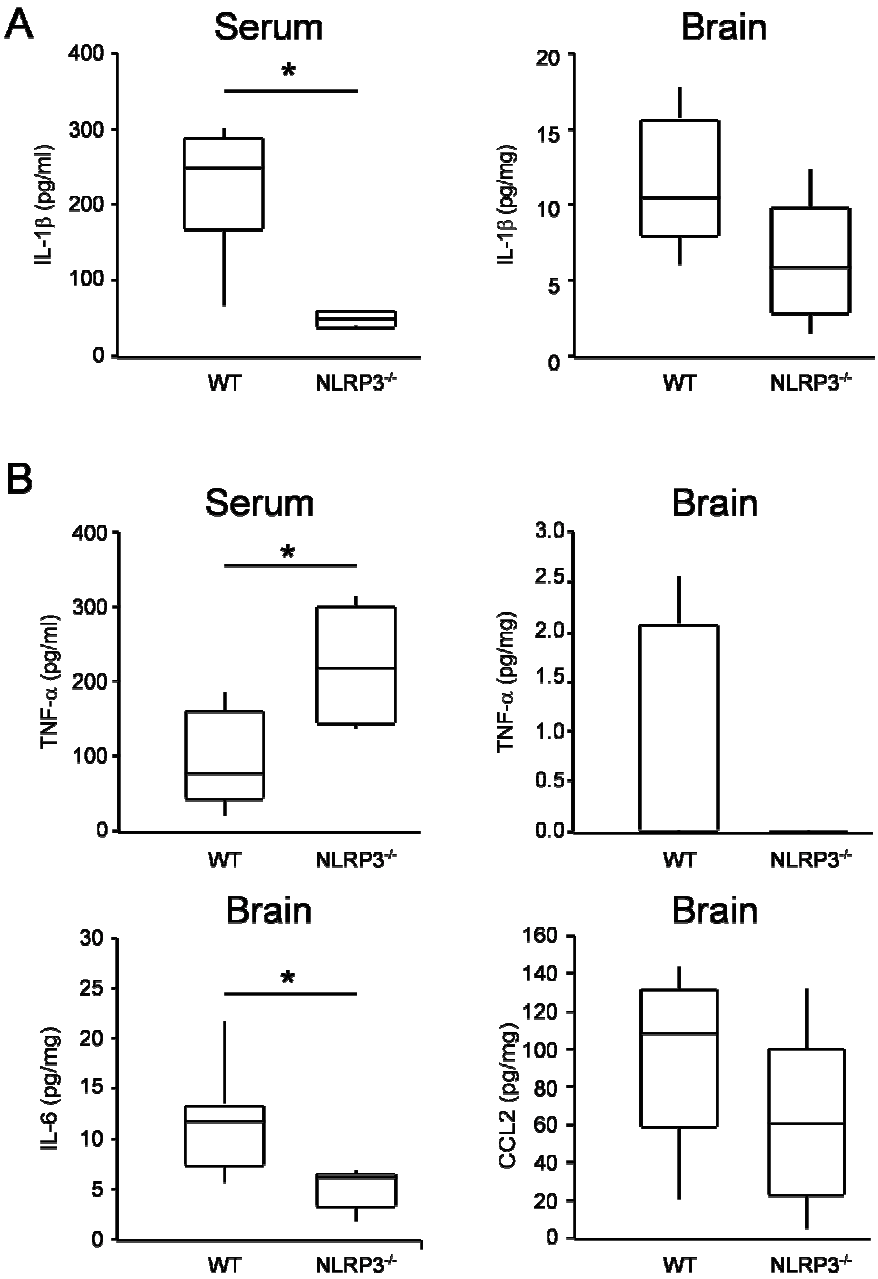

Figure 14 NLRP3$^{-/-}$ mice show a different cytokine profile during early phase of peripheral inflammation

Comparison of inflammatory cytokines levels 5 h after LPS injection in blood serum and brain samples of 4-6 months old WT and NLRP3$^{-/-}$ mice. **(A)** Box plots showing the comparison of IL-1β levels (medians per mouse) in the blood serum and the brain. Note, a significant decrease of IL-1β expression in the blood serum of NLRP3$^{-/-}$ mice and a trend towards reduced IL-1β levels in the brain. **(B)** Box plots showing the comparison of different cytokine levels (medians per mouse) in the blood serum (TNF-α) and in the brain (TNF-α, IL-6, and CCL2) of WT and NLRP3$^{-/-}$ mice. NLRP3$^{-/-}$ mice showed significantly increased blood serum levels of TNF-α when compared to WT mice. There were no detectable levels of TNF-α in the brain of NLRP3$^{-/-}$ mice and the levels in WT mice were comparably low. The brain levels of IL-6 in NLRP3$^{-/-}$ mice were significantly lower than in WT mice and there was a visible, but not significant tendency to lower levels of CCL2. The cytokine IL-10 was in both mouse strains not detectable in the brain (plot not shown). Statistic analyses were performed using Mann-Whitney test. Data were considered significantly different when $p \leq 0.05$. For exact p-values and numbers of experimental animals, see Table 4. (The experiments were performed with the help of Elizabeta Zirdum).

Table 4 Summary of the cytokine concentrations in WT and NLRP3$^{-/-}$ mice

Comparison of cytokine concentrations (median ± IQR) in the blood serum and in the brain of WT and NLRP3$^{-/-}$ mice 5 h after LPS injection.

Serum (pg/ml)	*WT 5h LPS*	*N°*	*NLRP3$^{-/-}$ 5h LPS*	*N°*	*p-value*	*Brain (pg/mg)*	*WT 5h LPS*	*N°*	*NLRP3$^{-/-}$ 5h LPS*	*N°*	*p-value*
IL-1β	248.59 ± 61.28	6	50.17 ± 18.76	4	0.01 *	**IL-1β**	10.5 ± 4.77	8	5.89 ± 3.08	5	0.065
TNF-α	76.23 ± 80.01	6	218.03 ± 134.26	5	0.03 *	**TNF-α**	0 ± 2.02	15	0 ± 0	5	0.123
						IL-6	11.78 ± 6.87	5	6.12 ± 1.57	5	0.008 *
						CCL2	108.08 ± 22.02	5	60.47 ± 26.75	5	0.31
						IL-10	0 ± 0	5	0 ± 0	5	-

All comparisons between the data sets were performed with Mann-Whitney test, *p≤ 0.05.

N°= number of experimental animals.

3.2.4.2 Cytokine profile of TNF-α$^{-/-}$ mice during the early phase of peripheral inflammation

In Figure 15 and Table 5, we compared the cytokine levels in TNF-α$^{-/-}$ mice with that observed in WT mice. Figure 15A shows box plots the TNF-α protein concentrations in blood serum and brain samples 5 h after LPS injection. In the brain of TNF-α$^{-/-}$ mice, no TNF-α protein was detected and thus, the TNF-α expression was significantly lower than in WT animals (p= 0.045, Mann-Whitney test). However, in four out of eight tested TNF-α$^{-/-}$ animals, the ELISA analysis reported measurable, although compared to WT animals clearly reduced levels of TNF-α protein in the blood serum (see Figure 15A and Table 5). Further, we found a significant reduction of IL-1β protein in the blood serum samples of TNF-α$^{-/-}$ mice compared to blood serum samples of WT animals (p= 0.014, Mann-Whitney test). Evaluation of the brain levels revealed a significant reduction of CCL2 in TNF-α$^{-/-}$ mice (p= 0.016, Mann-Whitney test) and apparently reduced levels of IL-1β and IL-6. Similar to the WT and NLRP3$^{-/-}$ mice, IL-10 was not detectable in the brains of TNF-α$^{-/-}$ mice (plot not shown, see Table 5).

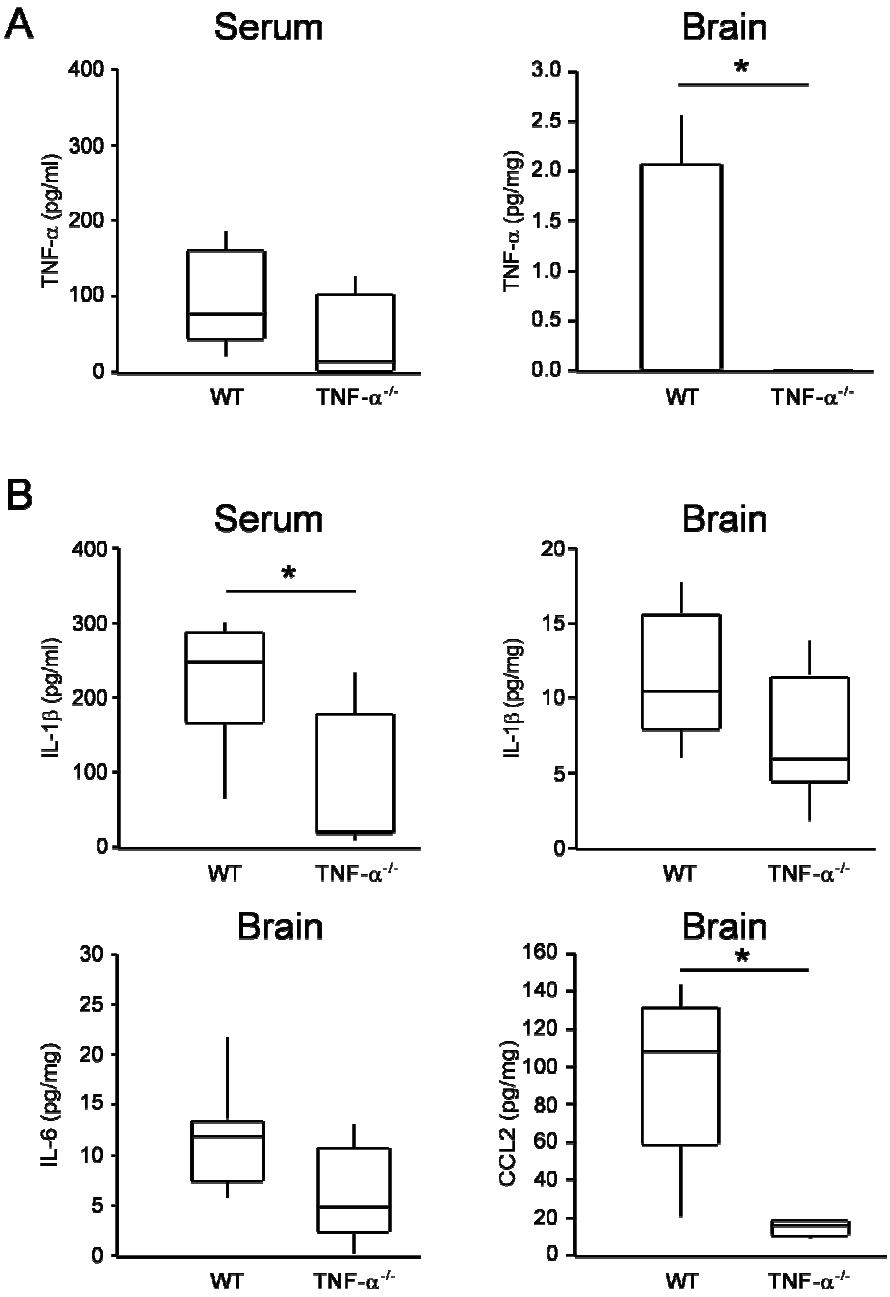

Figure 15 TNF-α$^{-/-}$ mice show a different cytokine profile during early phase of peripheral inflammation

Comparison of inflammatory cytokines levels 5 h after LPS injection in blood serum and brain samples of 4-6 months old WT and TNF-α$^{-/-}$ mice. **(A)** Box plots showing the comparison of TNF-α levels (medians per mouse) in blood serum and brain samples. The blood serum levels of TNF-α protein in TNF-α$^{-/-}$ mice appeared reduced compared to WT mice, but the effect was below statistical significance. In the brain, however, the TNF-α expression was significantly lower, compared to the expression in WT mice. **(B)** Box plots illustrating the blood serum levels of IL-1β and different brain cytokine levels (IL-1β, IL-6, and CCL2) in WT and TNF-α$^{-/-}$ mice. Note, significantly lower IL-1β levels in the blood serum of TNF-α$^{-/-}$ mice when compared to blood serum of WT animals. There was a slight but not significant reduction of IL-1β and IL-6 in the brain of TNF-α$^{-/-}$ mice and a significantly lower level of CCL2. The cytokine IL-10 was not detectable in the brain of both mouse strains (plot not shown). Statistic analyses were performed using Mann-Whitney test, data were considered significantly different when $p \leq 0.05$. For exact p-values and numbers of experimental animals, see Table 5. (Experiments were performed together with Elizabeta Zirdum).

Table 5 Summary of the cytokine concentrations in WT and TNF-α$^{-/-}$ mice

Comparison of cytokine concentrations (median ± IQR) in the blood serum and in the brain of WT and TNF-α$^{-/-}$ mice 5 h after LPS injection.

Serum (pg/ml)	*WT 5h LPS*	*N°*	*TNF-α$^{-/-}$ 5h LPS*	*N°*	*p-value*	*Brain (pg/mg)*	*WT 5h LPS*	*N°*	*TNF-α$^{-/-}$ 5h LPS*	*N°*	*p-value*
TNF-α	76.23 ± 80.01	6	13.42 ± 101.07	8	0.162	**TNF-α**	0 ± 2.02	15	0 ± 0	8	0.045*
IL-1β	248.59 ± 61.28	6	22.27 ± 113.69	7	0.014 *	**IL-1β**	10.5 ± 4.77	8	5.97 ± 2.19	7	0.142
						IL-6	11.78 ± 6.87	5	4.75 ± 3.86	5	0.129
						CCL2	108.08 ± 22.02	5	15.46 ± 2.86	4	0.016 *
						IL-10	0 ± 0	4	0 ± 0	4	-

All comparisons between the data sets were performed with Mann-Whitney test, *p≤ 0.05.

N°= number of experimental animals.

3.2.5 Effects of inflammation on microglial Ca^{2+}-signaling in NLRP3$^{-/-}$ and TNF-α$^{-/-}$ mice

After determination of the cytokine levels, we asked how the hyperactivity of microglia is influenced by the NLRP3 inflammasome and TNF-α. To address this question, we injected NLRP3$^{-/-}$ and TNF-α$^{-/-}$ mice with LPS, filled the microglial cells of these mice with the Ca^{2+}-sensor OGB-1 by means of electroporation, and evaluated the fractions of active and inactive cells 5 h after induction of inflammation (Figure 16).

The fraction of cells with spontaneous Ca^{2+}-transients in NLRP3$^{-/-}$ mice was strongly reduced compared to the fraction in control Iba1$^{GFP/+}$ mice. We measured a significant reduction from 79 % of active cells in Iba1$^{GFP/+}$ mice to only 25 % of active cells in the NLRP3$^{-/-}$ mice (p= 0.005, Fisher`s exact test). Further, the fraction of active and inactive cells in NLRP3$^{-/-}$ mice did not differ from the fractions of PBS-injected Iba1$^{GFP/+}$ mice (p= 0.445, Fisher`s exact test).

The influence of TNF-α on the microglial hyperactivity during inflammation was evaluated in TNF-α$^{-/-}$ mice. The fraction of active and inactive cells in LPS-injected TNF-α$^{-/-}$ mice was hereby significantly different from the fractions in PBS-injected Iba1$^{GFP/+}$ mice, with a higher fraction of active cells (p= 0.018, Fisher`s exact test). The fraction of spontaneously active cells decreased from 79 % in LPS-injected Iba1$^{GFP/+}$ mice to only 47 % in the TNF-α$^{-/-}$ mice. However, this effect did not reach the level of statistical significance (p= 0.147, Fisher`s exact test).

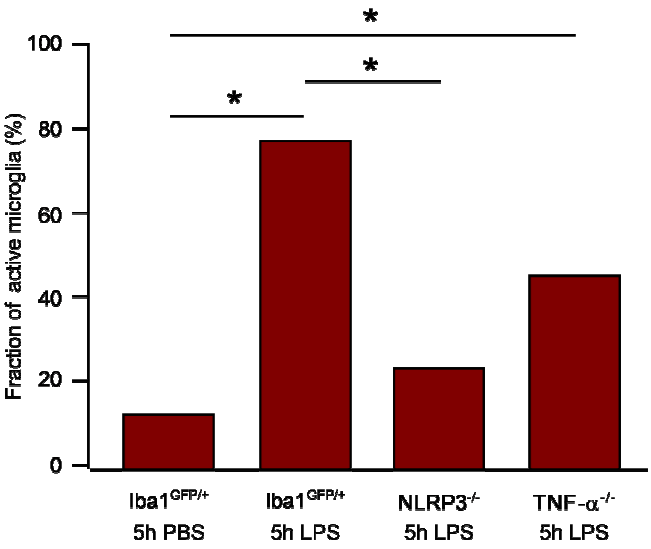

Figure 16 Influence of the NLRP3 inflammasome and TNF-α on inflammation-induced microglial Ca^{2+}-signaling

Bar graphs comparing the fraction of spontaneously active microglia in 4-6 months old Iba1$^{GFP/+}$, NLRP3$^{-/-}$, and TNF-α$^{-/-}$ mice 5 h after PBS or LPS injection. The fractions of active and inactive cells in Iba1$^{GFP/+}$ mice were significantly different 5 h after LPS injection when compared to the fractions 5 h after PBS injection (p= 0.001, Fisher`s exact test, same data set as in Figure 13). When comparing NLRP3$^{-/-}$ mice with Iba1$^{GFP/+}$ mice 5 h after LPS injection, there was a significant difference in the cell fractions (p= 0.005, Fisher`s exact test) with a clear decrease in the fraction of active cells in the NLRP3$^{-/-}$ mice. The signaling of microglia from NLRP3$^{-/-}$ mice resembled the signaling of PBS-injected mice (p= 0.445, Fisher`s exact test). Comparing the cell fractions of TNF-α$^{-/-}$ mice and Iba1$^{GFP/+}$ mice 5 h after LPS injection, revealed a decrease of the active cell fraction in TNF-α$^{-/-}$ mice, however, this effect was below the level of statistical significance (p= 0.147, Fisher's exact test). In comparison to PBS-injected Iba1$^{GFP/+}$ mice, the fractions of active cells in LPS-injected TNF-α$^{-/-}$ mice were significantly increased (p= 0.018, Fisher's exact test). We measured the cell fractions of Iba1$^{GFP/+}$ mice in 5 mice per group: with n= 22 cells for 5 h PBS and n= 14 cells for 5 h LPS. The fractions of NLRP3$^{-/-}$ mice were measured in 5 mice with n= 20 cells and the fractions of TNF-α$^{-/-}$ mice in 6 mice and n= 18 cells. (These experiments were performed by Dr. Bianca Brawek).

Taken together, these data identified a clear role of the NLRP3 inflammasome for the inflammation-induced microglial Ca^{2+}-signaling.

3.2.6 Expression of activation markers in microglia during a peripheral inflammation

3.2.6.1 Inflammation increases expression of microglial IL-1β

IL-1β is considered as one of the major inflammatory proteins. Within the brain, it is mainly produced by microglial cells (Pinteaux et al. 2002). To investigate the time course of the cortical IL-1β production under inflammatory conditions, we analyzed

the cortical expression of microglial marker Iba1 and the cytokine IL-1β at different time points after PBS or LPS injection by means of immunohistochemistry.

Figure 17A shows representative images of microglia and their IL-1β expression in control (PBS injections), during the early, and during the late phase of peripheral inflammation (LPS injections). In contrast to PBS controls, which were completely devoid of IL-1β positive cells, many IL-1β-positive microglial cells were found in LPS-injected animals, both 5 h, and 30 h after the LPS injection. To evaluate the cytokine production, we calculated the fractions of positive cells at the different time points after the injections (Figure 17B). A comparison of the 4 fractions revealed a significant difference in the expression of IL-1β (p= 0.001, Kruskal-Wallis test). When compared pair-wise in a post-hoc test, 5 h after LPS injection, microglia showed a visible increase in production of IL-1β, whereby the fraction of positive cells stayed below statistical significance when compared to PBS-injected controls (p= 0.144, Dunn`s multiple comparisons test). However, 30 h after LPS injection, the fraction of IL-1β positive cells was significantly increased when compared to 30 h after PBS injection (p= 0.008, Dunn`s multiple comparisons test). Notably, the fraction of IL-1β positive cells was not significantly different 5 h after LPS compared to 30 h after LPS injection (p= 1, Dunn`s multiple comparisons test).

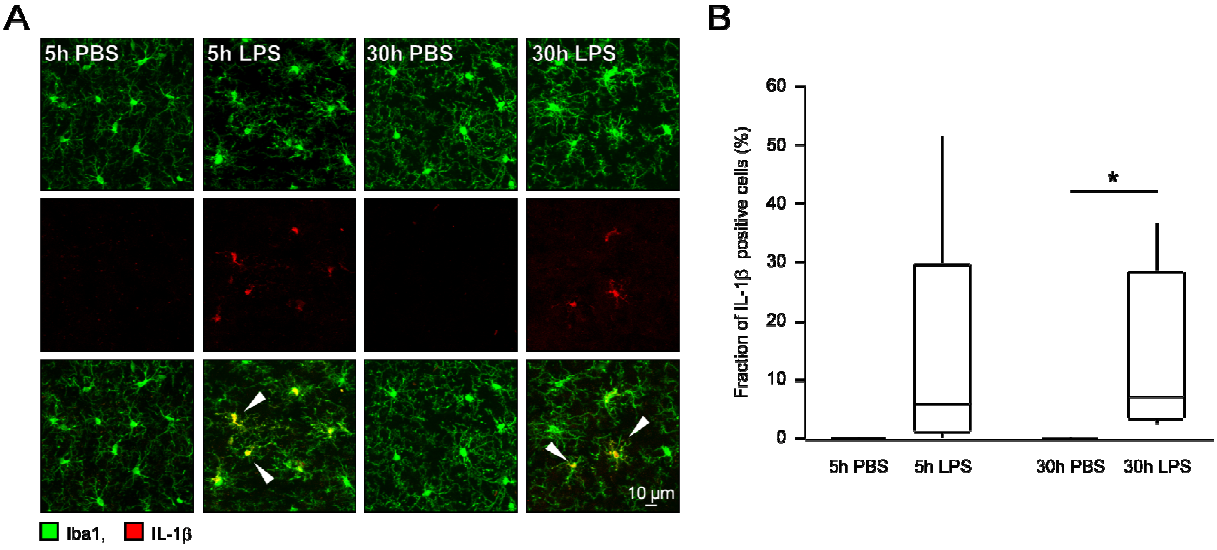

Figure 17 Increase in microglial IL-1β expression during peripheral inflammation

(A) MIP images (25 µm depths) of microglial cells labeled with anti-Iba1 and anti-IL-1β antibodies in the cortex of 4-6 months old WT mice at different time points after PBS or LPS injection. Arrowheads point to IL-1β positive microglia, which were only detected in LPS-injected mice **(B)** Box plots showing the medians

(per mouse) fractions of IL-1β positive cells 5 h and 30 h after PBS or LPS injection (n= 15 analyzed areas per mouse in 5 mice per group). Note, a significant change in the fraction of IL-1β positive cells during peripheral inflammation (p= 0.001, Kruskal-Wallis test). The Dunn`s multiple comparisons test revealed no significant difference in the IL-1β expression between 5 h PBS and 5 h LPS (p= 0.144) and a significant increase in the fraction of IL-1β positive microglia 30 h after LPS compared to 30 h after PBS (p= 0.008, Dunn`s multiple comparisons test). Comparing 5 h and 30 h after LPS injection revealed no significant difference of the IL-1β positive cell fraction (p= 1, Dunn`s multiple comparisons test). (The experiments were performed with the help of Daria Savitska).

3.2.6.2 Microglial CD68 expression is not influenced by the peripheral inflammation

Macrosialin, also known as cluster of differentiation 68 (CD68) is a macrophage-specific intracellular glycoprotein. In the CNS, it is mainly expressed by microglia. CD68 is localized within the lysosomes and endosomes of the cells and is associated with the clearance of cell debris, phagocytosis, as well as the recruitment of macrophages (Silva and Gordon 1999; Holness et al. 1993). As it is up-regulated under inflammatory conditions, it is commonly used as a microglial activation marker. To investigate the CD68 expression in our experimental model, we injected WT mice with PBS or LPS and stained fixed cortical slices with antibodies against Iba1 and CD68. Subsequently, we measured the intensities of the CD68 expression in microglia 5 h and 30 h after the injections.

Figure 18A shows typical staining patterns of Iba1 and CD68 in microglia. The evaluation of the intensities of the CD68 expression (Figure 18B) revealed no alteration in the CD68 expression between the different time points after PBS or LPS injection (p= 0.105, Kruskal-Wallis test).

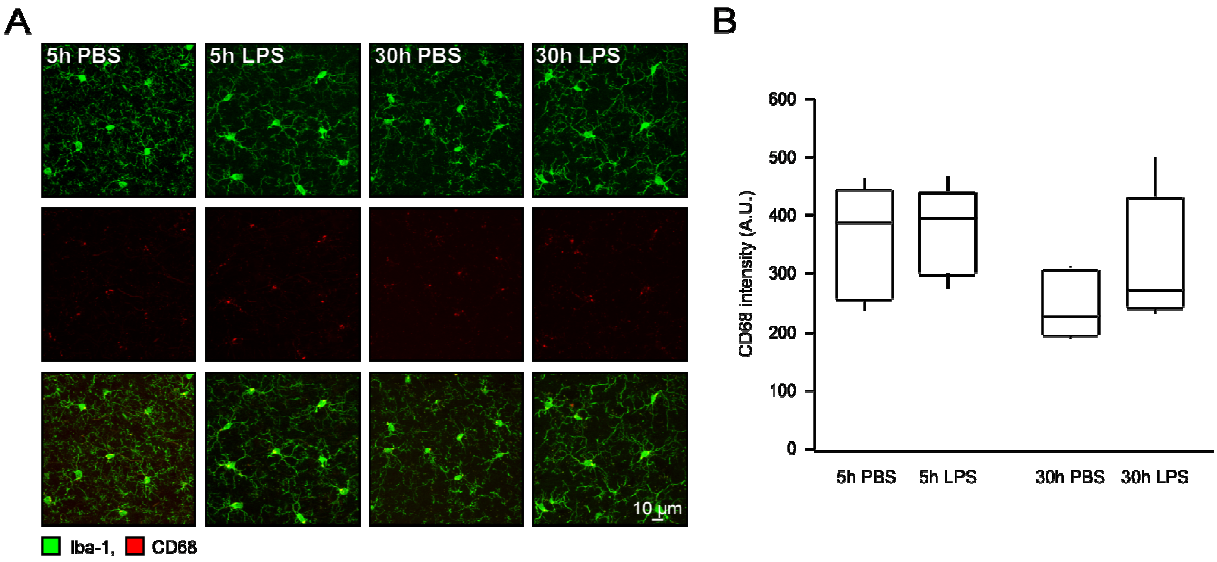

Figure 18 No change in microglial CD68 expression during peripheral inflammation

(A) MIP images (25 µm depths) of microglia labeled with anti-Iba1 and anti-CD68 antibodies in the cortex of 4-6 months old WT mice 5 h and 30 h after PBS or LPS injection. **(B)** Box plots showing the medians (per mouse) of the CD68 signal intensity in microglia at different time points after PBS or LPS injection (n= 6-10 analyzed areas per mouse, 5 mice per group). Note, no significant change in the CD68 signal intensity between these groups (p= 0.105, Kruskal-Wallis test). (These experiments were performed by Daria Savitska).

3.2.7 Inflammation leads to accelerated microglial process extension

Microglia have the ability to protect the brain tissue by sending their processes to a site of injury and to shield the surrounding brain parenchyma from toxic stimuli. Damaged cells release ATP and thereby attract microglial processes. An ATP-containing pipette can mimic a damaged cell and leads to microglial process extension towards the pipette (Davalos et al. 2005; Nimmerjahn, Kirchhoff, and Helmchen 2005; Schwendele et al. 2012). It is known that this property of microglia might be altered under pathological conditions like during neuroinflammation observed in a mouse model of Alzheimer`s disease (Brawek et al. 2014). To further characterize the functional properties of microglia in our model of peripheral inflammation, we measured the velocity of the process extensions towards an ATP-filled pipette at different time points during inflammation.

Figure 19A shows representative images of the microglial process movement towards the ATP-containing pipette over time. The experiments revealed a significant change in the process velocities (Figure 19B, p= 0.002, Kruskal-Wallis test).

Under inflammatory conditions, already 5 h after LPS injection, the cells showed a visible increase in the velocity of process extension towards the ATP-containing pipette. The velocity of the processes changed hereby from a mean value of 3.36 µm/min in PBS-injected mice to a value of 4.09 µm/min in the LPS-injected mice, whereby the increase stayed below statistical significance (p= 0.171, Dunn`s multiple comparisons test). Analyzing the process movements during the late phase of inflammation resulted in a further acceleration in the microglial process velocity. 30 h after LPS injection, the speed of the cell processes increased significantly from 3.48 µm/min 30 h after PBS injection to 4.67 µm/min 30 h after LPS injection (p= 0.039, Dunn`s multiple comparisons test).

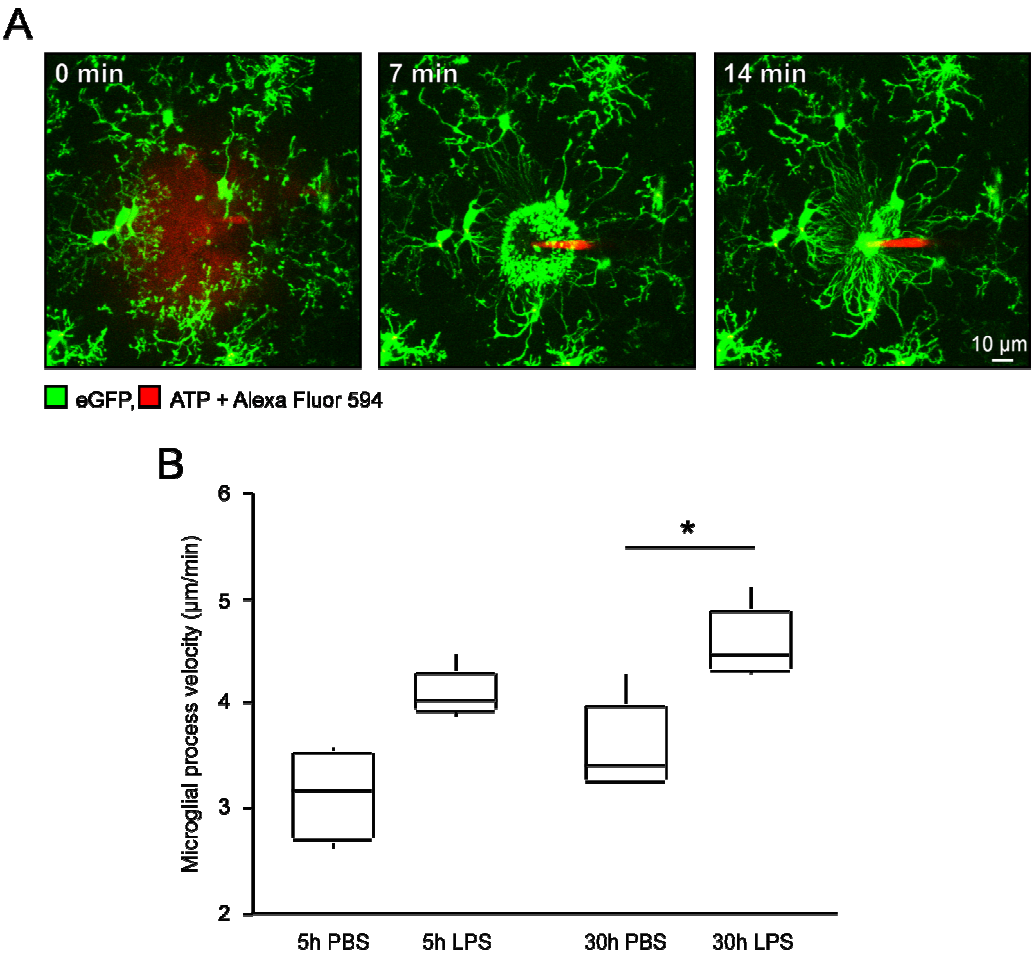

Figure 19 Increase of microglial process velocity during peripheral inflammation

(A) MIP images (70-90 µm below the cortical surface) of microglia in the motor cortex of a 5 months old Iba1$^{GFP/+}$ mouse 30 h after LPS injection. Images illustrate the process extension towards a pipette filled with ATP and Alexa Fluor 594 (red). **(B)** Comparison of the means (per mouse) of the microglial process velocity (µm/min)

between 5 h after LPS, 30 h after LPS and their corresponding PBS-controls (n= 2-7 areas per mouse in 5 mice per group). The process velocity during inflammation was significantly changed (p= 0.002, Kruskal-Wallis test). There was a visible but not significant increase in the velocity 5 h after LPS compared to 5 h after PBS injection (p= 0.171, Dunn`s multiple comparisons test). However, the process velocity increase reached the level of statistical significance 30 h after LPS injection when compared to 30 h after PBS injection (p= 0.039, Dunn`s multiple comparisons test).

Taken together, a peripheral inflammation can be divided into two phases. During the early phase, the cytokine levels are high and microglia react with strong Ca^{2+}-signals. During the late phase, when the cytokine levels are lowered, morphological changes start to take place, the IL-1β expression in microglia is up-regulated and the process velocity of the cells is markedly increased.

3.3 Neuronal functional properties during a peripheral inflammation

As microglia, also neurons have the capacity to react quickly to changes in their environment. In the following, we shifted the focus from the immune cells of the brain towards the neuronal network, to characterize the reactions of neurons to a peripheral inflammation.

3.3.1 Inflammation leads to hyperactivity of layer 2/3 neurons

The Ca^{2+}-sensor GCaMP6f provides a reliable reflection of the action potential firing in neurons (Chen et al. 2013). Inflammation was reported to affect neuronal activity. Injections of LPS, for example, were shown to alter the neuronal excitability in rats and increase their susceptibility to seizures (M. a Galic et al. 2008). Further, neurons in organotypic brain slices excited by topical application of LPS showed an increased frequency of spontaneous excitatory postsynaptic currents (EPSCs) (Pascual et al. 2012). However, how neurons react to peripheral inflammation in terms of their *in vivo* Ca^{2+}-signaling, and how their activity changes in the course of inflammation remains unclear. To answer the above questions, we injected a neuron-specific GCaMP6f-encoding viral construct into the motor cortex of WT mice and implanted a chronic cranial window above the injected area. Afterward, the frequency of spontaneously occurring neuronal Ca^{2+}-transients was measured in

neurons of layer 2/3 before (control) and at different time points after intraperitoneal PBS or LPS injections.

Representative images of GCaMP6f-labeled neurons are shown in Figure 20A and B. The spontaneous Ca^{2+}-transients of the imaged neurons (labeled with respective numbers) and the surrounding neuropil region (green dotted line) are illustrated in Figure 20C (PBS) and D (LPS).

Comparing the frequency of spontaneous Ca^{2+}-transients (transients/min) before and 5 h after LPS injection, with help of cumulative histograms of the frequencies, in all analyzed cells, revealed a clear rightward shift of the frequency after LPS injection (Figure 20F). This effect was absent in mice injected with PBS (Figure 20E).

The box plots in Figure 20G and H show the frequency of neuronal Ca^{2+}-transients of PBS- and LPS-injected mice as a function of time after the induction of the peripheral inflammation. The frequencies were normalized to the initial control measurements before the injections. Comparing the normalized frequencies of spontaneous Ca^{2+}-transients at different time points after PBS injection to the control measurement, carried out before the injection, with a repeated measures ANOVA, revealed no significant difference (Figure 20G, $p= 0.304$, Friedman`s test). In contrast, induction of a peripheral inflammation with LPS resulted in a significant increase in the neuronal frequency of the $Ca^{2+}$-transients (Figure 20H, $p= 0.001$, Friedman`s test). This effect was observed during the early phase of inflammation (control versus 5 h LPS, $p= 0.016$, Dunn`s multiple comparisons test). The frequency of Ca^{2+}-transients reached hereby a median value of 164 % of the initial frequency.

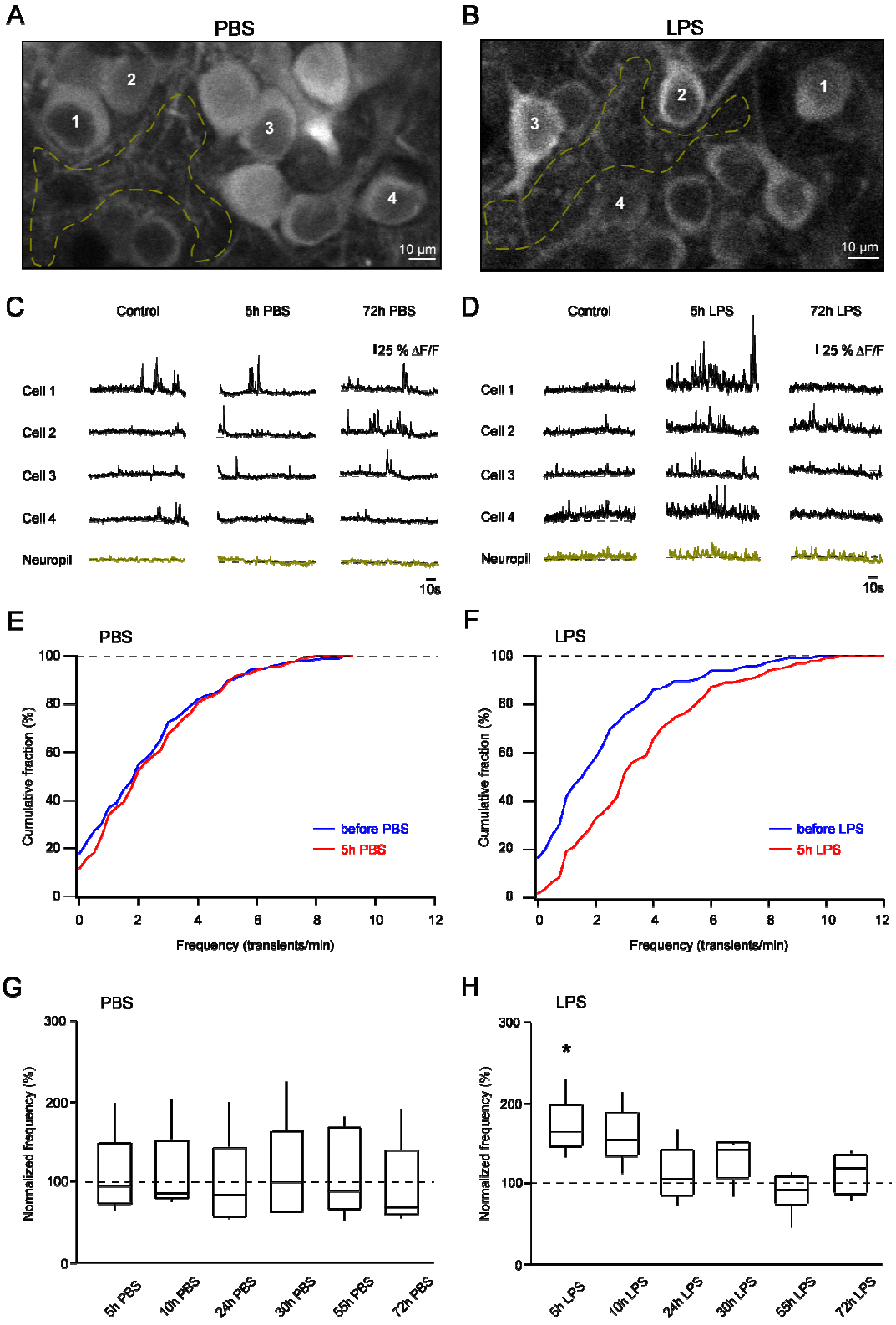

Figure 20 GCaMP6f-labeled neurons and increase in neuronal Ca^{2+}-signaling during peripheral inflammation

(A) and **(B)** MIP images (164 µm (A) and 186 µm (B) below the cortical surface) of GCaMP6f-labeled neurons in the motor cortex of 5 months old WT mice. **(C)** and **(D)** Spontaneous Ca^{2+}-transients recorded from neurons

(black traces) and neuropil (green trace), before (control), 5 h, and 72 h after PBS or LPS injection. The corresponding cells are marked with the respective numbers in panel (A) and (B). ΔF/F shows the normalized change in fluorescence. **(E)** and **(F)** Cumulative histograms of the frequency of neuronal Ca^{2+}-transients before and 5 h after PBS or LPS injection. Note, higher frequencies 5 h after LPS injection. **(G)** Box plots showing the medians (per mouse) of normalized neuronal frequency of Ca^{2+}-transients at different time points after PBS injection (n= 5 mice). PBS injections did not cause any significant change in the frequency of Ca^{2+}-transients (p= 0.304, Friedman`s test). **(H)** Box plots showing the medians (per mouse) of normalized frequency of $Ca^{2+}$-transients in neurons at different time points after LPS injection (n= 6 mice). Note a significant change in the frequency of $Ca^{2+}$-transients after LPS injection (p= 0.001, Friedman`s test). When compared to control condition, there was a significant frequency increase 5 h after LPS injection (p= 0.016, Dunn's multiple comparisons test).

3.3.2 Separation of somatic and neuropil Ca^{2+}-signals by independent component analysis

Labeling of neurons with GCaMP6f results in a broad staining of neuronal somata, dendrites, and axons (see Figure 20A and B). Ca^{2+}-signals can either occur either in neuronal cell bodies or in their processes located in the surrounding neuropil. Because the size of the brain area excited by a two-photon laser beam increases with an increase in the intensity of excitation light, signals collected from a given somatic region of interest, in reality, might originate from the surrounding neuropil. To discriminate between somatic and neuropil Ca^{2+}-signals, we reanalyzed the data obtained from the Ca^{2+}-measurements 5 h after PBS and LPS injection with "independent component analysis" (ICA). This method allows the identification of signals in cell somata occurring asynchronously (independently) with cytosol signals. At the same time, this mathematical approach eliminates somatic Ca^{2+}-signals occurring synchronously with that originating in the neuropil area.

3.3.2.1 Inflammation increases Ca^{2+}-signaling in neuronal somata

The frequency distributions of the asynchronous somatic Ca^{2+}-transients, before and after PBS (A) or LPS (B) injection, are shown in Figure 21A and B. It has to be noticed, however, that ICA revealed a high percentage of silent cells (i.e. either genuinely inactive cells or cells without independent Ca^{2+}-signals). In PBS-injected mice, around 15 % of the cells were silent. This number increased to 32 % in the LPS-injected mice. Also, after separation of independent somatic Ca^{2+}-signals by ICA, we observed no change of the frequency of Ca^{2+}-transients 5 h after PBS injection when compared to the control measurement (see cumulative histograms in Figure 21A). However, 5 h after LPS injection, there was a clear increase in the

frequency of independent somatic Ca^{2+}-transients when compared to the control condition (see Figure 21B).

The frequencies of the somatic Ca^{2+}-transients, normalized to the respective frequencies before PBS or LPS injection, are displayed in Figure 21C. Due to the high percentage of silent cells, we compared the 75^{th} percentiles of the frequency distributions (per mouse) instead of the medians. 5 h after PBS injection (Figure 21C), there was no significant frequency change of the independently active neurons ($p > 0.999$, Wilcoxon signed rank test). In contrast, the frequency of somatic Ca^{2+}-transients 5 h after LPS injection increased significantly, compared to the initial control measurement ($p = 0.031$, Wilcoxon signed rank test). This supports the previous results (see 3.3.1 and Figure 20G and H) and substantiates the excitatory effect of peripheral inflammation on cortical layer 2/3 neurons. To elucidate further properties of the somatic Ca^{2+}-signals, we analyzed the amplitudes of the Ca^{2+}-transients 5 h after LPS injection. We observed hereby a significant increase in the amplitudes of the somatic Ca^{2+}-transients during inflammation (Figure 21D, $p = 0.031$, Wilcoxon signed rank test).

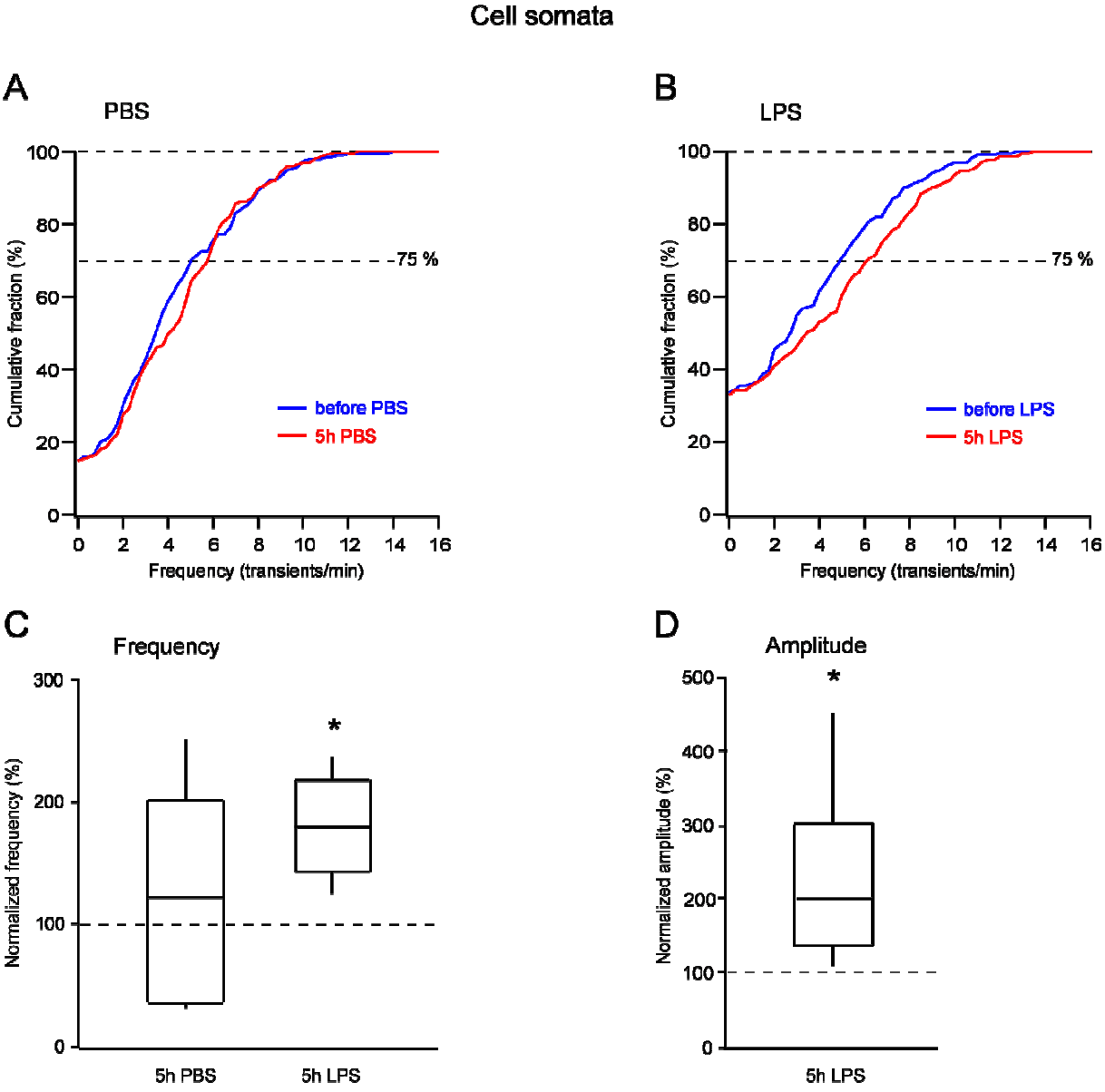

Figure 21 ICA reveals increase in frequency and amplitude of somatic Ca^{2+}-transients of layer 2/3 neurons during peripheral inflammation

(A) and **(B)** Cumulative histograms of the frequencies of the somatic Ca^{2+}-transients before and 5 h after PBS or LPS injection (results obtained from same datasets as the one shown in Figure 20). **(C)** Box plots showing the 75th percentiles (per mouse) of normalized frequencies of somatic Ca^{2+}-transients 5 h after PBS and LPS injection. Note, a significant increase in frequency of Ca^{2+}-transients 5 h after LPS injection ($p= 0.031$, Wilcoxon signed-rank test) and no frequency change after PBS injection ($p> 0.999$, Wilcoxon signed-rank test)**.** **(D)** Box plots showing the 75th percentiles (per mouse) of normalized amplitudes of somatic Ca^{2+}-transients 5 h after LPS injection. Note, a significant increase in the amplitude of Ca^{2+}-transients 5 h after LPS injection ($p= 0.031$, Wilcoxon signed-rank test).

3.3.2.2 Inflammation increases the amplitude of Ca^{2+}-transients in the neuropil

After investigation of the somatic Ca^{2+}-signals of layer 2/3 neurons, we focused on the Ca^{2+}-signals originating in the neuropil (Figure 22). When compared to control conditions before the injections, we found that neither PBS nor LPS injections affected the frequency of the Ca^{2+}-transients in the neuropil (Figure 22A, control versus 5 h PBS, $p> 0.999$ and control versus 5 h LPS, $p> 0.999$, Wilcoxon signed rank test). However, there was a clear increase in the amplitude of the neuropil Ca^{2+}-transients 5 h after LPS injection when compared to control (Figure 22B, $p= 0.031$, Wilcoxon signed rank test). In contrast, the signal amplitudes of PBS-injected mice did not change (Figure 22B, $p= 0.188$, Wilcoxon signed rank test).

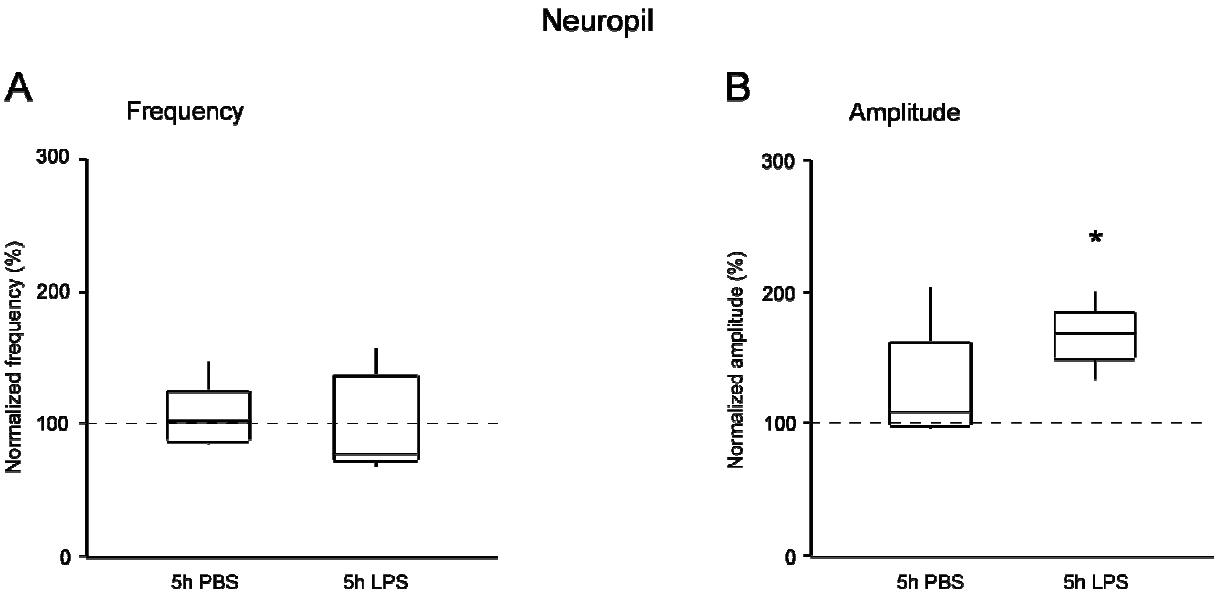

Figure 22 ICA reveals an increase in the amplitude of neuropil Ca^{2+}-transients during peripheral inflammation

(A) Box plots showing the medians (per mouse) of the normalized frequencies of Ca^{2+}-transients in the neuropil 5 h after PBS and LPS injection (results obtained from same datasets as the one shown in Figure 20). There was no change in the frequency of Ca^{2+}-transients in PBS- and LPS-injected mice ($p> 0.999$, Wilcoxon signed-rank test). **(B)** Box plots showing the medians (per mouse) of the normalized amplitude of Ca^{2+}-transients in the neuropil 5 h after PBS and LPS injection. Note, a significant increase in the amplitude of neuropil Ca^{2+}-transients 5 h after LPS injection ($p= 0.031$, Wilcoxon signed-rank test) but not after PBS injection ($p= 0.188$, Wilcoxon signed-rank test).

Taken together, neurons react to a peripheral inflammation with a pronounced increase in their Ca^{2+}-signaling. This effect was observed during the early phase of

inflammation, 5 h after the LPS challenge. An increased Ca^{2+}-signaling was hereby observed in both, the somata of the layer 2/3 neurons, where the frequency and the amplitude were increased and, in the neuropil, where solely the amplitude of the Ca^{2+}-signals was increased.

3.3.3 Effects of inflammation on presynaptic axonal Ca^{2+}-signals

Cortical layer 2/3 neurons receive excitatory input from pyramidal neurons of deeper layers (Shepherd et al. 2005). The described above experiments already indicated an excitatory effect of LPS in the neuronal somata (postsynapse). Therefore, in the next step, we analyzed how peripheral inflammation impacts presynaptic Ca^{2+}-signaling. To this end, we labeled neurons in layer 5 of the motor cortex with GCaMP6f. We then measured spontaneous Ca^{2+}-signals in their ascending axons in layer 1 before and after PBS or LPS injection through a chronic window.

3.3.3.1 Inflammation increases frequency of Ca^{2+}-transients in axons from the motor cortex

Figure 23A shows a typical axonal staining in layer 1 of the mouse motor cortex (individual axons marked by white arrowheads). The corresponding axonal Ca^{2+}-transients measured before (control) and after LPS injection (5 h LPS) are displayed in Figure 23B.

Cumulative histograms of the frequencies of axonal Ca^{2+}-transients (Figure 23C) indicated no influence of the PBS injection (left panel) and a somewhat higher frequency of axonal Ca^{2+}-transients after the LPS injection (right panel). A comparison of the amplitudes of the axonal Ca^{2+}-transients before and after LPS injection revealed a slight increase in the signal amplitude after LPS injection, with a median value reaching 117 % of the initial amplitude (Figure 23D). Nevertheless, this effect was below the level of statistical significance ($p= 0.156$, Wilcoxon signed rank test (one-tailed)). Figure 23E illustrates the normalized frequencies of axonal Ca^{2+}-transients after PBS or LPS injection. The LPS injection resulted hereby in a significant increase in the frequency of Ca^{2+}-transients with a median value reaching 133 % of the initial frequency ($p= 0.031$, Wilcoxon signed rank test (one-tailed)). The PBS injection did not alter the frequency of axonal Ca^{2+}-transients ($p= 0.250$, Wilcoxon signed rank test (one-tailed)).

3.3.3.2 Inflammation does not influence the frequency of Ca^{2+}-transients in axons from the somatosensory cortex

In addition to the inputs from deeper layers of the motor cortex, there are strong reciprocal connections between the somatosensory and the motor cortex (Suter and Shepherd 2015). To investigate the input from the somatosensory cortex, we labeled neurons in the somatosensory area with GCaMP6f and measured Ca^{2+}-signals in their axonal projections to layer 1 of the motor cortex before and after LPS injection. In contrast to the axons originating in the motor cortex, we did not observe any inflammation-induced increase in frequency of Ca^{2+}-transients in the axons from the somatosensory cortex (Figure 23F, $p= 0.125$, Wilcoxon signed rank test (one-tailed)).

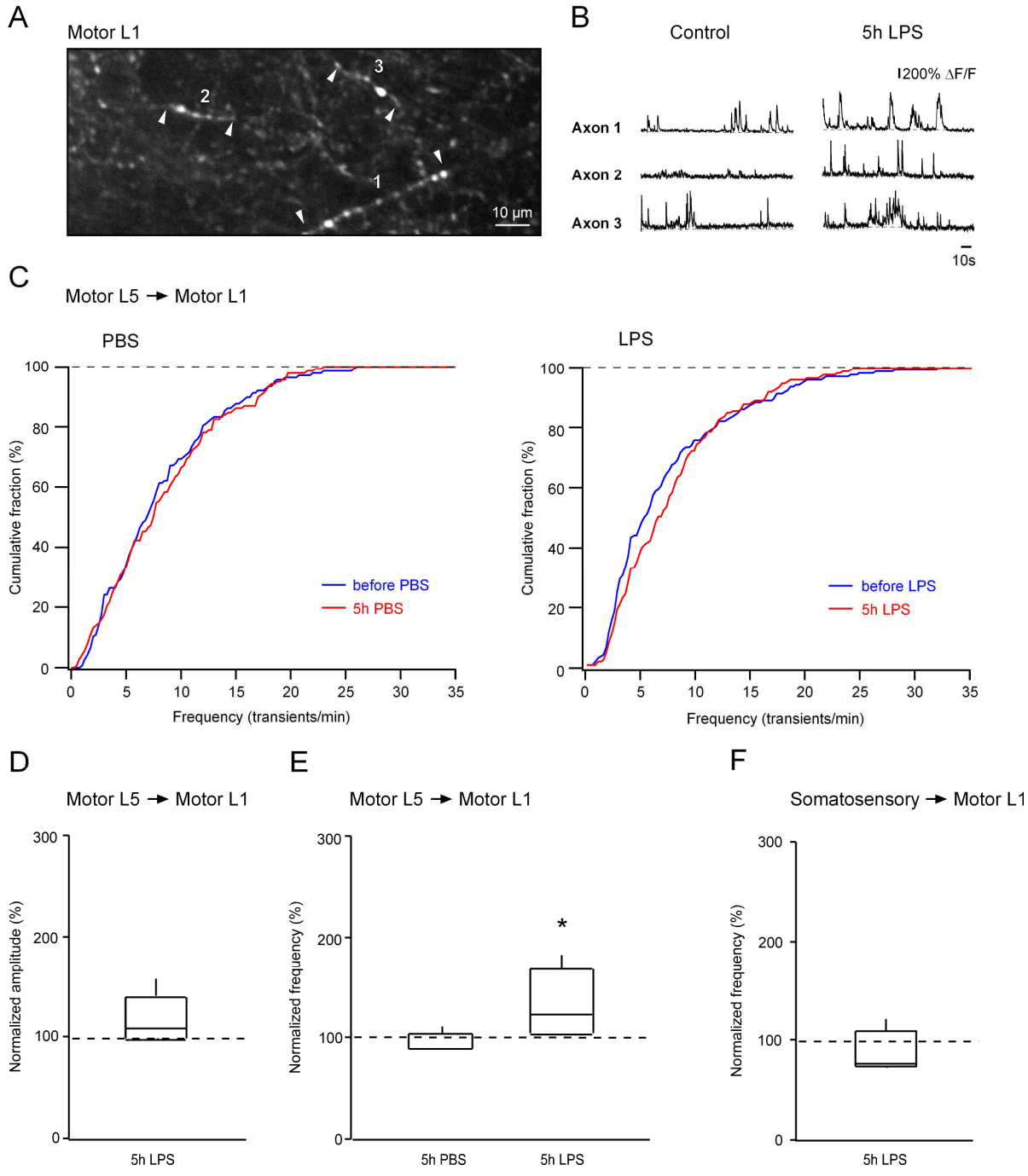

Figure 23 Increase in frequency of presynaptic Ca^{2+}-transients in axons from the motor but not the somatosensory cortex during peripheral inflammation

(A) Representative average intensity projection image (20 µm below the cortical surface) of GCaMP6f-labeled axons in layer 1 in the motor cortex of a 5 months old WT mouse. Individual axons are marked by white arrowheads. **(B)** Spontaneous Ca^{2+}-transients from axons recorded before (control) and 5 h after LPS injection. The corresponding axons are marked with the respective numbers in (A). ΔF/F shows the normalized change in fluorescence. **(C)** Cumulative histograms of the frequency of Ca^{2+}-transients in axons of layer 5 neurons in the motor cortex, before and 5 h after PBS or LPS injection (n= 5 mice per group). **(D)** Box plot showing the median (per mouse) of the normalized amplitude of Ca^{2+}-transients in axons from the motor cortex, 5 h after LPS injection

(p= 0.156, Wilcoxon signed-rank test (one-tailed)). **(E)** Box plots showing the medians (per mouse) of normalized frequencies of Ca^{2+}-transients in axons from the motor cortex 5 h after PBS and LPS injection. Note, a significant increase in the frequency of Ca^{2+}-transients 5 h after LPS injection (p= 0.031, Wilcoxon signed-rank test (one-tailed)), but not 5 h after PBS injection (p= 0.250, Wilcoxon signed-rank test (one-tailed)). **(F)** Box plot showing the medians (per mouse) of the normalized frequency of Ca^{2+}-transients in axons from the somatosensory cortex 5 h after LPS injection. LPS injection induced no increase in the frequency in axons from the somatosensory cortex (p= 0.125, Wilcoxon signed-rank test (one-tailed)).

3.3.4 Inflammation increases Ca^{2+}-signaling in layer 5 neurons of the motor cortex

Next, we measured Ca^{2+}-signals in the somata of layer 5 neurons in the motor cortex (at 450 to 600 µm depths). We injected mice with PBS or LPS before we "bulk-electroporated" neurons (Nagayama et al. 2007) in layer 5 with the small molecule Ca^{2+}-sensor Oregon Green BAPTA-1 (OGB-1). This method allowed to sparsely label neurons surrounding the tip of the labeling pipette and enabled sufficient visibility to image the Ca^{2+}-signals of the deep cortical neurons. The frequency of somatic Ca^{2+}-transients was measured 4-6 h after the LPS or PBS injection.

Representative images of cells electroporated after PBS (A) or LPS (B) injection with the corresponding somatic Ca^{2+}-transients (C and D) are shown in Figure 24. Cumulative histograms of the frequency of the Ca^{2+}-transients (Figure 24E) revealed a significant increase in frequency in mice injected with LPS when compared to PBS-injected mice (p= 0.045, Kolmogorov–Smirnov test). Comparing the medians (per mouse) of the frequency of Ca^{2+}-transients 5 h after PBS and LPS injection supported these results and revealed a significantly higher frequency of Ca^{2+}-transients in the layer 5 neurons after LPS injection (Figure 24F, p= 0.041, Mann-Whitney test (one-tailed)).

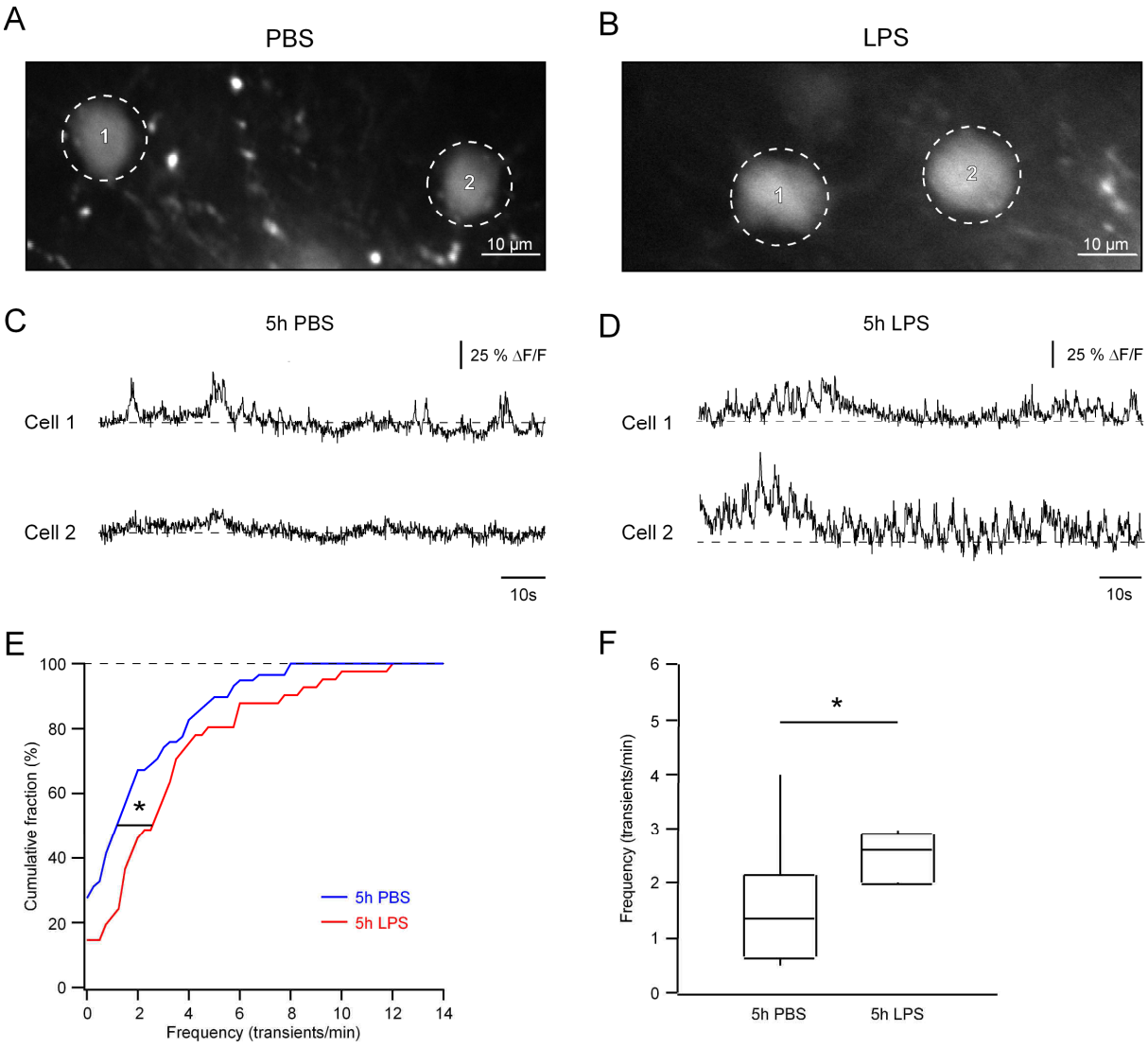

Figure 24 Increase in frequency of somatic Ca^{2+}-transients in layer 5 neurons of the motor cortex during peripheral inflammation

(A) and **(B)** Representative average intensity projection images (496 µm (A) and 538 µm (B) below the cortical surface) of OGB-1-labeled neurons in the motor cortex of 5 months old WT mice. Mice were injected either with PBS or with LPS. **(C)** and **(D)** Spontaneous Ca^{2+}-transients from electroporated neurons recorded 5 h after PBS or LPS injection, respectively. The corresponding neurons are marked with the respective numbers in (A and B). **(E)** Cumulative histograms of the frequency of somatic Ca^{2+}-transients ~5 h after the PBS and LPS injections. Note, a significant increase in frequency of the Ca^{2+}-transients in LPS-injected mice ($p= 0.045$, Kolmogorov-Smirnov test) **(F)** Box plots illustrating the medians (per mouse) of the frequency of Ca^{2+}-transients 5 h after PBS and LPS injection. Compared to PBS injections, there was a significant increase in frequency of the Ca^{2+}-transients after injection of LPS ($p= 0.041$, Mann-Whitney test (one-tailed)).

As the previous data have shown, the inflammation-induced Ca^{2+}-signaling increase is not only a feature of cortical neurons in layer 2/3. It can be also found in their presynaptic partners. Thus, in addition to observing increased frequency of Ca^{2+}-signals in axons originating in deeper layers of the motor cortex, similar results were also obtained when recording from somata of neurons in layer 5.

3.3.5 Inflammation decreases Ca^{2+}-signaling in inhibitory neurons

Around 20-30 % of the cortical neurons are inhibitory neurons (Markram et al. 2004). With the GCaMP6f-encoding viral construct, it was not possible to distinguish between neurons with excitatory or inhibitory properties. However, we aimed to know which cell type, in particular, is affected. To address this question, we used a VIAAT-Cre-GCaMP6 transgenic mouse line. These mice express the Cre recombinase under control of the VIAAT-promoter, which is exclusively active in inhibitory GABAergic neurons. We implanted a chronic window above the motor cortex of these mice and evaluated the spontaneous somatic Ca^{2+}-signaling of GCaMP6-labeled GABAergic neurons 5 h after PBS and LPS injection.

Figure 25A shows a representative image of two GABAergic cells. The corresponding spontaneous Ca^{2+}-transients of the imaged neurons before (control) and after LPS injection, are shown in Figure 25B. Cumulative histograms of the frequency of Ca^{2+}-transients before and 5 h after PBS injection indicated no change in the frequency of the Ca^{2+}-transients (Figure 25C). However, comparison of the frequency of Ca^{2+}-transients before and after LPS injection revealed a clear decrease in the frequency of the Ca^{2+}-transients during peripheral inflammation (Figure 25D). The box plots in Figure 25E illustrate the normalized frequency of Ca^{2+}-transients after PBS and LPS injection. We found no significant difference in the frequency of the Ca^{2+}-transients in inhibitory neurons after injection of PBS ($p= 0.125$, Wilcoxon signed-rank test), whereas LPS injection resulted in a significant decrease in the frequency of Ca^{2+}-transients (Figure 25E, $p= 0.031$, Wilcoxon signed-rank test).

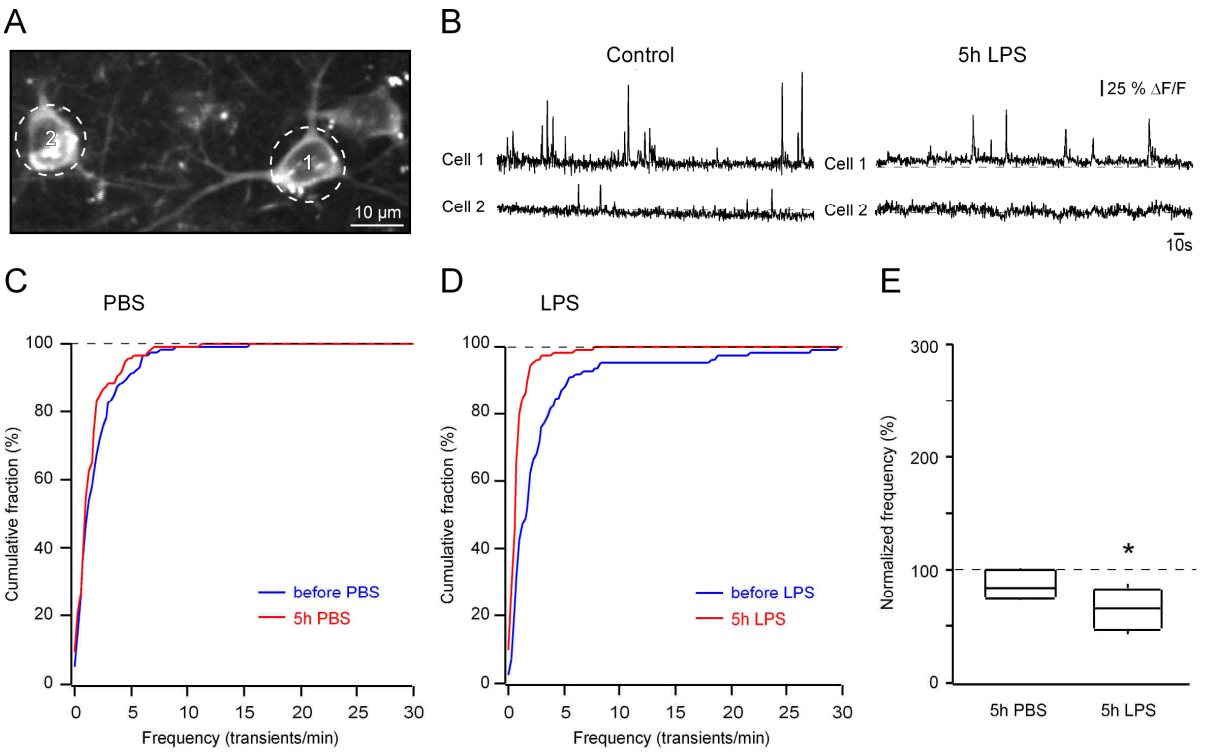

Figure 25 Decrease in frequency of Ca^{2+}-transients in inhibitory neurons during peripheral inflammation

(A) Representative MIP image (76-86 µm below the cortical surface) of GCaMP6-expressing GABAergic neurons in the motor cortex of a 5 months old VIAAT-Cre-GCaMP6 mouse. **(B)** Spontaneous Ca^{2+}-transients recorded from the neurons in (A), before (control) and 5 h after LPS injection. **(C)** and **(D)** Cumulative histograms of the frequency of somatic Ca^{2+}-transients before and 5 h after PBS or LPS injection. Data obtained from 4-6 months old VIAAT-Cre-GCaMP6 mice (n= 6 mice per group). **(E)** Box plots showing the medians (per mouse) of normalized frequency of somatic Ca^{2+}-transients 5 h after PBS and LPS injection. Note, a significant decrease in the frequency of somatic Ca^{2+}-transients in inhibitory neurons 5 h after LPS injection (p= 0.031, Wilcoxon signed-rank test), and no significant change in the frequency 5 h after PBS injection (p= 0.125, Wilcoxon signed-rank test).

3.3.6 Ca^{2+}-signaling in neurons of NLRP3$^{-/-}$ and TNF-α$^{-/-}$ mice

The Ca^{2+}-signaling of microglia was influenced by the NLRP3 inflammasome and to a minor extent by the cytokine TNF-α. However, the way how neurons react in absence of these inflammatory mediators remained elusive. To address this question, we labeled neurons of layer 2/3 in NLRP3$^{-/-}$ and TNF-α$^{-/-}$ mice with GCaMP6f and measured their spontaneous somatic Ca^{2+}-signaling through a chronic window before and after injection of LPS.

3.3.6.1 Basal spontaneous Ca^{2+}-signaling in neurons of NLRP3$^{-/-}$ and TNF-α$^{-/-}$ mice

First, we examined, whether the basal spontaneous Ca^{2+}-signaling in neurons of NLRP3$^{-/-}$ and TNF-α$^{-/-}$ animals differed from the signaling in WT animals. To this end, we compared the frequency of somatic Ca^{2+}-transients in neurons of NLRP3$^{-/-}$ and TNF-α$^{-/-}$ mice with the frequency of the Ca^{2+}-transients in neurons of WT mice.

The basal spontaneous Ca^{2+}-signaling in neurons of NLRP3$^{-/-}$ mice was clearly increased compared to WT mice. The NLRP3$^{-/-}$ mice showed a significantly higher frequency of Ca^{2+}-transients than WT animals (Figure 26A, p= 0.03, Mann-Whitney test).

In contrast, the basal spontaneous Ca^{2+}-signaling in neurons of TNF-α$^{-/-}$ mice did not differ from the signaling in neurons of WT animals. TNF-α$^{-/-}$ and WT mice showed comparable frequencies of spontaneous Ca^{2+}-transients (Figure 26B, p= 0.537, Mann-Whitney test).

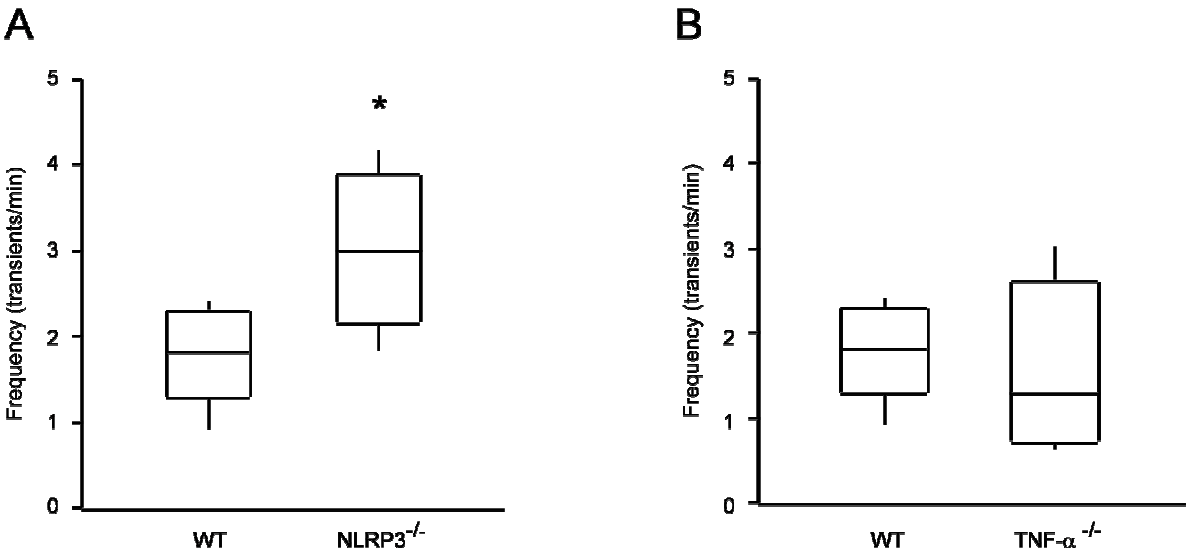

Figure 26 Influence of the deletion of NLRP3 inflammasome and TNF-α on basal spontaneous Ca^{2+}-signaling in layer 2/3 neurons of the motor cortex

Comparison of basal spontaneous Ca^{2+}-signaling in neurons of WT, NLRP3$^{-/-}$ and TNF-α$^{-/-}$ mice (n= 5 mice per group). **(A)** Box plots illustrating the medians (per mouse) of the frequency of Ca^{2+}-transients in neurons of WT and NLRP3$^{-/-}$ mice. Note, a significant increase in the frequency of the Ca^{2+}-transients in NLRP3$^{-/-}$ mice compared to WT animals (p= 0.03, Mann-Whitney test). **(B)** Box plots showing the medians (per mouse) of the frequency of Ca^{2+}-transients in neurons of WT and TNF-α$^{-/-}$ mice. There was no significant difference between the frequencies of spontaneous Ca^{2+}-transients in WT and TNF-α$^{-/-}$ animals (p= 0.537, Mann-Whitney test).

3.3.6.1 Effects of inflammation on Ca^{2+}-signaling in neurons of NLRP3$^{-/-}$ and TNF-α$^{-/-}$ mice

In a next step, we investigated whether the NLRP3 inflammasome and the cytokine TNF-α play a role for the neuronal Ca^{2+}-signaling during a peripheral inflammation. Therefore, we measured the spontaneous somatic Ca^{2+}-signaling in neurons of NLRP3$^{-/-}$ and TNF-α$^{-/-}$ mice, before and at different time points after LPS injection.

Figure 27A illustrates the normalized frequency of neuronal Ca^{2+}-transients in NLRP3$^{-/-}$ mice as a function of time after the induction of peripheral inflammation. Comparing the frequencies of the Ca^{2+}-transients to the initial control frequency with a repeated measures ANOVA, revealed no significant effect of LPS on the frequency of the Ca^{2+}-transients in NLRP3$^{-/-}$ mice ($p= 0.169$, Friedman`s test). The normalized frequencies of neuronal $Ca^{2+}$-transients in LPS-treated TNF-α$^{-/-}$ mice are shown in Figure 27B. A repeated measures ANOVA revealed a significant change in the frequency of $Ca^{2+}$-transients in the LPS-treated TNF-α$^{-/-}$ mice ($p= 0.026$, Friedman`s test), however, a post hoc comparison with the Dunn's multiple comparisons test stayed below statistical significance ($p> 0.05$). Cumulative histograms of the frequencies of the neuronal Ca^{2+}-transients in NLRP3$^{-/-}$ and TNF-α$^{-/-}$ mice before and 5 h after LPS injection are shown in Figure 27C and D. It is worth to note that 5 h after LPS injection, the NLRP3$^{-/-}$ mice showed a clear, although not significant (Figure 27A) increase in the frequency of Ca^{2+}-transients when compared to the initial control frequency (Figure 27C). Such frequency increase during the early phase of inflammation was not observed in the TNF-α$^{-/-}$ mice (Figure 27D).

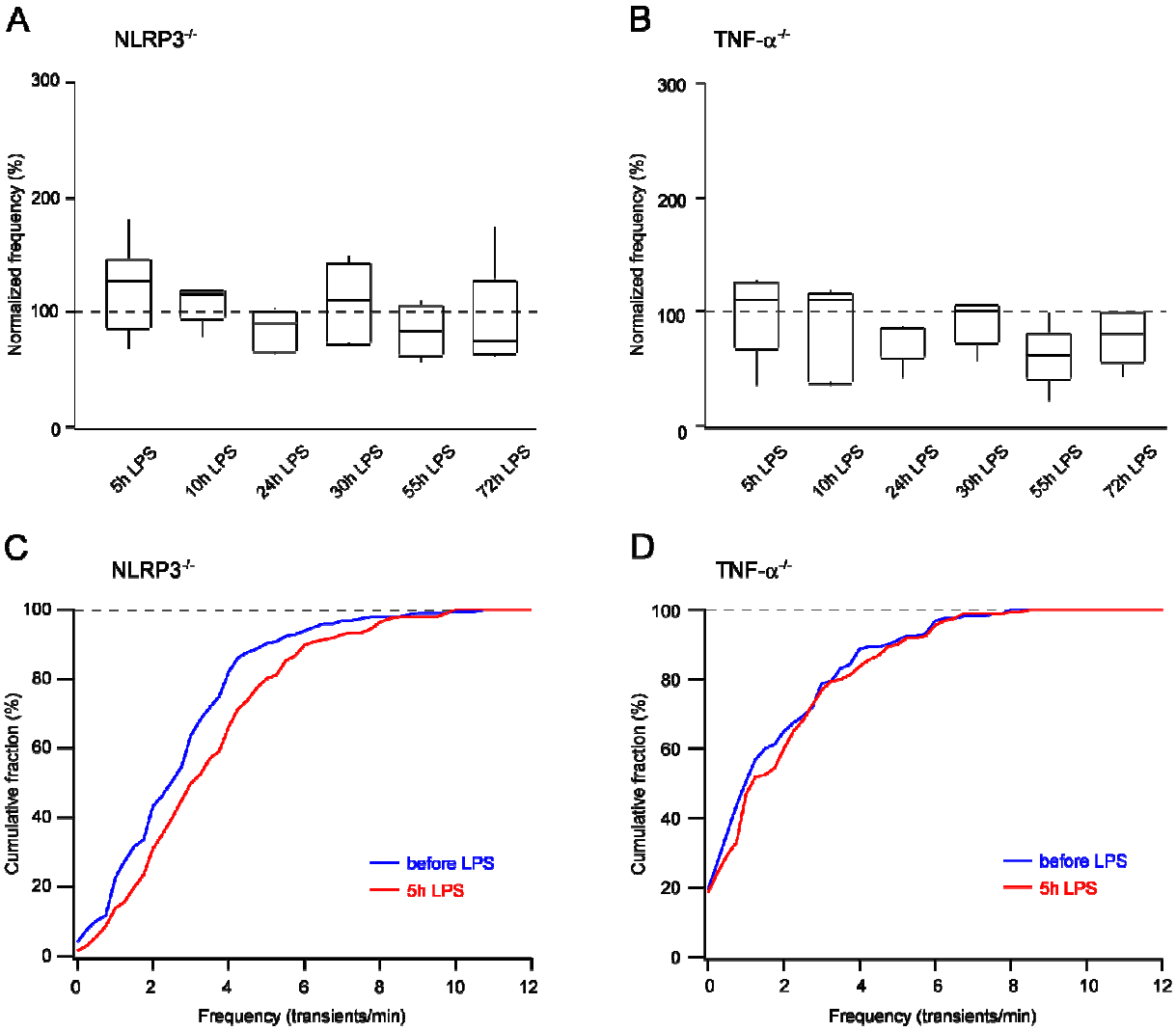

Figure 27 Influence of the deletion of NLRP3 inflammasome and TNF-α on the neuronal Ca^{2+}-signaling during peripheral inflammation

Spontaneous Ca^{2+}-signaling in neurons of 4-6 months old NLRP3$^{-/-}$ and TNF-α$^{-/-}$ animals at different time points during inflammation (n= 5 mice per group). **(A)** Box plots showing the medians (per mouse) of the normalized frequency of Ca^{2+}-transients in NLRP3$^{-/-}$ mice plotted as a function of time after injection of LPS. There was no significant change in the frequency of Ca^{2+}-transients in NLRP3$^{-/-}$ mice after LPS injection (p= 0.169, Friedman`s test). **(B)** Box plots illustrating the medians (per mouse) of the normalized frequency of Ca^{2+}-transients in TNF-α$^{-/-}$ mice. Frequencies plotted as a function of time after injection of LPS. The frequency of spontaneous Ca^{2+}-transients in TNF-α$^{-/-}$ mice was significantly changed after LPS injection (p= 0.024, Friedman`s test), but a post hoc Dunn's multiple comparisons test revealed no significant difference (p> 0.05). **(C)** and **(D)** Cumulative histograms of the frequencies of Ca^{2+}-transients before and 5 h after LPS injection in NLRP3$^{-/-}$ (C) and TNF-α$^{-/-}$ mice (D). Note, a higher frequency of Ca^{2+}-transients in NLRP3$^{-/-}$ mice 5 h after LPS injection, when compared to the frequency before injection. In contrast, injection of LPS seemed to have no excitatory influence on the frequency of Ca^{2+}-transients in TNF-α$^{-/-}$ mice.

To directly compare the effect of LPS in NLRP3$^{-/-}$ and WT mice, we plotted the frequencies of the Ca^{2+}-transients 5 h after LPS injection in a cumulative histogram (Figure 28A). Interestingly, there was no significant difference in the frequency of Ca^{2+}-transients between NLRP3$^{-/-}$ mice and WT animals (Figure 28A, p= 0.933, Kolmogorov-Smirnov test). Thus, the NLRP3$^{-/-}$ mice were able to reach a similar frequency of Ca^{2+}-transients during inflammation as WT animal. The lack of effect observed in Figure 27A was most probably due to the increased frequency of Ca^{2+}-transients found in these mice under control conditions.

In contrast, comparing the frequencies of Ca^{2+}-transients (5 h after LPS) between TNF-α$^{-/-}$ mice and WT mice (Figure 28B) revealed a significantly lower frequency of Ca^{2+}-transients in TNF-α$^{-/-}$ mice than in the WT animals (p< 0.001, Kolmogorov-Smirnov test).

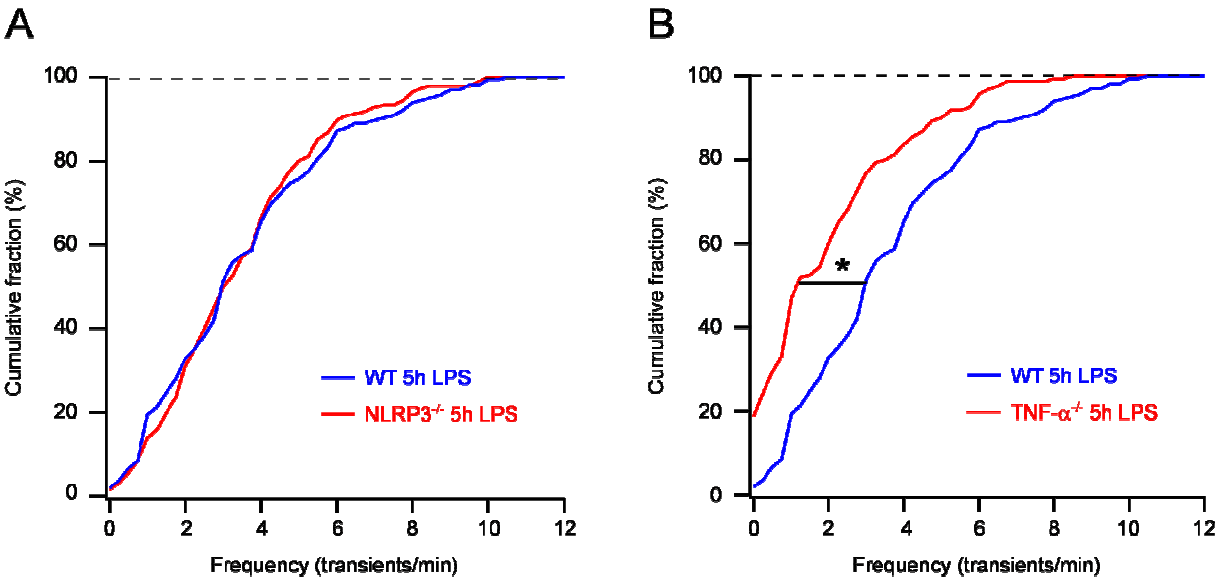

Figure 28 Comparison of the neuronal Ca^{2+}-signaling during peripheral inflammation in WT, NLRP3$^{-/-}$ and TNF-α$^{-/-}$ mice

(A) Cumulative histograms of the frequency of spontaneous neuronal Ca^{2+}-signals 5 h after LPS injection in WT and NLRP3$^{-/-}$ mice. Note, a comparable frequency of Ca^{2+}-transients in NLRP3$^{-/-}$ and WT mice (p= 0.933, Kolmogorov-Smirnov test). **(B)** Cumulative histograms of the frequency of spontaneous neuronal Ca^{2+}-signals 5 h after LPS injection in WT and TNF-α$^{-/-}$ mice. TNF-α$^{-/-}$ mice showed a significantly lower frequency of Ca^{2+}-transients after LPS injection than WT animals (p< 0.001, Kolmogorov-Smirnov test).

Taken together, inhibitory neurons react to a peripheral inflammation with a reduced frequency of spontaneous Ca^{2+}-transients. Further, a proper function of the NLRP3 inflammasome and the cytokine TNF-α seem to be important for the modulation of neuronal Ca^{2+}-signaling. We found that the NLRP3 inflammasome has an impact on the basal spontaneous Ca^{2+}-signaling in neurons but is apparently not responsible for the excitatory effect of LPS during inflammation. In contrast, the presence of TNF-α is not required for the spontaneous Ca^{2+}-signaling under control conditions. However, TNF-α seems to be important for the LPS-induced increase of spontaneous neuronal Ca^{2+}-signaling in the course of peripheral inflammation.

3.3.7 Effects of microglial depletion on the neuronal network

In the brain, the colony stimulating factor-1 (CSF-1) receptor is exclusively expressed on microglia. A blockade of this receptor yields a robust depletion of the cells (Elmore et al. 2014; Dagher et al. 2015). In the following experiments, we blocked microglial CSF-1 receptors in $Iba1^{GFP/+}$ mice to investigate whether the spontaneous neuronal Ca^{2+}-signaling depends on the presence of microglia.

3.3.7.1 CSF-1-receptor inhibition leads to microglial depletion

To confirm microglial depletion after CSF-1 receptor inhibition, we implanted a chronic window above the motor cortex of $Iba1^{GFP/+}$ mice and counted the numbers of microglia before and after feeding the animals with the CSF-1 receptor inhibitor PLX 5622 (Plexxikon Inc., USA) for 7 days.

Figure 29A shows images of the motor cortex of an $Iba1^{GFP/+}$ mouse before and after CSF-1 receptor inhibition. The quantifications of the microglial cell numbers before and after feeding with PLX 5622 are displayed in Figure 29B. PLX 5622 led to a significant reduction of microglial cells from a total number of 47.38 cells per imaging field (0-200 µm below the cortical surface) to a value of 6.58 cells per field ($p< 0.001$, Paired t-test).

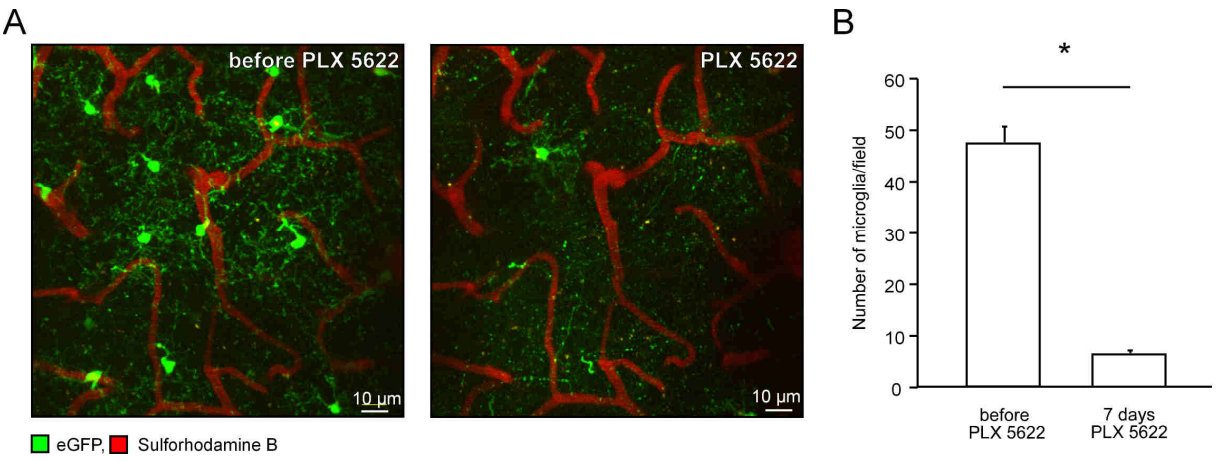

Figure 29 CSF-1 receptor inhibition leads to microglial depletion

(A) MIP images (50-100 µm below the cortical surface) in the motor cortex of a 5 months old Iba1$^{GFP/+}$ mouse before (left panel) and during (right panel, 7 day-long feeding period) feeding with the CSF-1 receptor inhibitor PLX 5622. Microglial eGFP is shown in green and blood vessels (in red) are stained by i.p. injections of sulforhodamine B. **(B)** Microglial number per imaging field (0-200 µm below the cortical surface, total volume 0.0062 mm^3) before and after microglial depletion via PLX 5622. Note, a significant reduction of the microglial number after feeding with PLX 5622 ($p < 0.001$, Paired t-test).

3.3.7.2 Microglial depletion decreases basal spontaneous Ca^{2+}-signaling in layer 2/3 neurons

Next, we wanted to investigate if the absence of microglia had an influence on the basal spontaneous Ca^{2+}-signaling in neurons. To this end, we labeled layer 2/3 motor cortical neurons of Iba1$^{GFP/+}$ mice with GCaMP6f and implanted a chronic window. Then, we imaged spontaneous Ca^{2+}-transients in these cells before and after feeding the mice for 7 days with the Plexxikon compound PLX 5622.

The distributions of the frequency of neuronal Ca^{2+}-transients before and after microglial depletion are shown in Figure 30A. We observed a clear increase in the number of silent neurons after microglial depletion, from 15 % of silent cells prior to depletion to 30 % of silent cells after feeding with PLX 5622. Further, our data revealed a decrease in the frequency of Ca^{2+}-transients after microglial depletion. Figure 30B shows the frequency of Ca^{2+}-transients in neurons after microglial depletion, normalized to the frequency of the Ca^{2+}-transients before depletion. Without microglia, neurons showed a significantly reduced frequency of Ca^{2+}-transients ($p = 0.042$, Wilcoxon signed-rank test), with a median value reaching only 64 % of the initial frequency.

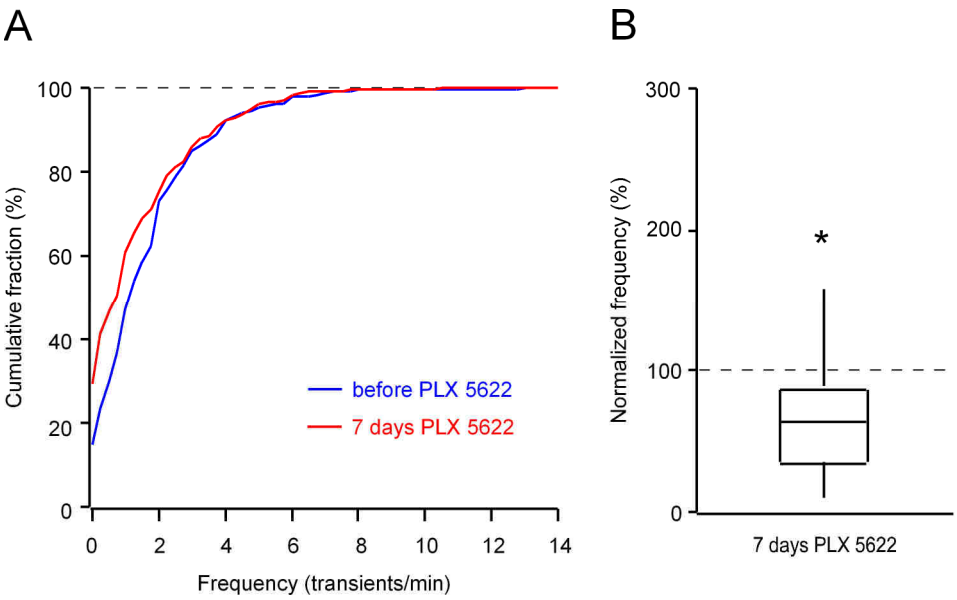

Figure 30 Microglial depletion decreases basal spontaneous Ca^{2+}-signaling in neurons

Effect of microglial depletion on spontaneous neuronal Ca^{2+}-signaling in the motor cortex of 4-6 months old $Iba1^{GFP/+}$ mice (n= 12 mice). **(A)** Cumulative histograms of the frequency of spontaneous Ca^{2+}-transients before and 7 days after CSF-1 receptor inhibition with PLX 5622. Note, a reduced frequency of Ca^{2+}-transients and a higher fraction of silent neurons after microglial depletion. **(B)** Box plot illustrating the medians (per mouse) of the normalized frequency of Ca^{2+}-transients 7 days after feeding PLX 5622. There was a significant decrease in the frequency of Ca^{2+}-transients under PLX 5622 treatment (p= 0.042, Wilcoxon signed-rank test).

3.3.7.3 Microglial depletion does not influence the inflammation-induced increase in Ca^{2+}-signaling in layer 2/3 neurons

To test the effect of microglial depletion on the inflammation-induced increase in neuronal Ca^{2+}-signaling, we measured the frequency of spontaneous Ca^{2+}-transients in GCaMP6f-labeled neurons of microglia-depleted mice before and 5 h after PBS or LPS injection.

The cumulative histograms in Figure 31A show the frequencies of Ca^{2+}-transients before microglial depletion with PLX 5622 (blue), before injecting PBS (green) and 5 h after PBS injection (red). The corresponding frequencies of Ca^{2+}-transients in the LPS-treated group of mice are illustrated in Figure 31B. As already shown above (see 3.3.7.2, Figure 30), microglial depletion led to a general decrease in the frequency of spontaneous Ca^{2+}-transients in neurons (Figure 31A and B, compare blue lines with green lines). However, injecting microglia-depleted mice with PBS had no effect on the frequency of the spontaneous neuronal Ca^{2+}-transients (Figure 31A, green line versus red line). In contrast, even in the absence of microglia,

the injection of LPS led to a remarkable increase in the frequency of Ca^{2+}-transients in neurons (Figure 31B, compare green line with red line). Figure 31C illustrates the normalized neuronal frequency of Ca^{2+}-transients 5 h after PBS and LPS injection, normalized to the frequencies measured in the same cells directly before the respective treatment. The LPS injection resulted in a significant increase in the frequency of the Ca^{2+}-transients, with a median value reaching 168 % of the initial frequency (p= 0.016, Wilcoxon signed-rank test). Injections of PBS had no effect on the spontaneous neuronal Ca^{2+}-signaling (p> 0.999, Wilcoxon signed-rank test).

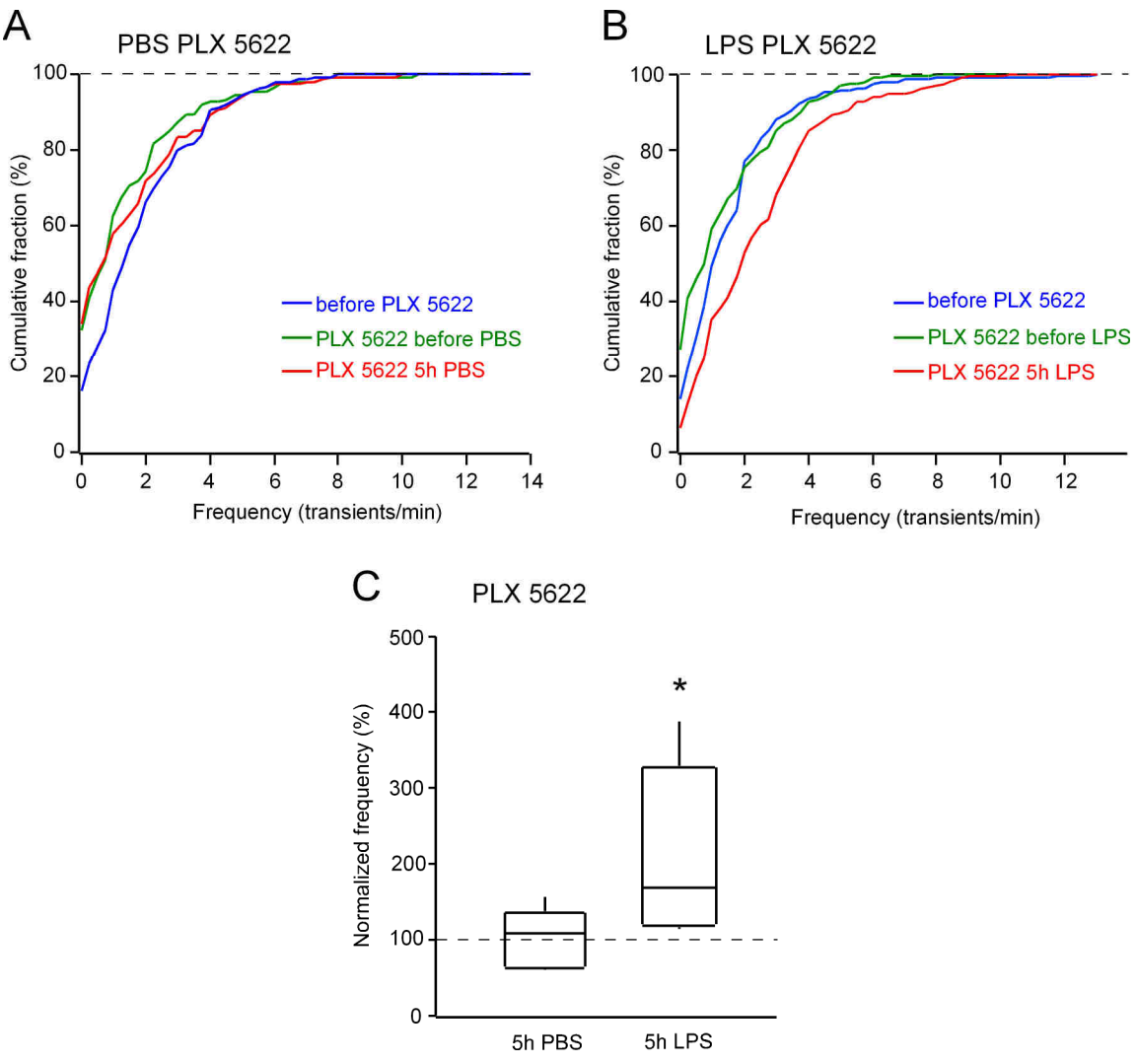

Figure 31 Microglial depletion does not influence the frequency of neuronal Ca^{2+}-transients during peripheral inflammation

Effects of microglial depletion on spontaneous neuronal Ca^{2+}-signaling in 4-6 months old $Iba1^{GFP/+}$ mice 5 h after PBS or LPS injection. **(A)** Cumulative histograms of the frequencies of Ca^{2+}-transients before feeding PLX 5622

(blue), 7 days after feeding PLX 5622/before PBS injection (green), and 5 h after PBS injection (red). Data from n= 5 mice. Note, a general decrease in the frequency of Ca^{2+}-transients after microglial depletion with PLX 5622. **(B)** Cumulative histograms of the frequencies of Ca^{2+}-transients before feeding PLX 5622 (blue), 7 days after PLX 5622/before LPS injection (green), and 5 h after LPS injection (red). Data obtained from n= 7 mice. LPS injection yielded a clear increase in the frequency of neuronal Ca^{2+}-transients in microglia-depleted mice. **(C)** Box plots illustrating medians (per mouse) of normalized frequency of Ca^{2+}-transients in neurons 5 h after PBS and LPS injection. Note that LPS injection induced a significant increase in the frequency of Ca^{2+}-transients ($p= 0.016$, Wilcoxon signed-rank test), whereas the PBS injection had no effect on the Ca^{2+}-signals ($p> 0.999$, Wilcoxon signed-rank test).

In summary, a blockade of microglial CSF-1 receptors led to an almost complete depletion of microglia within the brain, as evidenced by the *in vivo* imaging of layers 1-3 of the motor cortex. This depletion was accompanied by a general decrease in the basal spontaneous Ca^{2+}-signaling in cortical neurons. Nevertheless, microglial depletion did not affect the increase in neuronal Ca^{2+}-signaling during the early phase of peripheral inflammation.

4. Discussion

4.1 Inflammation-mediated increase of spontaneous network activity

Taken together, this work shows that under inflammatory conditions, the properties of the local cortical network in the intact *in vivo* brain are shifted towards a hyperactive state. Microglia, as well as neurons, react to peripheral inflammation, induced by LPS injections, with a clear increase of their spontaneous Ca^{2+}-signaling. By using *in vivo* two-photon Ca^{2+}-imaging, we characterized the behavior of these two cell types over time and provided insights into the mechanisms involved.

4.2. Microglia react to inflammation with up-regulation of their Ca^{2+}-signaling

After the systemic administration of LPS in mice, ELISA-based protein analysis confirmed that the inflammatory signal was transmitted from the periphery to the brain. We found a considerable increase in the brain cytokine concentration 5 h after LPS injection. During the initial phase of inflammation, this up-regulation was visible for most of the tested cytokines (IL-1β, TNF-α, IL-6, CCL2 and IL-10) in the periphery, as well as in the brain. Only the brain level of TNF-α did not increase to the statistically significant level and the brain level of IL-10 was below our detection threshold. Later during inflammation (30 h after LPS injection), the majority of cytokines returned to their control levels and did not differ any more from the corresponding PBS controls, pointing out the transient character of this acute cytokine response.

During the early phase of inflammation, microglia reacted with a pronounced up-regulation of their spontaneous Ca^{2+}-signaling. As was shown by our group previously, during physiological conditions, the spontaneous microglial Ca^{2+}-signaling is low (Eichhoff et al. 2011; see also Pozner et al. 2015). Consistently, after PBS injections the observed fraction of spontaneously active cells was low. In contrast, under pathological conditions (i.e. after LPS injection), we observed an early (already 5 h after LPS injection) and dramatic increase in the fraction of spontaneously active microglia. These results are consistent with the study of Pozner et al. 2015, who

showed that a moderate subcutaneous dose of LPS in the lower lip of GCaMP5-expressing mice provoked increased microglial Ca^{2+}-signals 12 h after the injection (Pozner et al. 2015). Notably, the pronounced increase in microglial Ca^{2+}-signaling occurred before the morphological activation of these cells. During the later phase of inflammation, when the brain concentrations of proinflammatory cytokines largely returned to control levels, the microglial hyperactivity decreased as well. These data suggest that microglia might sense the increase in the level of the proinflammatory cytokines and signal this change in brain homeostasis to other cells via up-regulation of their Ca^{2+}-signaling and initiation of Ca^{2+}-mediated signal cascades.

4.3 Ca^{2+} mediates effector functions of microglia

In general, a rise in the intracellular Ca^{2+}-concentration can be associated with different effector functions. These functions, for example, include cytoskeletal rearrangements that are underlying changes of cell's structure like altered morphology, process extension, migration towards an injury, engulfment of particles by phagocytosis or cell proliferation (Färber and Kettenmann 2006b; Bader et al. 1994; Korvers et al. 2016; Brawek et al. 2017; Koizumi et al. 2007). In this work, we investigated *in vivo* the inflammation-mediated changes in morphology of individual microglial cells over time. Consistent with previous data (Kozlowski and Weimer 2012; Kondo, Kohsaka, and Okabe 2011), this evaluation unveiled obvious inflammation-induced alterations of the cell's morphology, occurring, however, during the later phase of inflammation. Microglia showed a gradual change of the soma volume, with a clear tendency towards increased volume, beginning 30 h after LPS injection. *Ex vivo* analysis in brain slices supported this result and affirmed the switch to a "morphologically reactive state", 30 h after the induction of inflammation. In addition to morphological changes, the presence of Ca^{2+} was shown to be linked with cell proliferation (Korvers et al. 2016). Accordingly, we observed a trend towards an increased microglial density and an obviously higher number of cell doublets during the late stage of peripheral inflammation. The literature about microglial proliferation in response to a peripheral LPS stimulation is controversial. In a study using four daily i.p. injections of LPS (1.0 mg/kg), there were no signs of proliferation of cortical microglia labeled with the thymidine analog BrdU (Z. Chen et al. 2012).

However, in another study, single i.p. injections of LPS (0.5 mg, 1mg or 2.5 mg/kg) led to a dose-dependent increase of microglial proliferation in the mouse brain 5 days after the injections (Shankaran et al. 2007). Moreover, it was shown that there might be regional differences in the proliferation of microglia after one single i.p. injection of 1.0 mg/kg LPS. 36-48 h after LPS injection, BrdU labeling revealed, an increased proliferation of microglia in the fornix and dentate gyrus, but not in the cortex and corpus callosum of mice (Fukushima et al. 2015). Thus, proliferation likely depends on the stimulus strength, the injection protocol, the time point after infection and the analyzed brain region. Nevertheless, in this work, the late stage of inflammation was characterized by increased microglial numbers and microglial cells were found in close proximity to each other. This suggests that at least a subset of cortical microglia reacted to the inflammation-induced potentiation of the intracellular Ca^{2+}-signaling with an increase in cell division.

In vitro, activation of microglia with LPS was shown to correlate with a rise in the basal intracellular Ca^{2+}-levels and the release of inflammatory mediators such as nitric oxide, IL-12, IL-6, TNF-α, or IL-1β is dependent on Ca^{2+} (Hoffmann et al. 2003; Färber and Kettenmann 2006a). Here, we observed a clear inflammation-induced up-regulation of IL-1β. The fraction of IL-1β-expressing cells started to increase already 5 h after LPS injection and reached the level of statistical significance 30 h after LPS injection. This finding suggests that IL-1β represents one of the early signals involved in the microglia-mediated brain's reaction to peripheral inflammation.

In the healthy brain, endogenous levels of inflammatory cytokines are generally low. Consistently, we did not find any IL-1β-positive cells in PBS-injected control mice. Activation of the NLRP3 inflammasome represents a common pathway leading to production of IL-1β. It is known that the formation of the NLRP3 inflammasome is regulated by intracellular Ca^{2+}-levels (Murakami et al. 2012; Lee et al. 2012). Hence, the inflammation-induced microglial Ca^{2+}-signaling reported in this study might initiate the production of microglial IL-1β through activation of the NLRP3 inflammasome. Strikingly, the LPS-mediated expression of IL-1β was restricted to Iba1-expressing cells. This suggests that microglia are the only brain cells producing significant amounts of IL-1β in response to peripheral inflammation.

Like IL-1β, CD68 is a known marker of macrophage activation. The explicit role of CD68 is under debate, but it was associated with antigen processing and

presentation as well as phagocytic function of cells (Silva and Gordon 1999; Zotova et al. 2013; Rabinowitz and Gordon 1989). Therefore, we analyzed the expression of microglial CD68 before and during peripheral inflammation. However, in our model of inflammation, we did not observe any change in the expression of CD68.

Microglia have a surveillance function within the brain and can actively shield dying cells or lesion sites with their motile processes, to protect the brain from spreading of the damage (Davalos et al. 2005; Nimmerjahn, Kirchhoff, and Helmchen 2005). This requires fast directed process movements towards the side of injury (Davalos et al. 2005; Nimmerjahn, Kirchhoff, and Helmchen 2005). Similar effects can be observed in response to a point source of ATP (Davalos et al. 2005). Here, Ca^{2+}-ions are implicated in the modulation of cytoskeletal actin dynamics, that is required for the motility of cellular processes (Bader et al. 1994, Nimmerjahn, Kirchhoff, and Helmchen 2005; Hines et al. 2009). To evaluate how a peripheral LPS injection affects this microglial surveillance function, we determined the microglial process motility towards an ATP-containing pipette. Microglia showed a clear increase of their process velocity after LPS injection. Already during the early phase of inflammation, in the absence of any obvious morphological changes of the cells, the velocity of microglial processes was increased. During the later phase, when the morphological changes started to take place, this increase became even larger and reached the level of statistical significance. These results stand in contrast to other findings, reporting impaired process movements towards a laser-induced injury in LPS-injected mice (Gyoneva et al. 2014; Pozner et al. 2015). It is known that the activation of purinergic P_2Y_{12} receptors on the microglial surface plays an important role in this type of process motility. Experiments with P_2Y_{12} knock-out mice or blockers of the P_2Y_{12} receptors revealed clearly reduced velocity of directional process movements (Haynes et al. 2006; Davalos et al. 2005). Interestingly, P_2Y_{12} receptors were also reported to be down-regulated in microglia after direct stimulation with LPS. This down-regulation was shown in cells that transformed from a ramified state to a highly morphologically activated state (Haynes et al. 2006). A down-regulation of P_2Y_{12} receptors would generally suggest a decrease of the microglial process dynamics. However, as this work revealed an obvious increase in the process velocity after LPS injection, the underlying mechanism seems to be more complex. The inconsistency in the literature about LPS-treated mice is presumably

due to differences in the experimental procedures. Microglial dynamics might change, for example, with the strength of the stimulus and the time of investigation, in respect to the time of LPS injection. In our study, for example, higher process velocity was observed 30 h after LPS injection as compared to 5 h after LPS injection. Such experimental differences can influence the activation state of microglia and thus affect their properties. Further, also the nature of the activation stimulus can explain the disparity in the results. A focal laser injury (with a lesion area of 10-15 µm) likely results in the release of different inflammatory mediators, probably activating many more different receptors than a single point source of ATP (Davalos et al., 2005). However, consistent with our data, microglia in a mouse model of epilepsy were reported to react to a pipette filled with the purinergic receptor agonist 2-methylthio-ADP with a markedly higher velocity of process movements. Furthermore, this study showed that the microglial expression of P_2Y_{12} receptors was up-regulated in their mice (Avignone, Ulmann, and Inserm 2008). Comparable results were also observed in mouse models with AD-related pathology. Highly activated cells close to amyloid-β plaques did not participate in the directed process movements towards an ATP-containing pipette, whereas morphologically less activated microglia, in a greater distance to the plaques, showed significantly increased process velocities (Brawek et al. 2014; Krabbe et al. 2013). Either way, all these findings suggest that the velocity of directed microglial process movement strongly depends on the activation state of the cells. The more the cells adopt a morphologically activated/amoeboid state, the less efficiently they can react to danger signals like ATP. This loss of process motility appears to require a given level of activation. We measured the highest process velocity 30 h after LPS injection, the time when first morphological changes were observed. Therefore, the switch of the cells towards a less dynamic state with reduced process motilities seems to be preceded by an initial phase of increased cell process motility. To our knowledge, this work is the first to report an acceleration of directed process movements during the LPS-induced peripheral inflammation. Inflammatory processes are regulated by a balance of pro and anti-inflammatory factors. During pathological conditions, as well as during the normal process of aging, microglia can adapt to the conditions and show a more reactive, so-called “primed state” (Dilger and Johnson 2008; Norden and Godbout 2013). However, during prolonged or chronic inflammatory

influences like, for example, Alzheimer`s disease, microglia can get “frustrated”, a condition characterized by, for example, a decreased phagocytic ability, altered surveillance functions with a reduced reactivity of the cells (Brawek et al. 2014; Hickman, Allison, and Khoury 2009). Thus, a reduced velocity of cell processes after LPS injection might mark the switch of microglia towards a frustrated state. As we did observe an increase in reactivity in our model of inflammation, our cells probably remained in a “primed state”.

In summary, peripheral inflammation can initiate several different effector functions of microglia in the brain. These include morphological adaptations, proliferation, cytokine expression, and altered process dynamics. All these alterations might be triggered by exaggerated microglial Ca^{2+}-signaling, taking place as early as 5 h after LPS injection.

4.4 Microglial hyperactivity requires activation of NLRP3 inflammasome

Microglia exposed to cell- or tissue injuries, as well as activated microglial cells in the vicinity of amyloid beta plaques in the brain of mice with AD-pathology, were reported to show an increased frequency of intracellular Ca^{2+}-transients (Eichhoff, Brawek, and Garaschuk 2011; Brawek et al. 2014; Pozner et al. 2015). These Ca^{2+}-signals were associated with a disturbed tissue homeostasis and minor cell or tissue damages in the microenvironment of the cells. Factors, released by damaged tissues, such as ATP, might activate metabotropic and ionotropic purinergic P2 receptors on the microglial surface and mediate either Ca^{2+}-release from intracellular stores or Ca^{2+}-influx from the extracellular space (Eichhoff, Brawek, and Garaschuk 2011; Brawek et al. 2014).

Microglia express several surface receptors for potential danger signals that enable them to sense inflammation or changes in their environment. In addition to the purinergic receptors, the latter include receptors for prostaglandins, complement factors, chemokines and proinflammatory cytokines, like TNF-α or IL-1β (Färber and Kettenmann 2006b; Färber and Kettenmann 2006a). Inflammatory conditions can lead to an up-regulation of such receptors (Choi et al. 2007; Bemelmans, Gouma, and Buurman 1993; Reinisch et al. 1994) and the activation of all of these receptors can be linked to elevated levels of $[Ca^{2+}]_i$ (T Möller et al. 1997;

Thomas Möller 2002; Färber and Kettenmann 2006b). Therefore, it is likely that the rapid increase of inflammatory mediators during the early phase of inflammation was sensed by microglia through activation of such surface receptors, and thus triggered the exaggerated Ca^{2+}-signaling of these cells.

In vitro data have shown that stimulation of murine microglial cells and astrocytes, as well as human epithelial cells and macrophages, with LPS, leads to increased levels of extracellular ATP (Ferrari et al. 1997; Pascual et al. 2012; Bodin and Burnstock 1998). Additionally, there are evidences from *in vivo* experiments that LPS stimulation promotes increased levels of extracellular ATP in the periphery and in the brain (Cauwels et al. 2014; Gourine et al. 2007). Hence, one possible mechanism leading to increased Ca^{2+}-signaling is LPS-mediated release of ATP from endothelial cells or resident cells of brain parenchyma like microglia or astrocytes. The released ATP, in turn, might be sensed by microglia through activation of P2 receptors, thereby promoting the exaggerated Ca^{2+}-signaling of microglia.

Other *in vitro* studies have shown that stimulation of microglial cell cultures with the proinflammatory cytokine TNF-α leads to increased $[Ca^{2+}]_i$. As this increase was also present in cells in a Ca^{2+}-free solution, an intracellular source of Ca^{2+} was suggested to be responsible for this cytokine-mediated increase of $[Ca^{2+}]_i$ (McLarnon et al. 2001). Similarly, application of IL-1β was reported to trigger an increase of $[Ca^{2+}]_i$ in microglial cell cultures through release of Ca^{2+} from intracellular sources (Goghari et al. 2000). Further, for IL-1β it is known that it can lead to increased $[Ca^{2+}]_i$ through activation of “alternative” signaling pathways. The “classical” pathway includes the activation of the IL-1 Type-I receptors (IL-1RI). After binding of IL-1β to IL-1RI, the IL-1RAcP receptor subunit is recruited, leading to the association of the adapter protein myeloid differentiation primary response 88 (MyD88) and the activation of the IL-1 receptor-associated protein kinase (IRAK). The formation of this protein complex finally results in the activation of the transcription factor NF-κB. In further “alternative” pathways, however, IL-1β can lead to the recruitment of the phosphatidylinositol-4,5-bisphosphate 3-kinase (IP_3K) or the activation of mitogen-activated protein kinases (MAPK) and protein kinase C (PKC), leading to increased $[Ca^{2+}]_i$ (Auron 1998; Spörri et al. 2001).

Taken together, these data suggest that also cytokines and the activation of microglial cytokine receptors can be involved in the increased Ca^{2+}-signaling during the early phase of inflammation.

However, because the current knowledge about microglial Ca^{2+}-signaling emerged predominantly from cell culture experiments and data from microglia in the intact living brain are still rare, the mechanisms that trigger microglial Ca^{2+}-signals *in vivo* are largely elusive. With this work, we were able to add another facet to the understanding of microglial Ca^{2+}-signaling in the living brain. We demonstrated for the first time a clear link between the incidence of spontaneous microglial Ca^{2+}-signals during peripheral LPS-induced inflammation and the NLRP3 inflammasome.

We found that in comparison to cells of WT mice, microglia from $NLRP3^{-/-}$ mice showed no microglial hyperactivity during the early phase of LPS-induced inflammation. This suggests that an intact NLRP3 inflammasome and likely also the concomitant production of inflammatory cytokines, like IL-1β or IL-18, seem to be essential for the inflammation-induced Ca^{2+}-signaling in microglia.

As many different stimuli are leading to inflammasome activation, the NLRP3 inflammasome is known as a sensor of cellular damage or stress (Walsh, Muruve, and Power 2014). It can get activated by harmful stimuli, such as amyloid beta, viral, fungal and bacterial components, by K^+-efflux from microglia, induced, for example, by extracellular stimulation with ATP, by reactive oxygen species (ROS), lysosomal destabilization or mitochondrial damage (Walsh, Muruve, and Power 2014; Murakami et al. 2012). Activation of NLRP3 inflammasome is usually preceded by a priming stimulus (e.g. bacterial LPS), leading to the activation of PAMPs and the subsequent transcription of NLRP3 protein complex subunits and cytokine precursors. Then, a second stimulus such as extracellular ATP or Ca^{2+} triggers the NLRP3 protein complex formation and the maturation and release of the proinflammatory cytokines. Due to the large variability of the stimuli leading to NLRP3 inflammasome activation, there is no general mechanism underlying the activation of NLRP3 inflammasomes.

However, a study analyzing ATP-stimulated macrophages *in vitro* suggested that activation of the NLRP3 inflammasome is mediated by P2 receptors and involves Ca^{2+}-mobilization from intracellular as well as from extracellular sources (Murakami et al. 2012). The study revealed by application of pharmaceutical blockers

that the NLRP3 inflammasome activation is regulated by pathways including the activation of phospholipase C (PLC) and inositol trisphosphate (IP_3), leading to Ca^{2+}-release from the endoplasmic reticulum (ER), as well as by a pathway activating store-operated calcium channels (SOC). The increased levels of Ca^{2+} were hereby further linked to damages of mitochondria and a concomitant activation of the NLRP3 inflammasome (Murakami et al. 2012). That NLRP3 inflammasome activation is mediated by Ca^{2+}-release from the ER was substantiated by another study. The authors proposed that ATP or extracellular Ca^{2+} bind to calcium-sensing receptors (CASR) on the surface of microglia. This binding activates PLC through G-protein-coupled receptors, with the result of an IP_3-mediated Ca^{2+}-release from the ER. The increased level of Ca^{2+}, then, activates the NLRP3 complex and triggers the caspase 1 dependent maturation of IL-1β (Lee et al. 2012). According to this, it seems clear that the inflammasome activation is regulated by intracellular Ca^{2+}-signals. However, to our knowledge, the idea that a depletion of the NLRP3 inflammasome is inhibiting microglial Ca^{2+}-signaling has not been reported before.

Due to the fact that systemic injection of LPS led to a strong up-regulation of inflammatory cytokines in our mice, it is reasonable to speculate that LPS injection also might have triggered the up-regulation of potential inflammasome activators, like extracellular ATP or Ca^{2+}. Such activators could have stimulated CASRs or P2 receptors on the microglial surface, resulting in a Ca^{2+}-dependent activation of the NLRP3 inflammasome. The initiated maturation and release of IL-1β might have triggered an autocrine feedback loop, activating microglial IL-1β receptors and thereby further increasing the Ca^{2+}-signaling of microglia during inflammation.

Interestingly, and in contrast to the NLRP3$^{-/-}$ mice, the inflammatory Ca^{2+}-signals of microglia in TNF-α$^{-/-}$ mice did not differ from the respective Ca^{2+}-signals in WT mice. This leads to the conclusion, that even if application of TNF-α in microglial cell cultures leads to increased levels of intracellular Ca^{2+} *in vitro* (McLarnon et al. 2001), microglia *in vivo* behave differently and the cytokine TNF-α seems to play a less important role for microglial hyperactivity during inflammation.

However, to further analyze the origin of microglial Ca^{2+}-signals we measured the serum and brain cytokine levels of the respective the knock-out mice. Compared to WT mice, 5 h after LPS injection NLRP3$^{-/-}$ mice showed significantly lower

IL-1β levels in the periphery, but just a trend towards lower levels in the brain. The presence of measurable IL-1β levels in these mice suggests that there must be additional NLRP3-independent mechanisms of IL-1β production. Even if in our experiments, 100 % of the IL-1β-expressing cells in WT mice were Iba1-positive (i.e. microglia), we cannot rule out different sources or pathways of IL-1β production in the NLRP3$^{-/-}$ mice. Such pathways might include the cleavage of pro-IL-1β into its active form by the action of serine- or metalloproteases derived from neutrophils and macrophages (Cassel et al. 2014; Lukens et al. 2014; Netea et al. 2015). Another option would be the activation of different inflammasome complexes. A relatively strong LPS stimulus in mice was, for example, shown to up-regulate the NLRP1 inflammasome expression in neurons, leading to caspase 1 activation and the production of IL-1β (Kaushal et al. 2015). Moreover, in addition to the reduced levels of IL-1β, the NLRP3$^{-/-}$ mice were characterized by a general trend towards decreased cytokine levels during the early phase of inflammation. Solely the level of TNF-α in the blood of these mice was significantly higher than in WT mice, suggesting a compensatory increase of this cytokine. However, as we did not observe significant differences in the LPS-induced Ca^{2+}-signals between WT and TNF-α$^{-/-}$ mice, this compensatory increase of TNF-α protein seems to be irrelevant for microglial Ca^{2+}-signaling.

A similar tendency to lower cytokine levels was observed in the TNF-α$^{-/-}$ mice. This fact is not surprising, taking into account that the cytokine production is often regulated by complex cascades of reciprocal interactions (Amiot et al. 1997). Surprisingly, some of the TNF-α$^{-/-}$ mice had measurable levels of TNF-α protein in the blood serum after injection of LPS. One possible explanation might be a strong LPS-induced up-regulation of soluble TNF-α receptors in these mice, interfering with the ELISA-antibodies, as it was already shown for WT mice (Bemelmans et al., 1993). The brains of TNF-α$^{-/-}$ mice, as expected, did not contain any measurable amounts of TNF-α protein. Although the inflammatory cytokines were elevated under inflammatory conditions compared to PBS controls, the cytokine responses were generally reduced in both knock-out strains. Since we observed an inflammation-induced microglial hyperactivity in the TNF-α$^{-/-}$ mice, but not in the NLRP3$^{-/-}$ mice, it seems rather unlikely, that the general reduction in the level of cytokines (present in both knock-out strains) is responsible for the absence of microglial Ca^{2+}-signals in the

NLRP3$^{-/-}$ mice. This suggests that microglial hyperactivity is mediated to a large extent by activation of the NLRP3 inflammasome. However, as the fraction of active cells in TNF-α$^{-/-}$ mice during inflammation seemed to be slightly decreased compared to WT mice, it is probably a combination of both, the NLRP3 inflammasome activation and the action of inflammatory cytokines contributing to the microglial hyperactivity during systemic LPS infection.

Taken together, in the periphery as well as in the brain, cytokines had their highest expression during the early phase of inflammation. At this time point, the spontaneous activity in microglia was the highest. Thus, microglial Ca^{2+}-signals can serve as a sensor or an early marker of inflammation. In mice without functional NLRP3 inflammasome, microglia were not able to increase their Ca^{2+}-signaling after stimulation with LPS. In WT mice, the late stage of peripheral inflammation was accompanied by morphological changes of microglia, higher process motilities and microglial IL-1β production, all representing the effector functions of these immune cells. We hypothesize that the NLRP3 inflammasome operates as a Ca^{2+}-dependent sensor of inflammation-induced stress factors, promoting microglial hyperactivity. The heightened Ca^{2+}-signaling, in turn, might trigger the metamorphosis of microglia from the initial “surveillance” state towards the late “effector” state during peripheral inflammation.

4.5 Inflammation induces neuronal hyperactivity in different parts of the cortical network

Like microglia, neurons showed a clear response to peripheral inflammation. LPS induced a pronounced hyperactivity of Ca^{2+}-signaling in cortical neurons. Similar to microglial cells, the neurons showed their strongest response to LPS during the early phase of inflammation (5 h after LPS injection). At later time points, the frequency of Ca^{2+}-signals started to decrease and finally returned to the baseline. This implicates, that also neurons have a certain sensor function, recognizing changes in the concentration of stress factors like ATP or a strong up-regulation of inflammatory mediators in the organism.

We observed increased spontaneous neuronal Ca^{2+}-signaling in different parts of the neural network in the motor cortex. Thus, increases in Ca^{2+}-signaling were present postsynaptically, in the somata of layer 2/3 pyramidal neurons. Using independent

component analysis (ICA), we separated a subpopulation of these neurons with asynchronous Ca^{2+}-signals. Also, this subpopulation showed a reliable increase in frequency of somatic Ca^{2+}-transients 5 h after LPS injection when compared to PBS-injected controls. Stimulation of GCaMP6f-labeled murine neuronal cell cultures with different cytokines such as TNF-α, IFN-y or IL-1β was recently reported to increase the synchronicity of Ca^{2+}-signals in neurons (Clarkson et al. 2017). Because a peripheral LPS injection studied here leads to the up-regulation of such proinflammatory mediators in the brain, it is likely that this treatment increased the synchronicity of the neuronal network activity. As ICA removes all cells active synchronously with the neuropil (and usually also with each other), this can explain a strong LPS-induced increase in the fraction of silent cells, as observed in our experiments. In contrast to increased frequency of somatic Ca^{2+}-transients, we did not observe an increase in frequency of Ca^{2+}-transients in the neuropil. Instead, we observed a significant increase in the amplitude of the neuropil Ca^{2+}-signals after LPS injection. The cortical neuropil was reported to consist to > 50 % of axons and presynaptic boutons, to around 30 % of dendrites and dendritic spines, to 10 % of glial processes, and to another 10 % of other structures like extracellular space (Chklovskii, Schikorski, and Stevens 2002). As we used a neuron-specific viral vector to deliver GCaMP6f into the cells, a glial contribution to the neuropil Ca^{2+}-signal can be neglected. Nevertheless, as GCaMP6f labels both, axonal and dendritic structures, a clear discrimination of the source of the neuropil Ca^{2+}-signal was not possible.

Among others, apical dendrites of layer 2/3 cortical neurons in the motor cortex get inputs from cells of deeper cortical layers (Shepherd et al. 2005). To gain insights into the local circuitry, we proved in another set of experiments that the inflammation-induced increase in Ca^{2+}-signaling was also present in the presynaptic partners of the layer 2/3 cells. Axons arising from motor cortical neurons of layer 5, revealed a clearly increased frequency of Ca^{2+}-transients 5 h after LPS injection. Further, as we observed a tendency to increased amplitudes in these axonal projections, it is likely that the increased amplitudes of Ca^{2+}-transients observed in the neuropil, can be attributed to the signaling in presynaptic axonal structures. Interestingly, although the somatosensory cortex and the motor cortex are strongly interconnected (Donoghue and Parham 1983; Kaneko, Caria, and Asanuma 1994; B. M.

Hooks et al. 2011; Mao et al. 2011), we did not observe any increase in the frequency of Ca^{2+}-transients in axons from the somatosensory cortex. As the somatosensory cortex is relevant for the signal transmission during pain (Backonja 1996; Bushnell et al. 1999), it is rather unlikely that inflammation-induced pain was modifying the neuronal Ca^{2+}-signaling in our experiments.

However, the results imply that there is a specific pathway modulating the neuronal activity during inflammation. It could be either a rather local inflammatory signal transfer or a signal transmission arising from deeper regions of the brain, like the thalamus. The motor cortex lacks a distinctly visible cortical layer 4. However, a laminar zone on the border of layer 5 was reported to provide similar functions, with excitatory inputs from the thalamus and excitatory outputs to layer 2/3 neurons (Yamawaki et al. 2014; Bryan M. Hooks et al. 2013). The fact that we measured a significant increase in Ca^{2+}-signaling in neurons of the motor cortical layer 5 would support the hypothesis that our inflammatory signal might have its origin in thalamic regions. In contrast, signal transmission through lateral long-range connections, at least from the somatosensory areas, seems rather unlikely.

4.6 Neuronal hyperactivity critically depends on TNF-α

So far, the mechanisms underlying inflammation-induced neuronal network hyperactivity are not clear. Several studies have provided evidence that the release of inflammatory mediators, as the one initiated by stimulation with LPS in this study, is linked to the increased excitability of neurons. Increased levels of CCL2, IL-1β or TNF-α, for example, were linked to greater susceptibility of rodents to seizures (Samland et al. 2003; Cerri et al. 2016; Vezzani et al. 2002; Riazi et al. 2008). Furthermore, for example, the action of IL-6 was reported to increase the neuronal activity in rats, as measured by *in vivo* electrophysiological recordings after i.p. injection of LPS (Palin et al. 2009). And CCL2, IL-1β, and TNF-α were also shown to enhance the function of NMDA receptors, leading to higher neuronal activities (Zhou et al. 2011; Wheeler et al. 2009; Viviani et al. 2003). Especially the proinflammatory cytokine TNF-α appears to play a major role in the heightened neuronal signaling during inflammation. It was reported that application of TNF-α to hippocampal slices results in an increase of excitatory and a decrease of inhibitory

synaptic transmission. This process was assumed to be regulated by trafficking of AMPA and $GABA_A$ receptors (Stellwagen et al., 2005).

Our data show that compared to WT mice, basal spontaneous Ca^{2+}-signaling of TNF-$\alpha^{-/-}$ mice remained unchanged. Moreover, TNF-$\alpha^{-/-}$ mice did not react with neuronal hyperactivity to induction of peripheral inflammation. Thus, TNF-α seems to be an important modulator of neuronal Ca^{2+}-signaling under inflammatory conditions. This stands in contrast to the results obtained from microglial cells. Also, the dysfunction of the NLRP3 inflammasome had less impact on the spontaneous neuronal Ca^{2+}-signaling during inflammation than in microglia. Peripheral injections of LPS did not result in a significant increase in Ca^{2+}-signaling in neurons of NLRP3$^{-/-}$ mice. However, the lack of inflammation-induced increase in the frequency of Ca^{2+}-transients in NLRP3$^{-/-}$ mice was probably due to a higher basal spontaneous Ca^{2+}-signaling in these mice. This higher basal spontaneous Ca^{2+}-signaling might have led to an occlusion effect so that the relative change in frequency did not reach the level of statistical significance. The reason for higher basal spontaneous Ca^{2+}-signaling in neurons of these mice remains unknown. As the NLRP3 inflammasome is mainly expressed in microglia, a malfunction of these cells with a disrupted communication between microglia and neurons might be involved.

4.7 LPS-induced inhibition of GABAergic neurons promotes neuronal hyperactivity

Usually, the brain activity is balanced by the activation of excitatory glutamatergic and inhibitory GABAergic neurons. Focusing on GABAergic cells during inflammation, revealed that the excitatory effect of LPS was absent in this cell type. Moreover, inhibitory cells responded with a clear reduction in the frequency of their Ca^{2+}-transients 5 h after LPS injection. This indicates that the overall increase in spontaneous Ca^{2+}-signaling observed in the GCaMP6-labeled neurons of layer 2/3 can be attributed to a reduced GABAergic inhibition of the local network. In addition to the already mentioned potential TNF-α-mediated change in $GABA_A$ receptor trafficking (Stellwagen et al., 2005), LPS-activated microglia were reported to specifically displace inhibitory GABAergic synapses in the rodent motor cortex thereby leading to an increased neuronal activity (Z. Chen et al. 2014a). Further, in GCaMP6-labeled neuronal cell cultures, the presence of Interferon-γ (IFN-γ), IL-1β

and TNF-α was shown to induce synchronous firing of neurons. Especially the action of IL-1β was hereby assumed to mediate this synchronicity, probably through inhibition of inhibitory GABAergic cells (Clarkson, et al., 2017).

Hence, the activation of cytokine-producing cells in combination with the presence of inflammatory cytokines like TNF-α might have changed the balance of excitation and inhibition in the network, resulting in increased Ca^{2+}-signaling of excitatory neurons.

Taken together, neurons are able to sense peripheral inflammation. A malfunction of the NLRP3 inflammasome in microglia, with a concomitant hampered production of IL-1β and IL-18, mainly leads to an increased basal spontaneous Ca^{2+}-signaling in neurons. A deficiency of TNF-α production, instead, clearly impairs neuronal hyperactivity during inflammation. This suggests a TNF-α-mediated mechanism underlying the excitatory LPS effect in neurons. Additionally, inhibitory GABAergic cells show a reduced frequency of spontaneous Ca^{2+}-transients after LPS injection, presumably promoting the overall excitatory effect of LPS.

4.8 Neuronal hyperactivity is independent of microglia

Our results revealed how microglia and neurons react individually to a moderate peripheral inflammatory stimulus. The question that remained was how these cells interact with each other. The view that microglia are important partners of neurons in the at least “quad-partite synapse” is meanwhile accepted (Schafer, Lehrman, and Stevens 2013). Microglia can release various factors to actively shape the neuronal activity and several publications emphasized the great importance of microglia during different inflammatory conditions like epilepsy, ischemia, Alzheimer`s or Parkinson`s disease etc. (Streit, Mrak, and Griffin 2004; Hanisch and Kettenmann 2007). In this respect, it is very surprising that the inflammation-induced neuronal hyperactivity seems to be independent of microglial cells. So far, how the presence of microglia shapes the neuronal activity is not entirely clear. Strikingly, previous studies reported, that a complete depletion of microglia from the brain, namely the removal of 5-12 % of all brain cells (Lawson et al., 1990), resulted in no obvious signs of cognitive impairments in mice (Elmore et al. 2014; Acharya et al. 2016). Further studies demonstrated that the depletion of microglia is correlated with a reduced loss of dendritic spines and neurons in mouse models of Alzheimer`s disease. Thus, the lack of microglia might even result in an improved memory and increased cognitive

abilities of mice with AD pathology (Spangenberg et al. 2016). This implicates a rather detrimental role of microglia under chronic inflammatory circumstances like during Alzheimer's disease.

Another work, in contrast, emphasized the protective role of microglial cells. It revealed that microglial depletion increased the severity of acute brain injury in mice after cerebral ischemia (Szalay et al. 2016). Interestingly, this study also revealed that the absence of microglia prevented KCl-induced occurrence of “spreading depolarizations” in ischemic as well as in non-ischemic brains. These results are rather surprising and somehow contradictive to the protective role of microglia, because “spreading depolarizations” are generally known to occur under pathological conditions, like after ischemia and are associated with the facilitation of neuronal cell death. The authors claimed that the absence of microglia resulted hereby in a somehow dysregulated Ca^{2+}-response in neurons leading to an increased neuronal death under the ischemic conditions.

How microglia influence the neuronal Ca^{2+}-signaling is generally not well understood. However, we can confirm with our *in vivo* results, that absence of microglia is associated with a changed neuronal activity. Furthermore, we provided different insights how the removal of microglia affects the murine brain. First, we showed, that microglial depletion leads to a general reduction of the basal spontaneous Ca^{2+}-signaling in neurons. Even if we did not observe obvious behavioral changes in microglia-depleted mice, there was a clear “silencing effect” on the neuronal network activity. Second, we found that depletion of microglia played no role in the neuronal hyperactivity during peripheral inflammation. Hence, despite the absence of the main immune cells of the brain, the neuronal network was able to react to a peripheral inflammation with an increased Ca^{2+}-signaling. This leads to the assumption, that at least the inflammation-induced neuronal Ca^{2+}-signaling is regulated through a yet unknown microglia-independent mechanism. During inflammation, microglia classically have been considered to be the main source of proinflammatory cytokines like TNF-α in the CNS (Olmos and Lladó 2014). However, the fact that we observed no LPS-induced Ca^{2+}-signaling increase in neurons of TNF-$\alpha^{-/-}$ mice, but a clear hyperactivity in microglia-depleted mice, hints that TNF-α or other inflammatory factors from different sources might have mediated this effect. The presence of astrocytes, for example, was reported not to be affected after CSF-1 receptor

inhibition. Thus, one possible mechanism is that astrocytes produced proinflammatory mediators. This, in turn, might have led to the increased spontaneous neuronal Ca^{2+}-signaling in excitatory neurons after LPS injection.
Even though, this work provided multiple pieces of evidence how particular *in vivo* brain cells react to a moderate inflammatory insult, more experiments would be needed to get a complete picture of the underlying mechanisms of the complex interactions between the brain cells and their hyperactivity during peripheral inflammation.

4.9 Conclusion

Based on the findings of this work, I propose following mechanisms how peripheral inflammation affects the *in vivo* functional properties of the cortical neural network (see Figure 32):
Early after a moderate bacterial infection in the periphery, the cytokine levels in the blood increase dramatically. This increase is paralleled by a concomitant rise of cytokines within the brain. Microglia and neurons individually sense the up-regulation of the inflammatory mediators and possible changes in the tissue homeostasis. Both cell types have hereby in common, that they react with a pronounced hyperactivity.
In neurons, it is especially the proinflammatory cytokine TNF-α, which is responsible for the inflammation-induced increase in Ca^{2+}-signaling. Further, the hyperactivity appears mainly to be a feature of excitatory neurons. TNF-α, probably in combination with other inflammatory factors might promote the increased neuronal excitation through inhibiting GABAergic interneurons.
In contrast to neurons, the microglial Ca^{2+}-signals seem to be less dependent on the action of TNF-α. The hyperactivity of microglia is rather regulated through the activation of the NLRP3 inflammasome complex and an increase in the level of proinflammatory cytokines. The NLRP3 inflammasome might function hereby as a Ca^{2+}-dependent sensor of inflammation-induced stress factors (i.e. ATP). After sensing these factors, it might promote microglial Ca^{2+}-signaling in an autocrine loop, by initiating the secretion of further inflammatory factors as IL-1β or IL-18.
Different effector functions of microglia can be linked to intracellular Ca^{2+}-signals. Therefore, the pronounced Ca^{2+}-signaling in microglia during inflammation might trigger the microglial switch from an early “sensor state” to a late “effector state” of

the cells. In this late state, microglia react with cytoskeletal rearrangements, leading to an activated morphology, an increase of cell proliferation or higher process reactivity, to actively fight the danger of inflammation.

Interestingly, basal spontaneous Ca^{2+}-signaling in neurons is dependent on the activation of the NLRP3 inflammasome complex, which is mainly expressed in microglial cells. A malfunction of the NLPR3 inflammasome complex results in a pronounced increase in Ca^{2+}-signaling of neurons.

In contrast, blocking the communication of microglia and neurons by complete removal of microglial cells from the brain results in silencing of the neuronal Ca^{2+}-signaling. Remarkably, the inflammation-induced hyperactivity seems to be independent of the presence of microglia.

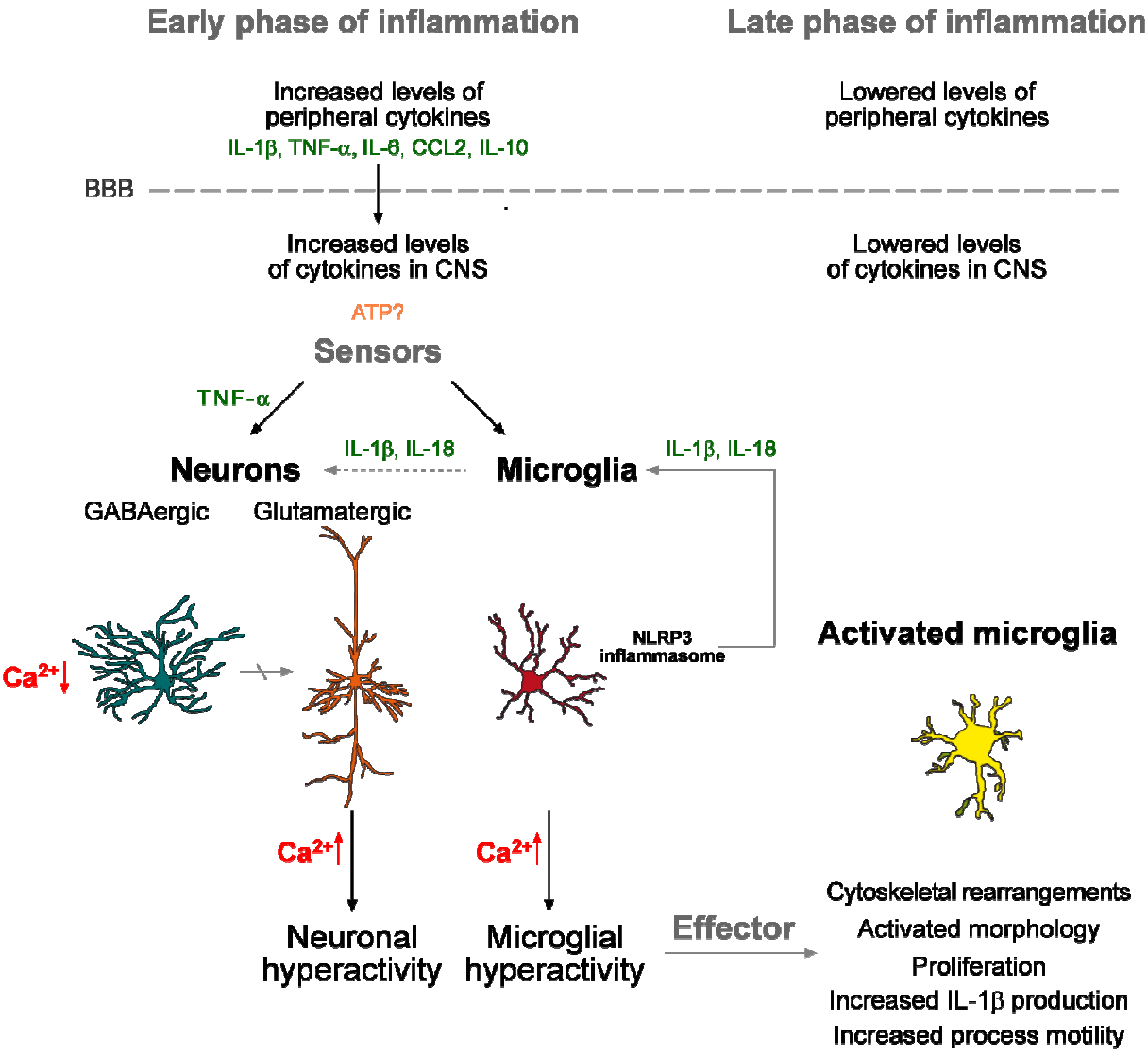

Figure 32 Effects of peripheral inflammation on *in vivo* functional properties of cortical networks

A peripheral inflammation in mice, induced by i.p. injections of bacterial LPS has different effects on the *in vivo* functional properties of different elements of cortical networks. The inflammation can be classified into two phases. During the early phase, there is a prominent increase in the level of different cytokines (IL-1β, TNF-α, IL-6, CCL-2 or IL-10) in the periphery. This inflammatory cytokine signal from the periphery is transmitted over the blood-brain barrier (BBB) and leads to a mirrored cytokine response within the central nervous system (CNS). During this phase, neurons and microglia act as sensors, sensing the increased level of cytokines or other released inflammatory mediators as, for example, adenosine triphosphate (ATP). Subsequently, both cell types show markedly increased Ca^{2+}-signaling (hyperactivity). The hyperactivity of neurons is hereby a feature of glutamatergic neurons. They are able to sense and react to the inflammation in a TNF-α-dependent mechanism. In contrast, inhibitory neurons show reduced Ca^{2+}-signaling, and the reduced inhibition is probably promoting the excitation of glutamatergic neurons.

The hyperactivity of microglia is dependent on the NLRP3 inflammasome. The activation of the NLRP3 inflammasome is Ca^{2+}-dependent. It is responsible for the maturation of IL-1β and IL-18, which, in turn, might promote the strong Ca^{2+}-signaling in microglia. Microglia can shape the activity of neurons in different ways. Neurons react to the absence of the microglial NLRP3 inflammasome and the presumed concomitant reduction of IL-1β and IL-18 with an increased basal Ca^{2+}-signaling. A complete depletion of microglia, in turn, results in a reduced basal Ca^{2+}-signaling in neurons. Remarkably, despite the lack of microglia, neurons still sense the inflammation and react with hyperactivity.

The late phase of inflammation is characterized by reduced levels of inflammatory mediators in the periphery and in the CNS. Ca^{2+} in microglia is associated with different effector functions of cells. Their increased Ca^{2+}-signaling during the early phase leads to a switch from the “sensor function” to the “effector function”. During the late phase, microglia show cytoskeletal rearrangements, an activated morphology, a higher rate of proliferation, enhanced IL-1β-expression and accelerated process velocity.

5. References

Acharya, Munjal M., Kim N. Green, Barrett D. Allen, Allison R. Najafi, Amber Syage, Harutyun Minasyan, Mi T. Le, et al. 2016. “Elimination of Microglia Improves Cognitive Function Following Cranial Irradiation.” *Scientific Reports* 6 (July): 1–11. doi:10.1038/srep31545.

Albiger, B., S. Dahlberg, B. Henriques-Normark, and S. Normark. 2007. “Role of the Innate Immune System in Host Defence against Bacterial Infections: Focus on the Toll-like Receptors.” *Journal of Internal Medicine* 261 (6): 511–28. doi:10.1111/j.1365-2796.2007.01821.x.

Álvarez-Rodríguez, Lorena, Marcos López-Hoyos, Pedro Muñoz-Cacho, and Víctor Manuel Martínez-Taboada. 2012. “Aging Is Associated with Circulating Cytokine Dysregulation.” *Cellular Immunology* 273 (2): 124–32. doi:10.1016/j.cellimm.2012.01.001.

Amiot, F, C Fitting, K J Tracey, J M Cavaillon, and F Dautry. 1997. “Lipopolysaccharide-Induced Cytokine Cascade and Lethality in LT Alpha/TNF Alpha-Deficient Mice.” *Molecular Medicine (Cambridge, Mass.)* 3 (12): 864–75.

Askew, Katharine, Kaizhen Li, Adrian Olmos-Alonso, Fernando Garcia-Moreno, Yajie Liang, Philippa Richardson, Tom Tipton, et al. 2017. “Coupled Proliferation and Apoptosis Maintain the Rapid Turnover of Microglia in the Adult Brain.” *Cell Reports* 18 (2): 391–405. doi:10.1016/j.celrep.2016.12.041.

Auron, P E. 1998. “The Interleukin 1 Receptor: Ligand Interactions and Signal Transduction.” *Cytokine & Growth Factor Reviews* 9 (3–4): 221–37. doi:10.1016/s1359-6101(98)00018-5.

Avignone, Elena, Lauriane Ulmann, and U Inserm. 2008. “Status Epilepticus Induces a Particular Microglial Activation State Characterized by Enhanced Purinergic Signaling” 28 (37): 9133–44. doi:10.1523/JNEUROSCI.1820-08.2008.

Backonja, Misha-Miroslav. 1996. “Primary Somatosensory Cortex and Pain Perception: Yes Sir, Your Pain Is in Your Head (Part I).” *Pain Forum* 5 (3). American Pain Society: 174–80. doi:10.1016/S1082-3174(96)80026-2.

Bader, Marie-France -F, Laurent Taupenot, Gabrielle Ulrich, Dominique Aunis, and Jaroslava Ciesielski-Treska. 1994. “Bacterial Endotoxin Induces [Ca2+]i Transients and Changes the Organization of Actin in Microglia.” *Glia* 11 (4): 336–44. doi:10.1002/glia.440110406.

Ban, E., G. Milon, N. Prudhomme, G. Fillion, and F. Haour. 1991. “Receptors for Interleukin-1 (α and β) in Mouse Brain: Mapping and Neuronal Localization in Hippocampus.” *Neuroscience* 43 (1): 21–30. doi:10.1016/0306-4522(91)90412-H.

Basu, Anirban, J. Kyle Krady, and Steven W. Levison. 2004. “Interleukin-1: A Master Regulator of Neuroinflammation.” *Journal of Neuroscience Research* 78 (2): 151–56. doi:10.1002/jnr.20266.

Bemelmans, M H, D J Gouma, and W A Buurman. 1993. “LPS-Induced STNF-Receptor Release in Vivo in a Murine Model. Investigation of the Role of Tumor Necrosis Factor, IL-1, Leukemia Inhibiting Factor, and IFN-Gamma.” *Journal of Immunology (Baltimore, Md. : 1950)* 151 (10): 5554–62.

Berridge, M J, P Lipp, and M D Bootman. 2000. “The Versatility and Universality of Calcium Signalling.” *Nature Reviews. Molecular Cell Biology* 1 (1): 11–21. doi:10.1038/35036035.

Biber, Knut, Harald Neumann, Kazuhide Inoue, and Hendrikus W.G.M. Boddeke. 2007. “Neuronal ‘On’ and ‘Off’ Signals Control Microglia.” *Trends in Neurosciences* 30 (11): 596–602. doi:10.1016/j.tins.2007.08.007.

Bicks, Lucy K., Hiroyuki Koike, Schahram Akbarian, and Hirofumi Morishita. 2015. “Prefrontal Cortex and Social Cognition in Mouse and Man.” *Frontiers in Psychology* 6 (NOV): 1–15. doi:10.3389/fpsyg.2015.01805.

Bodin, P., and G. Burnstock. 1998. “Increased Release of ATP from Endothelial Cells during Acute Inflammation.” *Inflammation Research* 47 (8): 351–54.

doi:10.1007/s000110050341.

Brawek, Bianca, and Olga Garaschuk. 2013. “Microglial Calcium Signaling in the Adult, Aged and Diseased Brain.” *Cell Calcium* 53 (3): 159–69. doi:10.1016/j.ceca.2012.12.003.

———. 2017. “Monitoring in Vivo Function of Cortical Microglia.” *Cell Calcium* 64. Elsevier Ltd: 109–17. doi:10.1016/j.ceca.2017.02.011.

Brawek, Bianca, Yajie Liang, Daria Savitska, Kaizhen Li, Natalie Fomin-thunemann, Yury Kovalchuk, Elizabeta Zirdum, Johan Jakobsson, and Olga Garaschuk. 2017. “A New Approach for Ratiometric in Vivo Calcium Imaging of Microglia.” *Scientific Reports*. Springer US, 1–13. doi:10.1038/s41598-017-05952-3.

Brawek, Bianca, Bernd Schwendele, Karin Riester, Shinichi Kohsaka, Chommanad Lerdkrai, Yajie Liang, and Olga Garaschuk. 2014. “Impairment of in Vivo Calcium Signaling in Amyloid Plaque-Associated Microglia.” *Acta Neuropathologica* 127 (4): 495–505. doi:10.1007/s00401-013-1242-2.

Brionne, Thomas C, Ina Tesseur, Eliezer Masliah, and Tony Wyss-Coray. 2003. “Loss of TGF-Beta 1 Leads to Increased Neuronal Cell Death and Microgliosis in Mouse Brain.” *Neuron* 40 (6): 1133–45. doi:10.1016/S0896-6273(03)00766-9.

Busche, Marc Aurel, Gerhard Eichhoff, Helmuth Adelsberger, Dorothee Abramowski, Karl-Heinz Wiederhold, Christian Haass, Matthias Staufenbiel, Arthur Konnerth, and Olga Garaschuk. 2008. “Clusters of Hyperactive Neurons near Amyloid Plaques in a Mouse Model of Alzheimer’s Disease.” *Science (New York, N.Y.)* 321 (5896): 1686–89. doi:10.1126/science.1162844.

Bushnell, M C, G H Duncan, R K Hofbauer, B Ha, J I Chen, and B Carrier. 1999. “Pain Perception: Is There a Role for Primary Somatosensory Cortex?” *Proceedings of the National Academy of Sciences of the United States of America* 96 (14): 7705–9. doi:10.1073/pnas.96.14.7705.

Cardona, Astrid E, Erik P Pioro, Margaret E Sasse, Volodymyr Kostenko, Sandra M Cardona, Ineke M Dijkstra, DeRen Huang, et al. 2006. “Control of Microglial Neurotoxicity by the Fractalkine Receptor.” *Nature Neuroscience* 9 (7): 917–24. doi:10.1038/nn1715.

Cassel, S. L., J. R. Janczy, X. Bing, S. P. Wilson, A. K. Olivier, J. E. Otero, Y. Iwakura, et al. 2014. “Inflammasome-Independent IL-1 Mediates Autoinflammatory Disease in Pstpip2-Deficient Mice.” *Proceedings of the National Academy of Sciences* 111 (3): 1072–77. doi:10.1073/pnas.1318685111.

Cauwels, A., E. Rogge, B. Vandendriessche, S. Shiva, and P. Brouckaert. 2014. “Extracellular ATP Drives Systemic Inflammation, Tissue Damage and Mortality.” *Cell Death and Disease* 5 (3). Nature Publishing Group: e1102-7. doi:10.1038/cddis.2014.70.

Cerri, C., S. Genovesi, M. Allegra, F. Pistillo, U. Puntener, A. Guglielmotti, V. H. Perry, Y. Bozzi, and M. Caleo. 2016. “The Chemokine CCL2 Mediates the Seizure-Enhancing Effects of Systemic Inflammation.” *Journal of Neuroscience* 36 (13): 3777–88. doi:10.1523/JNEUROSCI.0451-15.2016.

Chen, Tsai-wen, Trevor J Wardill, Yi Sun, Stefan R Pulver, Sabine L Renninger, Amy Baohan, Eric R Schreiter, et al. 2013. “Ultrasensitive Fluorescent Proteins for Imaging Neuronal Activity.” *Nature* 499: 295–300. doi:10.1038/nature12354.

Chen, Zhihong, Walid Jalabi, Weiwei Hu, Hyun-Joo Park, John T Gale, Grahame J Kidd, Rodica Bernatowicz, et al. 2014a. “Microglial Displacement of Inhibitory Synapses Provides Neuroprotection in the Adult Brain.” *Nature Communications* 5 (July). Nature Publishing Group: 4486. doi:10.1038/ncomms5486.

Chen, Zhihong, Walid Jalabi, Karl B Shpargel, Kenneth T Farabaugh, Ranjan Dutta, Xinghua Yin, Grahame J Kidd, Cornelia C Bergmann, Stephen a Stohlman, and Bruce D Trapp. 2012. “Lipopolysaccharide-Induced Microglial Activation and Neuroprotection against Experimental Brain Injury Is Independent of Hematogenous TLR4.” *The Journal of Neuroscience : The Official Journal of the Society for Neuroscience* 32 (34): 11706–15. doi:10.1523/JNEUROSCI.0730-12.2012.

Chklovskii, Dmitri B., Thomas Schikorski, and Charles F. Stevens. 2002. “Wiring Optimization in Cortical Circuits.” *Neuron* 34 (3): 341–47. doi:10.1016/S0896-6273(02)00679-7.

Choi, Hyun B., Jae K. Ryu, Seung U. Kim, and James G. McLarnon. 2007. “Modulation of the Purinergic P2X7 Receptor Attenuates Lipopolysaccharide-Mediated Microglial Activation and Neuronal Damage in Inflamed Brain.” *Journal of Neuroscience* 27 (18): 4957–68. doi:10.1523/JNEUROSCI.5417-06.2007.

Clarkson, Benjamin D.S., Robert J. Kahoud, Christina B. McCarthy, and Charles L. Howe. 2017. “Inflammatory Cytokine-Induced Changes in Neural Network Activity Measured by Waveform Analysis of High-Content Calcium Imaging in Murine Cortical Neurons.” *Scientific Reports* 7 (1). Springer US: 1–13. doi:10.1038/s41598-017-09182-5.

Czapski, Grzegorz A., Magdalena Cakala, Malgorzata Chalimoniuk, Barbara Gajkowska, and Joanna B. Strosznajder. 2007. “Role of Nitric Oxide in the Brain during Lipopolysaccharide-Evoked Systemic Inflammation.” *Journal of Neuroscience Research* 85 (April): 1694–1703. doi:10.1002/jnr.21294.

Dagher, Nabil N., Allison R. Najafi, Kara M. Neely Kayala, Monica R. P. Elmore, Terra E. White, Rodrigo Medeiros, Brian L. West, and Kim N. Green. 2015. “Colony-Stimulating Factor 1 Receptor Inhibition Prevents Microglial Plaque Association and Improves Cognition in 3xTg-AD Mice.” *Journal of Neuroinflammation* 12 (1). Journal of Neuroinflammation: 139. doi:10.1186/s12974-015-0366-9.

Dantzer, R. 2009. “Cytokine, Sickness Behaviour, and Depression.” *Immunology and Allergy Clinics of North America* 29 (2): 247–64. doi:10.1016/j.iac.2009.02.002.Cytokine.

Davalos, Dimitrios, Jaime Grutzendler, Guang Yang, Jiyun V Kim, Yi Zuo, Steffen Jung, Dan R Littman, Michael L Dustin, and Wen-Biao Gan. 2005. “ATP Mediates Rapid Microglial Response to Local Brain Injury in Vivo.” *Nature Neuroscience* 8 (6): 752–58. doi:10.1038/nn1472.

De Jong, E. K. 2005. “Vesicle-Mediated Transport and Release of CCL21 in Endangered Neurons: A Possible Explanation for Microglia Activation Remote from a Primary Lesion.” *Journal of Neuroscience* 25 (33): 7548–57. doi:10.1523/JNEUROSCI.1019-05.2005.

De Paola, Vincenzo, Anthony Holtmaat, Graham Knott, Sen Song, Linda Wilbrecht, Pico Caroni, and Karel Svoboda. 2006. “Cell Type-Specific Structural Plasticity of Axonal Branches and Boutons in the Adult Neocortex.” *Neuron* 49 (6): 861–75. doi:10.1016/j.neuron.2006.02.017.

Deckert, Martina, Jonathon D. Sedgwick, Elena Fischer, and Dirk Schlüter. 2006. “Regulation of Microglial Cell Responses in Murine Toxoplasma Encephalitis by CD200/CD200 Receptor Interaction.” *Acta Neuropathologica* 111 (6): 548–58. doi:10.1007/s00401-006-0062-z.

Dénes, Adám, Szilamér Ferenczi, and Krisztina J Kovács. 2011. “Systemic Inflammatory Challenges Compromise Survival after Experimental Stroke via Augmenting Brain Inflammation, Blood- Brain Barrier Damage and Brain Oedema Independently of Infarct Size.” *Journal of Neuroinflammation* 8 (1). BioMed Central Ltd: 164. doi:10.1186/1742-2094-8-164.

Deverman, Benjamin E., and Paul H. Patterson. 2009. “Cytokines and CNS Development.” *Neuron* 64 (1). Elsevier Inc.: 61–78. doi:10.1016/j.neuron.2009.09.002.

Dilger, Ryan N, and Rodney W Johnson. 2008. “Aging, Microglial Cell Priming, and the Discordant Central Inflammatory Response to Signals from the Peripheral Immune System.” *Journal of Leukocyte Biology* 84 (4): 932–39. doi:10.1189/jlb.0208108.

Donoghue, Johnp P., and Carol Parham. 1983. “Afferent Connections of the Lateral Agranular Field of the Rat Motor Cortex.” *Journal of Comparative Neurology* 217 (4): 390–404. doi:10.1002/cne.902170404.

Dragunow, M., and R. Faull. 1989. “The Use of C-Fos as a Metabolic Marker in Neuronal Pathway Tracing.” *Journal of Neuroscience Methods* 29 (3): 261–65. doi:10.1016/0165-0270(89)90150-7.

Eichhoff, Gerhard, Bianca Brawek, and Olga Garaschuk. 2011. “Microglial Calcium Signal

Acts as a Rapid Sensor of Single Neuron Damage in Vivo ☆." *Biochimica et Biophysica Acta - Molecular Cell Research* 1813 (5). Elsevier B.V.: 1014–24. doi:10.1016/j.bbamcr.2010.10.018.

Elmore, Monica R P, Allison R. Najafi, Maya A. Koike, Nabil N. Dagher, Elizabeth E. Spangenberg, Rachel A. Rice, Masashi Kitazawa, et al. 2014. "Colony-Stimulating Factor 1 Receptor Signaling Is Necessary for Microglia Viability, Unmasking a Microglia Progenitor Cell in the Adult Brain." *Neuron* 82 (2). Elsevier Inc.: 380–97. doi:10.1016/j.neuron.2014.02.040.

Etkin, A, T Egner, and R Kalisch. 2011. "Emotional Processing in Anterior Cingulate and Medial Prefrontal." *Trends in Cognitive Sciences* 15 (2): 85–93. doi:10.1016/j.tics.2010.11.004.Emotional.

Eyo, Ukpong B., and Long Jun Wu. 2013. "Bidirectional Microglia-Neuron Communication in the Healthy Brain." *Neural Plasticity* 2013. doi:10.1155/2013/456857.

Färber, Katrin, and Helmut Kettenmann. 2006a. "Functional Role of Calcium Signals for Microglial Function." *Glia*, no. March: 656–65. doi:10.1002/glia.

———. 2006b. "Purinergic Signaling and Microglia." *Pflugers Archiv European Journal of Physiology* 452 (5): 615–21. doi:10.1007/s00424-006-0064-7.

Ferrari, By Davide, Paola Chiozzi, Simonetta Falzoni, Stefania Hanau, and Francesco Di Virgilio. 1997. "Microglial Cells Stimulated with Bacterial Endotoxin" 185 (3): 22–25.

Ferrier, D. 1874. "Experiments on the Brain of Monkeys." *Proceedings of the Royal Society of London* 23 (156–163): 409–30. doi:10.1098/rspl.1874.0058.

Fritsch, G., and E. Hitzig. 2009. "Electric Excitability of the Cerebrum (Über Die Elektrische Erregbarkeit Des Grosshirns)." *Epilepsy and Behavior* 15 (2). Elsevier Inc.: 123–30. doi:10.1016/j.yebeh.2009.03.001.

Fukushima, Shohei, Eriko Furube, Masanobu Itoh, Toshihiro Nakashima, and Seiji Miyata. 2015. "Robust Increase of Microglia Proliferation in the Fornix of Hippocampal Axonal Pathway after a Single LPS Stimulation." *Journal of Neuroimmunology* 285. Elsevier B.V.: 31–40. doi:10.1016/j.jneuroim.2015.05.014.

Gadek-Michalska, A, and J Bugajski. 2004. "Role of Prostaglandins and Nitric Oxide in the Lipopolysaccharide-Induced ACTH and Corticosterone Response." *Journal of Physiology and Pharmacology* 55 (3): 663–75. http://www.ncbi.nlm.nih.gov/pubmed/15381835.

Galic, Michael A., Kiarash Riazi, and Quentin J. Pittman. 2012. "Cytokines and Brain Excitability." *Front Neuroendocrinol* 33 (1): 116–25. doi:10.1016/j.yfrne.2011.12.002.

Galic, Michael a, Kiarash Riazi, James G Heida, Abdeslam Mouihate, Neil M Fournier, Sarah J Spencer, Lisa E Kalynchuk, G Campbell Teskey, and Quentin J Pittman. 2008. "Postnatal Inflammation Increases Seizure Susceptibility in Adult Rats." *The Journal of Neuroscience : The Official Journal of the Society for Neuroscience* 28 (27): 6904–13. doi:10.1523/JNEUROSCI.1901-08.2008.

Gao, Fei, Zhiqiang Liu, Wei Ren, and Wen Jiang. 2014. "Acute Lipopolysaccharide Exposure Facilitates Epileptiform Activity via Enhanced Excitatory Synaptic Transmission and Neuronal Excitability in Vitro." *Neuropsychiatric Disease and Treatment* 10: 1489–95. doi:10.2147/NDT.S65695.

Garaschuk, O., and A. Konnerth. 1997. "Dual Role of Ryanodine-Sensitive Calcium Stores in Central Neurons." *Neurophysiology* 29: 199–204. http://link.springer.com/article/10.1007/BF02461229.

Garaschuk, Olga, and Oliver Griesbeck. 2010. "Calcium Measurement Methods" 43 (1): 101–17. doi:10.1007/978-1-60761-476-0.

Gee, J. Michael, Nathan A. Smith, Fernando R. Fernandez, Michael N. Economo, Daniela Brunert, Markus Rothermel, S. Craig Morris, et al. 2014. "Imaging Activity in Neurons and Glia with a Polr2a-Based and Cre-Dependent GCaMP5G-IRES-TdTomato Reporter Mouse." *Neuron*, August. Elsevier Inc., 1–15. doi:10.1016/j.neuron.2014.07.024.

Ginhoux, Florent, Melanie Greter, Marylene Leboeuf, Sayan Nandi, Peter See, Mark F Mehler, Simon J Conway, et al. 2010. "Fate Mapping Analysis Reveals That Adult

Microglia Derive from Primitive Macrophages." *Science* 330 (6005): 841–45. doi:10.1126/science.1194637.Fate.

Goghari, Vikram, Sonia Franciosi, Seung U. Kim, Yong Beom Lee, and James G. McLarnon. 2000. "Acute Application of Interleukin-1beta Induces Ca2+ Responses in Human Microglia." *Neuroscience Letters* 281 (2–3): 83–86. doi:10.1016/S0304-3940(00)00824-7.

Gourine, Alexander V., Nicholas Dale, Enrique Llaudet, Dmitry M. Poputnikov, K. Michael Spyer, and Valery N. Gourine. 2007. "Release of ATP in the Central Nervous System during Systemic Inflammation: Real-Time Measurement in the Hypothalamus of Conscious Rabbits." *Journal of Physiology* 585 (1): 305–16. doi:10.1113/jphysiol.2007.143933.

Grienberger, Christine, and Arthur Konnerth. 2012. "Imaging Calcium in Neurons." *Neuron* 73 (5). Elsevier Inc.: 862–85. doi:10.1016/j.neuron.2012.02.011.

Gyoneva, Stefka, Dimitrios Davalos, Dipankar Biswas, Sharon a Swanger, Ethel Garnier-Amblard, Francis Loth, Katerina Akassoglou, and Stephen F Traynelis. 2014. "Systemic Inflammation Regulates Microglial Responses to Tissue Damage in Vivo." *Glia* 62 (8): 1345–60. doi:10.1002/glia.22686.

Hanisch, Uwe-Karsten K, and Helmut Kettenmann. 2007. "Microglia: Active Sensor and Versatile Effector Cells in the Normal and Pathologic Brain." *Nature Neuroscience* 10 (11): 1387–94. doi:10.1038/nn1997.

Hanke, Mark L., and Tammy Kielian. 2011. "Toll-like Receptors in Health and Disease in the Brain: Mechanisms and Therapeutic Potential." *Cli Sci* 121 (9): 367–87. doi:10.1042/CS20110164.

Hatsopoulos, Nicholas G. 2010. "Columnar Organization in the Motor Cortex." *Cortex* 46 (2): 270–71. doi:10.1016/j.cortex.2008.07.005.

Hayashi et al. 2006. "Potentiation of the NMDA Receptor-Mediated Responses Through the Activation of the Glycine Site by Microglia Secreting Soluble Factors." *Glia* 55 (14): 1416–25. doi:10.1002/glia.

Haynes, Sharon E., Gunther Hollopeter, Guang Yang, Dana Kurpius, Michael E. Dailey, Wen Biao Gan, and David Julius. 2006. "The P2Y12 Receptor Regulates Microglial Activation by Extracellular Nucleotides." *Nature Neuroscience* 9 (12): 1512–19. doi:10.1038/nn1805.

Henry, C J, Y Huang, A Wynne, M Hanke, J Himler, M T Bailey, J F Sheridan, and J P Godbout. 2008. "Minocycline Attenuates Lipopolysaccharide (LPS)-Induced Neuroinflammation, Sickness Behavior, and Anhedonia." *J Neuroinflammation* 5: 15. doi:10.1186/1742-2094-5-15.

Hickman, Suzanne E, Elizabeth K Allison, and Joseph El Khoury. 2009. "Microglial Dysfunction and Defective β-Amyloid Clearance Pathways in Aging Alzheimer's Disease Mice." *Journal of Neuroscience* 28 (33): 8354–60. doi:10.1523/JNEUROSCI.0616-08.2008.Microglial.

Hines, Dustin J, Hyun B Choi, Rochelle M Hines, Anthony G Phillips, and Brian a MacVicar. 2013. "Prevention of LPS-Induced Microglia Activation, Cytokine Production and Sickness Behavior with TLR4 Receptor Interfering Peptides." *PloS One* 8 (3): e60388. doi:10.1371/journal.pone.0060388.

Hines, Dustin J, Rochelle M Hines, Sean J Mulligan, and Brian A Macvicar. 2009. "Microglia Processes Block the Spread of Damage in the Brain and Require Functional Chloride Channels." *Glia* 57 (15): 1610–18. doi:10.1002/glia.20874.

Hirasawa, T., K. Ohsawa, Y. Imai, Y. Ondo, C. Akazawa, S. Uchino, and Shinichi Kohsaka. 2005. "Visualization of Microglia in Living Tissues Using Iba1-EGFP Transgenic Mice." *Journal of Neuroscience Research* 81 (3): 357–62. doi:10.1002/jnr.20480.

Hoek, R. M. 2000. "Down-Regulation of the Macrophage Lineage Through Interaction with OX2 (CD200)." *Science* 290 (5497): 1768–71. doi:10.1126/science.290.5497.1768.

Hoffmann, Anja, Oliver Kann, Carsten Ohlemeyer, Uwe-Karsten Hanisch, and Helmut Kettenmann. 2003. "Elevation of Basal Intracellular Calcium as a Central Element in the

Activation of Brain Macrophages (Microglia): Suppression of Receptor-Evoked Calcium Signaling and Control of Release Function." *The Journal of Neuroscience* 23 (11): 4410–19. doi:23/11/4410 [pii].

Holness, C. L., R. P. Da Silva, J. Fawcett, S. Gordon, and D. L. Simmons. 1993. "Macrosialin, a Mouse Macrophage-Restricted Glycoprotein, Is a Member of the Lamp/Lgp Family." *Journal of Biological Chemistry* 268 (13): 9661–66.

Hoogland, Inge C M, Carin Houbolt, David J van Westerloo, Willem A van Gool, and Diederik van de Beek. 2015. "Systemic Inflammation and Microglial Activation: Systematic Review of Animal Experiments." *Journal of Neuroinflammation* 12 (1). Journal of Neuroinflammation: 114. doi:10.1186/s12974-015-0332-6.

Hooks, B. M., S. Andrew Hires, Ying Xin Zhang, Daniel Huber, Leopoldo Petreanu, Karel Svoboda, and Gordon M.G. Shepherd. 2011. "Laminar Analysis of Excitatory Local Circuits in Vibrissal Motor and Sensory Cortical Areas." *PLoS Biology* 9 (1). doi:10.1371/journal.pbio.1000572.

Hooks, Bryan M., Tianyi Mao, Diego A. Gutnisky, Naoki Yamawaki, Karel Svoboda, and Gordon M. G. Shepherd1. 2013. "Organization of Cortical and Thalamic Input to Pyramidal Neurons in Mouse Motor Cortex." *J Neurosci* 33 (2): 748–60. doi:doi:10.1523/JNEUROSCI.4338-12.2013.

Hyvärinen, Aapo, Juha Karhunen, and Erkki Oja. 2001. "Independent Component Analysis." *Applied and Computational Harmonic Analysis* 21 (1): 135–44. doi:10.1002/0471221317.

Ji, Guangju, Morris E. Feldman, Ke Yu Deng, Kai Su Greene, Jason Wilson, Jane C. Lee, Robyn C. Johnston, et al. 2004. "Ca2+-Sensing Transgenic Mice: Postsynaptic Signaling in Smooth Muscle." *Journal of Biological Chemistry* 279 (20): 21461–68. doi:10.1074/jbc.M401084200.

Jiang, X., S. Shen, C. R. Cadwell, P. Berens, F. Sinz, A. S. Ecker, S. Patel, and A. S. Tolias. 2015. "Principles of Connectivity among Morphologically Defined Cell Types in Adult Neocortex." *Science* 350 (6264): aac9462-aac9462. doi:10.1126/science.aac9462.

Judkewitz, Benjamin, Matteo Rizzi, Kazuo Kitamura, and Michael Häusser. 2009. "Targeted Single-Cell Electroporation of Mammalian Neurons in Vivo." *Nature Protocols* 4 (6): 862–69. doi:10.1038/nprot.2009.56.

Jung, S., J. Aliberti, P. Graemmel, M. J. Sunshine, G. W. Kreutzberg, A. Sher, and D. R. Littman. 2000. "Analysis of Fractalkine Receptor CX3CR1 Function by Targeted Deletion and Green Fluorescent Protein Reporter Gene Insertion." *Molecular and Cellular Biology* 20 (11): 4106–14. doi:10.1128/MCB.20.11.4106-4114.2000.

Kaneko, T, M A Caria, and H Asanuma. 1994. "Information Processing within the Motor Cortex. I. Responses of Morphologically Identified Motor Cortical Cells to Stimulation of the Somatosensory Cortex." *The Journal of Comparative Neurology* 345 (2): 161–71. doi:10.1002/cne.903450202.

Kaushal, V., R. Dye, P. Pakavathkumar, B. Foveau, J. Flores, B. Hyman, B. Ghetti, B. H. Koller, and A. C. LeBlanc. 2015. "Neuronal NLRP1 Inflammasome Activation of Caspase-1 Coordinately Regulates Inflammatory Interleukin-1-Beta Production and Axonal Degeneration-Associated Caspase-6 Activation." *Cell Death and Differentiation* 22 (10). Nature Publishing Group: 1676–86. doi:10.1038/cdd.2015.16.

Kerr, Jason N D, David Greenberg, and Fritjof Helmchen. 2005. "Imaging Input and Output of Neocortical Networks in Vivo." *Proceedings of the National Academy of Sciences of the United States of America* 102 (39): 14063–68. doi:10.1073/pnas.0506029102.

Kettenmann, H., U.-K. Hanisch, M. Noda, and A. Verkhratsky. 2011. "Physiology of Microglia." *Physiological Reviews* 91 (2): 461–553. doi:10.1152/physrev.00011.2010.

Kirkcaldie, Matthew T.K. 2012. *Neocortex*. *The Mouse Nervous System*. Elsevier Inc. doi:10.1016/B978-0-12-369497-3.10004-4.

Klein, Robyn S, Eugene Lin, Bo Zhang, Andrew D Luster, Judy Tollett, Melanie A Samuel, Michael Engle, and Michael S Diamond. 2005. "Neuronal CXCL10 Directs CD8+ T-Cell Recruitment and Control of West Nile Virus Encephalitis." *Journal of Virology* 79 (17):

11457–66. doi:10.1128/JVI.79.17.11457-11466.2005.

Koizumi, Schuichi, Yukari Shigemoto-Mogami Kaoru Nasu-Tada, Yoichi Shinozaki1, Keiko Ohsawa, Makoto Tsuda Bhalchandra V., JoshiKenneth A., Jacobson, Shinichi Kohsaka, and Kazuhide Inoue. 2007. "UDP Acting at P2Y6 Receptors Is a Mediator of Microglial Phagocytosis." *Nature* 446: 1091–95. doi:10.1038/nature05704.

Kondo, Satoru, Shinichi Kohsaka, and Shigeo Okabe. 2011. "Long-Term Changes of Spine Dynamics and Microglia after Transient Peripheral Immune Response Triggered by LPS in Vivo." *Molecular Brain* 4 (1). BioMed Central Ltd: 27. doi:10.1186/1756-6606-4-27.

Korvers, Laura, Amanda de Andrade Costa, Martin Mersch, Vitali Matyash, Helmut Kettenmann, and Marcus Semtner. 2016. "Spontaneous Ca2+ Transients in Mouse Microglia." *Cell Calcium* 60 (6). Elsevier Ltd: 396–406. doi:10.1016/j.ceca.2016.09.004.

Kovács, Zsolt, Arpád Dobolyi, Gábor Juhász, and Katalin a Kékesi. 2014. "Lipopolysaccharide Induced Increase in Seizure Activity in Two Animal Models of Absence Epilepsy WAG/Rij and GAERS Rats and Long Evans Rats." *Brain Research Bulletin* 104C (April). Elsevier Inc.: 7–18. doi:10.1016/j.brainresbull.2014.03.003.

Kozlowski, Cleopatra, and Robby M. Weimer. 2012. "An Automated Method to Quantify Microglia Morphology and Application to Monitor Activation State Longitudinally in Vivo." *PLoS ONE* 7 (2): 1–9. doi:10.1371/journal.pone.0031814.

Krabbe, Grietje, Annett Halle, Vitali Matyash, Jan L Rinnenthal, Gina D Eom, Ulrike Bernhardt, Kelly R Miller, Stefan Prokop, Helmut Kettenmann, and Frank L Heppner. 2013. "Functional Impairment of Microglia Coincides with Beta-Amyloid Deposition in Mice with Alzheimer-like Pathology." *PloS One* 8 (4): e60921. doi:10.1371/journal.pone.0060921.

Krueger, J M, J Fang, P Taishi, Z Chen, T Kushikata, and J Gardi. 1998. "Sleep. A Physiologic Role for IL-1 Beta and TNF-Alpha." *Annals of the New York Academy of Sciences*. doi:10.1111/j.1749-6632.1998.tb08323.x.

Lamkanfi, Mohamed, and Vishva M. Dixit. 2012. "Inflammasomes and Their Roles in Health and Disease." *Annual Review of Cell and Developmental Biology* 28 (1): 137–61. doi:10.1146/annurev-cellbio-101011-155745.

Lawson, L.J., V.H. Perry, P. Dri, and S. Gordon. 1990. "Heterogeneity in the Distribution and Morphology of Microglia in the Normal Adult Mouse Brain." *Neuroscience* 39 (1): 151–70. doi:10.1016/0306-4522(90)90229-W.

Lee, Geun-Shik, Naeha Subramanian, Andrew I. Kim, Ivona Aksentijevich, Raphaela Goldbach-Mansky, David B. Sacks, Ronald N. Germain, Daniel L. Kastner, and Jae Jin Chae. 2012. "The Calcium-Sensing Receptor Regulates the NLRP3 Inflammasome through Ca2+ and CAMP." *Nature* 492 (7427): 123–27. doi:10.1038/nature11588.

Lev-Ram, V., and A. Grinvald. 1987. "Activity-Dependent Calcium Transients in Central Nervous System Myelinated Axons Revealed by the Calcium Indicator Fura-2." *Biophysical Journal* 52 (4): 571–76. doi:10.1016/S0006-3495(87)83246-0.

Limatola, Cristina, Clotilde Lauro, Myriam Catalano, Maria Teresa Ciotti, Cristina Bertollini, Silvia Di Angelantonio, Davide Ragozzino, and Fabrizio Eusebi. 2005. "Chemokine CX3CL1 Protects Rat Hippocampal Neurons against Glutamate-Mediated Excitotoxicity." *Journal of Neuroimmunology* 166 (1–2): 19–28. doi:10.1016/j.jneuroim.2005.03.023.

Liu, W., Y. Tang, and J. Feng. 2011. "Cross Talk between Activation of Microglia and Astrocytes in Pathological Conditions in the Central Nervous System." *Life Sciences* 89 (5–6). Elsevier Inc.: 141–46. doi:10.1016/j.lfs.2011.05.011.

Lu, Yong Chen, Wen Chen Yeh, and Pamela S. Ohashi. 2008. "LPS/TLR4 Signal Transduction Pathway." *Cytokine* 42 (2): 145–51. doi:10.1016/j.cyto.2008.01.006.

Lukens, J. R., J. M. Gross, C. Calabrese, Y. Iwakura, M. Lamkanfi, P. Vogel, and T.-D. Kanneganti. 2014. "Critical Role for Inflammasome-Independent IL-1 Production in Osteomyelitis." *Proceedings of the National Academy of Sciences* 111 (3): 1066–71. doi:10.1073/pnas.1318688111.

Mank, Marco, Alexandre Ferrao Santos, Stephan Direnberger, Thomas D. Mrsic-Flogel,

Sonja B. Hofer, Valentin Stein, Thomas Hendel, et al. 2008. “A Genetically Encoded Calcium Indicator for Chronic in Vivo Two-Photon Imaging.” *Nature Methods* 5 (9): 805–11. doi:10.1038/nmeth.1243.

Mao, Tianyi, Deniz Kusefoglu, Bryan M. Hooks, Daniel Huber, Leopoldo Petreanu, and Karel Svoboda. 2011. “Long-Range Neuronal Circuits Underlying the Interaction between Sensory and Motor Cortex.” *Neuron* 72 (1). Elsevier Inc.: 111–23. doi:10.1016/j.neuron.2011.07.029.

Markram, Henry, Maria Toledo-Rodriguez, Yun Wang, Anirudh Gupta, Gilad Silberberg, and Caizhi Wu. 2004. “Interneurons of the Neocortical Inhibitory System.” *Nature Reviews Neuroscience* 5 (10): 793–807. doi:10.1038/nrn1519.

Masocha, Willias. 2009. “Systemic Lipopolysaccharide (LPS)-Induced Microglial Activation Results in Different Temporal Reduction of CD200 and CD200 Receptor Gene Expression in the Brain.” *Journal of Neuroimmunology* 214 (1–2). Elsevier B.V.: 78–82. doi:10.1016/j.jneuroim.2009.06.022.

Mazzoni, Alberto, Frederic D. Broccard, Elizabeth Garcia-Perez, Paolo Bonifazi, Maria Elisabetta Ruaro, and Vincent Torre. 2007. “On the Dynamics of the Spontaneous Activity in Neuronal Networks.” *PLoS ONE* 2 (5). doi:10.1371/journal.pone.0000439.

McCoy, Melissa K, and Malú G Tansey. 2008. “TNF Signaling Inhibition in the CNS: Implications for Normal Brain Function and Neurodegenerative Disease.” *Journal of Neuroinflammation* 5 (1): 45. doi:10.1186/1742-2094-5-45.

McLarnon, J. G., S. Franciosi, X. Wang, J. H. Bae, H. B. Choi, and S. U. Kim. 2001. “Acute Actions of Tumor Necrosis Factor-α on Intracellular Ca2+ and K+ Currents in Human Microglia.” *Neuroscience* 104 (4): 1175–84. doi:10.1016/S0306-4522(01)00119-1.

McMahan, C J, J L Slack, B Mosley, D Cosman, S D Lupton, L L Brunton, C E Grubin, J M Wignall, N A Jenkins, and C I Brannan. 1991. “A Novel IL-1 Receptor, Cloned from B Cells by Mammalian Expression, Is Expressed in Many Cell Types.” *The EMBO Journal* 10 (10): 2821–32. http://www.pubmedcentral.nih.gov/articlerender.fcgi?artid=452992&tool=pmcentrez&rendertype=abstract.

Meuth, Sven G., Ole J. Simon, Alexander Grimm, Nico Melzer, Alexander M. Herrmann, Philipp Spitzer, Peter Landgraf, and Heinz Wiendl. 2008. “CNS Inflammation and Neuronal Degeneration Is Aggravated by Impaired CD200-CD200R-Mediated Macrophage Silencing.” *Journal of Neuroimmunology* 194 (1–2): 62–69. doi:10.1016/j.jneuroim.2007.11.013.

Miyamoto, Akiko, Hiroaki Wake, Andrew J Moorhouse, and Junichi Nabekura. 2013. “Microglia and Synapse Interactions: Fine Tuning Neural Circuits and Candidate Molecules.” *Frontiers in Cellular Neuroscience* 7 (May): 70. doi:10.3389/fncel.2013.00070.

Möller, T, C Nolte, R Burger, A Verkhratsky, and H Kettenmann. 1997. “Mechanisms of C5a and C3a Complement Fragment-Induced [Ca2+]i Signaling in Mouse Microglia.” *Journal of Neuroscience* 17 (2): 615–24. http://eutils.ncbi.nlm.nih.gov/entrez/eutils/elink.fcgi?dbfrom=pubmed&id=8987784&retmode=ref&cmd=prlinks%5Cnpapers3://publication/uuid/A3CFA1A7-DE38-4D4C-B4C7-5E94F9893FEA.

Möller, Thomas. 2002. “Calcium Signaling in Microglial Cells.” *Glia* 40 (2): 184–94. doi:10.1002/glia.10152.

Molyneaux, Bradley J, Paola Arlotta, Joao R L Menezes, and Jeffrey D Macklis. 2007. “Neuronal Subtype Specification in the Cerebral Cortex.” *Nature Reviews. Neuroscience* 8 (6): 427–37. doi:10.1038/nrn2151.

Moriguchi, Shigeki, Yoshito Mizoguchi, Yoshiro Tomimatsu, Yoshinori Hayashi, Tomoko Kadowaki, Yoshifumi Kagamiishi, Nobuo Katsube, et al. 2003. “Potentiation of NMDA Receptor-Mediated Synaptic Responses by Microglia.” *Molecular Brain Research* 119 (2): 160–69. doi:10.1016/j.molbrainres.2003.09.007.

Mott, Ryan T., Ghania Ait-Ghezala, Terrence Town, Takashi Mori, Martina Vendrame, Jin

Zeng, Jared Ehrhart, Michael Mullan, and Jun Tan. 2004. “Neuronal Expression of CD22: Novel Mechanism for Inhibiting Microglial Proinflammatory Cytokine Production.” *Glia* 46 (4): 369–79. doi:10.1002/glia.20009.

Mountcastle, Vernon B. 1997. “The Columnar Organization of the Neocortex.” *Brain* 120 (4): 701–22. doi:10.1093/brain/120.4.701.

Murakami, T., J. Ockinger, J. Yu, V. Byles, A. McColl, A. M. Hofer, and T. Horng. 2012. “Critical Role for Calcium Mobilization in Activation of the NLRP3 Inflammasome.” *Proceedings of the National Academy of Sciences* 109 (28): 11282–87. doi:10.1073/pnas.1117765109.

Nagayama, Shin, Shaoqun Zeng, Wenhui Xiong, Max L. Fletcher, Arjun V. Masurkar, Douglas J. Davis, Vincent A. Pieribone, and Wei R. Chen. 2007. “In Vivo Simultaneous Tracing and Ca2+ Imaging of Local Neuronal Circuits.” *Neuron* 53 (6): 789–803. doi:10.1016/j.neuron.2007.02.018.

Nava Catorce, Miryam, and Goar Gevorkian. 2016. “LPS-Induced Murine Neuroinflammation Model: Main Features and Suitability for Pre-Clinical Assessment of Nutraceuticals.” *Current Neuropharmacology* 14 (2): 155–64. doi:10.2174/1570159X14666151204122017.

Netea, Mihai G., Frank L. van de Veerdonk, Jos W.M. van der Meer, Charles A. Dinarello, and Leo A.B. Joosten. 2015. “Inflammasome-Independent Regulation of IL-1-Family Cytokines.” *Annual Review of Immunology* 33 (1): 49–77. doi:10.1146/annurev-immunol-032414-112306.

Nimmerjahn, Axel, Frank Kirchhoff, and Fritjof Helmchen. 2005. “Resting Microglial Cells Are Highly Dynamic Surveillants of Brain Parenchyma in Vivo.” *Science* 308 (May): 1314–19. doi:10.1126/science.1110647.

Norden, D M, and J P Godbout. 2013. “Review: Microglia of the Aged Brain: Primed to Be Activated and Resistant to Regulation.” *Neuropathology and Applied Neurobiology* 39 (1): 19–34. doi:10.1111/j.1365-2990.2012.01306.x.

Ohki, Kenichi, Sooyoung Chung, Yeang H. Ch’ng, Prakash Kara, and R. Clay Reid. 2005. “Functional Imaging with Cellular Resolution Reveals Precise Micro-Architecture in Visual Cortex.” *Nature* 433 (7026): 597–603. doi:10.1038/nature03274.

Olmos, Gabriel, and Jerònia Lladó. 2014. “Tumor Necrosis Factor Alpha: A Link between Neuroinflammation and Excitotoxicity.” *Mediators of Inflammation* 2014. doi:10.1155/2014/861231.

Palin, Karine, Marie L Moreau, Julie Sauvant, Hélène Orcel, Agnès Nadjar, Anne Duvoid-Guillou, Jennifer Dudit, Alain Rabié, and Françoise Moos. 2009. “Interleukin-6 Activates Arginine Vasopressin Neurons in the Supraoptic Nucleus during Immune Challenge in Rats.” *American Journal of Physiology. Endocrinology and Metabolism* 296 (6): E1289–99. doi:10.1152/ajpendo.90489.2008.

Palomero-Gallagher, Nicola, and Karl Zilles. 2015. *Isocortex*. *The Rat Nervous System*. Fourth Edi. Elsevier Inc. doi:10.1016/B978-0-12-374245-2.00022-X.

Paolicelli, Rosa C., Giulia Bolasco, Francesca Pagani, Laura Maggi, Maria Scianni, Patrizia Panzanelli, Maurizio Giustetto, et al. 2011. “Synaptic Pruning by Microglia Is Necessary for Normal Brain Development.” *Science (New York, N.Y.)* 1456 (July): 10–13. doi:10.1126/science.1202529.

Pascual, O., S. Ben Achour, P. Rostaing, A. Triller, and A. Bessis. 2012. “Microglia Activation Triggers Astrocyte-Mediated Modulation of Excitatory Neurotransmission.” *Proceedings of the National Academy of Sciences* 109 (4): E197–205. doi:10.1073/pnas.1111098109.

Perry, and Holmes Cunningham. 2007. “Systemic Inflammation and in Neurodegeneration” 7 (February): 161–67.

Petersen, Mark A., and Michael E. Dailey. 2004. “Diverse Microglial Motility Behaviors during Clearance of Dead Cells in Hippocampal Slices.” *Glia* 46 (2): 195–206. doi:10.1002/glia.10362.

Pinteaux, Emmanuel, Lisa C. Parker, Nancy J. Rothwell, and Giamal N. Luheshi. 2002.

"Expression of Interleukin-1 Receptors and Their Role in Interleukin-1 Actions in Murine Microglial Cells." *Journal of Neurochemistry* 83 (4): 754–63. doi:10.1046/j.1471-4159.2002.01184.x.

Pozner, Amir, Ben Xu, Sierra Palumbos, J. Michael Gee, Petr Tvrdik, and Mario R. Capecchi. 2015. "Intracellular Calcium Dynamics in Cortical Microglia Responding to Focal Laser Injury in the PC::G5-TdT Reporter Mouse." *Frontiers in Molecular Neuroscience* 8 (May): 1–10. doi:10.3389/fnmol.2015.00012.

Prevedel, Robert, Aart J. Verhoef, Alejandro J. Pernía-Andrade, Siegfried Weisenburger, Ben S. Huang, Tobias Nöbauer, Alma Fernández, et al. 2016. "Fast Volumetric Calcium Imaging across Multiple Cortical Layers Using Sculpted Light." *Nature Methods* 13 (12): 1021–28. doi:10.1038/nmeth.4040.

Rabinowitz, S, and S Gordon. 1989. "Differential Expression of Membrane Sialoglycoproteins in Exudate and Resident Mouse Peritoneal Macrophages." *J Cell Sci* 93 (Pt 4): 623–30.

Reinisch, N, M Wolkersdorfer, C M Kahler, K Ye, C A Dinarello, and C J Wiedermann. 1994. "Interleukin-1 Receptor Type I MRNA in Mouse Brain as Affected by Peripheral Administration of Bacterial Lipopolysaccharide." *Neuroscience Letters* 166 (2): 165–67.

Riazi, Kiarash, Michael a Galic, J Brent Kuzmiski, Winnie Ho, Keith a Sharkey, and Quentin J Pittman. 2008. "Microglial Activation and TNFalpha Production Mediate Altered CNS Excitability Following Peripheral Inflammation." *Proceedings of the National Academy of Sciences of the United States of America* 105 (44): 17151–56. doi:10.1073/pnas.0806682105.

Rodgers, Krista M, Mark R Hutchinson, Alexis Northcutt, Steven F Maier, Linda R Watkins, and Daniel S Barth. 2009. "The Cortical Innate Immune Response Increases Local Neuronal Excitability Leading to Seizures." *Brain : A Journal of Neurology* 132 (Pt 9): 2478–86. doi:10.1093/brain/awp177.

Samland, Helen, Salvador Huitron-Resendiz, Eliezer Masliah, Jose Criado, Steven J. Henriksen, and Iain L. Campbell. 2003. "Profound Increase in Sensitivity to Glutamatergic- but Not Cholinergic Agonist-Induced Seizures in Transgenic Mice with Astrocyte Production of IL-6." *Journal of Neuroscience Research* 73 (2): 176–87. doi:10.1002/jnr.10635.

Santello, Mirko, and Andrea Volterra. 2012. "TNFalpha in Synaptic Function: Switching Gears." *Trends in Neurosciences* 35 (10): 638–47. doi:10.1016/j.tins.2012.06.001.

Schafer, Dorothy P., Emily K. Lehrman, Amanda G. Kautzman, Ryuta Koyama, Alan R. Mardinly, Ryo Yamasaki, Richard M. Ransohoff, Michael E. Greenberg, Ben A. Barres, and Beth Stevens. 2012. "Microglia Sculpt Postnatal Neural Circuits in an Activity and Complement-Dependent Manner." *Neuron* 74 (4). Elsevier Inc.: 691–705. doi:10.1016/j.neuron.2012.03.026.

Schafer, Dorothy P, Emily K Lehrman, and Beth Stevens. 2013. "The 'Quad-Partite' Synapse: Microglia-Synapse Interactions in the Developing and Mature CNS." *Glia* 61 (1): 24–36. doi:10.1016/j.jneumeth.2010.08.011.Autogenic.

Schwendele, Bernd, Bianca Brawek, Marina Hermes, and Olga Garaschuk. 2012. "High-Resolution in Vivo Imaging of Microglia Using a Versatile Nongenetically Encoded Marker." *European Journal of Immunology* 42 (8): 2193–96. doi:10.1002/eji.201242436.

Shadlen, Michael N., and William T. Newsome. 1994. "Noise, Neural Codes and Cortical Organization." *Current Opinion in Neurobiology* 4 (4): 569–79. doi:10.1016/0959-4388(94)90059-0.

Shankaran, Mahalakshmi, Michael E. Marino, Robert Busch, Carole Keim, Chelsea King, Jean Lee, Salena Killion, Mohamad Awada, and Marc K. Hellerstein. 2007. "Measurement of Brain Microglial Proliferation Rates In Vivo in Response to Neuroinflammatory Stimuli: Application to Drug Discovery." *Journal of Neuroscience Research* 85 (11): 2352–59. doi:10.1002/jnr.

Shepherd, Gordon M.G., Armen Stepanyants, Ingrid Bureau, Dmitri Chklovskii, and Karel Svoboda. 2005. "Geometric and Functional Organization of Cortical Circuits." *Nature Neuroscience* 8 (6): 782–90. doi:10.1038/nn1447.

Silva, Rosângela P. DA, and Siamon Gordon. 1999. “Phagocytosis Stimulates Alternative Glycosylation of Macrosialin (Mouse CD68), a Macrophage-Specific Endosomal Protein.” *Biochemical Journal* 338 (3): 687. doi:10.1042/0264-6021:3380687.

Sims, J., C. March, D Cosman, M. Widmer, H. MacDonald, C. McMahan, C. Grubin, et al. 1988. “CDNA Expression Cloning of the IL-1 Receptor, a Member of the Immunoglobulin Superfamily.” *Science* 241 (4865): 585–89. doi:10.1126/science.2969618.

Spangenberg, Elizabeth E., Rafael J. Lee, Allison R. Najafi, Rachel A. Rice, Monica R.P. Elmore, Mathew Blurton-Jones, Brian L. West, and Kim N. Green. 2016. “Eliminating Microglia in Alzheimer’s Mice Prevents Neuronal Loss without Modulating Amyloid-β Pathology.” *Brain* 139 (4): 1265–81. doi:10.1093/brain/aww016.

Spörri, Bernhard, Matthias Bickel, Dirk Dobbelaere, Joel Machado, and Daniel Lottaz. 2001. “Soluble Interleukin-1 Receptor - Reverse Signaling in Innate Immunoregulation.” *Cytokine and Growth Factor Reviews* 12 (1): 27–32. doi:10.1016/S1359-6101(00)00020-4.

Steinmetz, Nicholas A., Christina Buetfering, Jerome Lecoq, Christian R. Lee, Andrew J. Peters, Elina A. K. Jacobs, Philip Coen, et al. 2017. “Aberrant Cortical Activity in Multiple GCaMP6-Expressing Transgenic Mouse Lines.” *Eneuro* 4 (5): ENEURO.0207-17.2017. doi:10.1523/ENEURO.0207-17.2017.

Stellwagen, David, Eric C Beattie, Jae Y Seo, and Robert C Malenka. 2005. “Differential Regulation of AMPA Receptor and GABA Receptor Trafficking by Tumor Necrosis Factor-Alpha.” *The Journal of Neuroscience : The Official Journal of the Society for Neuroscience* 25 (12): 3219–28. doi:10.1523/JNEUROSCI.4486-04.2005.

Stellwagen, David, and Robert C. Malenka. 2006. “Synaptic Scaling Mediated by Glial TNF-α.” *Nature* 440 (7087): 1054–59. doi:10.1038/nature04671.

Stevens, Beth, Nicola J. Allen, Luis E. Vazquez, Gareth R. Howell, Karen S. Christopherson, Navid Nouri, Kristina D. Micheva, et al. 2007. “The Classical Complement Cascade Mediates CNS Synapse Elimination.” *Cell* 131 (6): 1164–78. doi:10.1016/j.cell.2007.10.036.

Stosiek, Christoph, Olga Garaschuk, Knut Holthoff, and Arthur Konnerth. 2003. “In Vivo Two-Photon Calcium Imaging of Neuronal Networks.” *Proceedings of the National Academy of Sciences of the United States of America* 100 (12): 7319–24. doi:10.1073/pnas.1232232100.

Streit, Wolfgang J., Robert E. Mrak, and W. Sue T Griffin. 2004. “Microglia and Neuroinflammation: A Pathological Perspective.” *Journal of Neuroinflammation* 1: 1–4. doi:10.1186/1742-2094-1-14.

Sullivan, Megan R., Axel Nimmerjahn, Dmitry V. Sarkisov, Fritjof Helmchen, and Samuel S.-H. Wang. 2005. “In Vivo Calcium Imaging of Circuit Activity in Cerebellar Cortex.” *Journal of Neurophysiology* 94 (2): 1636–44. doi:10.1152/jn.01013.2004.

Suter, Benjamin A, and Gordon M G Shepherd. 2015. “Reciprocal Interareal Connections to Corticospinal Neurons in Mouse M1 and S2.” *The Journal of Neuroscience : The Official Journal of the Society for Neuroscience* 35 (7): 2959–74. doi:10.1523/JNEUROSCI.4287-14.2015.

Szalay, Gergely, Bernadett Martinecz, Nikolett Lénárt, Zsuzsanna Környei, Barbara Orsolits, Linda Judák, Eszter Császár, et al. 2016. “Microglia Protect against Brain Injury and Their Selective Elimination Dysregulates Neuronal Network Activity after Stroke.” *Nature Communications* 7 (May). doi:10.1038/ncomms11499.

Takahashi, Kazuya, Christian D.P. Rochford, and Harald Neumann. 2005. “Clearance of Apoptotic Neurons without Inflammation by Microglial Triggering Receptor Expressed on Myeloid Cells-2.” *The Journal of Experimental Medicine* 201 (4): 647–57. doi:10.1084/jem.20041611.

Tallini, Y. N., M. Ohkura, B.-R. Choi, G. Ji, K. Imoto, R. Doran, J. Lee, et al. 2006. “Imaging Cellular Signals in the Heart in Vivo: Cardiac Expression of the High-Signal Ca2+ Indicator GCaMP2.” *Proceedings of the National Academy of Sciences* 103 (12): 4753–

58. doi:10.1073/pnas.0509378103.

Tan, Jun, Terrence Town, and Michael Mullan. 2000. “CD45 Inhibits CD40L-Induced Microglial Activation via Negative Regulation of the Src/P44/42 MAPK Pathway.” *Journal of Biological Chemistry* 275 (47): 37224–31. doi:10.1074/jbc.M002006200.

Taylor, D. L. 2005. “Stimulation of Microglial Metabotropic Glutamate Receptor MGlu2 Triggers Tumor Necrosis Factor -Induced Neurotoxicity in Concert with Microglial-Derived Fas Ligand.” *Journal of Neuroscience* 25 (11): 2952–64. doi:10.1523/JNEUROSCI.4456-04.2005.

Terrando, Niccolò, António Rei Fidalgo, Marcela Vizcaychipi, Mario Cibelli, Daqing Ma, Claudia Monaco, Marc Feldmann, and Mervyn Maze. 2010. “The Impact of IL-1 Modulation on the Development of Lipopolysaccharide-Induced Cognitive Dysfunction.” *Critical Care* 14 (3): R88. doi:10.1186/cc9019.

Tian, Lin, S Andrew Hires, Tianyi Mao, Daniel Huber, M Eugenia Chiappe, Sreekanth H Chalasani, Leopoldo Petreanu, et al. 2009. “Imaging Neural Activity in Worms, Flies and Mice with Improved GCaMP Calcium Indicators.” *Nature Methods* 6 (12). Nature Publishing Group: 875–81. doi:10.1038/nmeth.1398.

Tremblay, Marie-Ève, Rebecca L Lowery, and Ania K Majewska. 2010. “Microglial Interactions with Synapses Are Modulated by Visual Experience.” *PLoS Biology* 8 (11): e1000527. doi:10.1371/journal.pbio.1000527.

Vezzani, Annamaria, Daniela Moneta, Cristina Richichi, Marisa Aliprandi, Stephanie J. Burrows, Teresa Ravizza, Carlo Perego, and M. Grazia De Simoni. 2002. “Functional Role of Inflammatory Cytokines and Antiinflammatory Molecules in Seizures and Epileptogenesis.” *Epilepsia* 43 (SUPPL. 5): 30–35. doi:10.1046/j.1528-1157.43.s.5.14.x.

Vitkovic, L, Jp Konsman, J Bockaert, R Dantzer, V Homburger, and C Jacque. 2000. “Cytokine Signals Propagate through the Brain.” *Molecular Psychiatry* 5: 604–15. doi:10.1038/sj.mp.4000851.

Viviani, B, S Bartesaghi, F Gardoni, A Vezzani, M M Behrens, T Bartfai, M Binaglia, et al. 2003. “Interleukin-1beta Enhances NMDA Receptor-Mediated Intracellular Calcium Increase through Activation of the Src Family of Kinases.” *The Journal of Neuroscience : The Official Journal of the Society for Neuroscience* 23 (25): 8692–8700. doi:23/25/8692 [pii].

Wake, Hiroaki, Andrew J Moorhouse, Shozo Jinno, Shinichi Kohsaka, and Junichi Nabekura. 2009. “Resting Microglia Directly Monitor the Functional State of Synapses In Vivo and Determine the Fate of Ischemic Terminals.” *The Journal of Neuroscience : The Official Journal of the Society for Neuroscience* 13 (29): 3974–80. doi:10.1523/JNEUROSCI.4363-08.2009.

Walsh, John G, Daniel a Muruve, and Christopher Power. 2014. “Inflammasomes in the CNS.” *Nature Reviews. Neuroscience* 15 (2): 84–97. doi:10.1038/nrn3638.

Wenzel, Michael, Jordan P. Hamm, Darcy S. Peterka, and Rafael Yuste. 2017. “Reliable and Elastic Propagation of Cortical Seizures in Vivo Michael.” *Cell Reports* 19 (13): 2681–2693. doi:doi:10.1016/j.celrep.2017.05.090.

Wesche, Holger, Christian Korherr, Werner Falk, Klaus Resch, Michael U Martin, and Michael Kracht. 1997. “The Interleukin-1 Receptor Accessory Protein (IL-1RAcP) Is Essential for IL-1-Induced Activation of Interleukin-1 Receptor-Associated Kinase (IRAK) and Stress-Activated Protein Kinases (SAP Kinases).” *The Journal of Biological Chemistry* 272 (12): 7727–31. doi:10.1074/jbc.272.12.7727.

Wheeler, David, Edward Knapp, Veera V R Bandaru, Yue Wang, David Knorr, Christophe Poirier, Mark P Mattson, Jonathan D Geiger, and Norman J Haughey. 2009. “TNFα-Induced Neutral Sphingomyelinase-2 Modulates Synaptic Plasticity by Controlling the Membrane Insertion of NMDA Receptors.” *Journal of Neurochemistry* 109 (5): 1237–49. doi:10.1111/j.1471-4159.2009.06038.x.TNF.

Whiteside, M. B., N. Quan, and M. Herkenharn. 1999. “Induction of Pituitary Cytokine Transcripts by Peripheral Lipopolysaccharide.” *Journal of Neuroendocrinology* 11 (2): 115–20. doi:10.1046/j.1365-2826.1999.00297.x.

Witter, Menno. 2012. *Hippocampus*. *The Mouse Nervous System*. Elsevier Inc. doi:10.1016/B978-0-12-369497-3.10005-6.

Wohleb, Eric S. 2016. “Neuron-Microglia Interactions in Mental Health Disorders: ‘For Better, and for Worse.’” *Frontiers in Immunology* 7 (NOV): 1–13. doi:10.3389/fimmu.2016.00544.

Xi, X, and L A Toth. 2000. “Lipopolysaccharide Effects on Neuronal Activity in Rat Basal Forebrain and Hypothalamus during Sleep and Waking.” *Am.J.Physiol Regul.Integr.Comp Physiol* 278 (3): R620–27.

Yamawaki, N, K Borges, B a Suter, K D Harris, and G M Shepherd. 2014. “A Genuine Layer 4 in Motor Cortex with Prototypical Synaptic Circuit Connectivity.” *Elife* 3: e05422. doi:10.7554/eLife.05422.

Zariwala, Hatim a, Bart G Borghuis, Tycho M Hoogland, Linda Madisen, Lin Tian, Chris I De Zeeuw, Hongkui Zeng, Loren L Looger, Karel Svoboda, and Tsai-Wen Chen. 2012. “A Cre-Dependent GCaMP3 Reporter Mouse for Neuronal Imaging in Vivo.” *The Journal of Neuroscience : The Official Journal of the Society for Neuroscience* 32 (9): 3131–41. doi:10.1523/JNEUROSCI.4469-11.2012.

Zhang, Jun-Ming, and Jianxiong An. 2007. “Cytokines, Inflammation and Pain.” *Int Anesthesiol Clin.* 45 (2): 27–37. doi:10.1097/AIA.0b013e318034194e.Cytokines.

Zhao, Boyu, and Joan P. Schwartz. 1998. “Involvement of Cytokines in Normal CNS Development and Neurological Diseases: Recent Progress and Perspectives.” *Journal of Neuroscience Research* 52 (1): 7–16. doi:10.1002/(SICI)1097-4547(19980401)52:1<7::AID-JNR2>3.0.CO;2-I.

Zhou, Hongmei Tang, Jianuo Liu, Jun Dong, and Huangui Xiong. 2011. “Chemokine CCL2 Modulation of Neuronal Excitability and Synaptic Transmission in Rat Hippocampal Slices” 49 (18): 1841–50. doi:10.1016/j.jacc.2007.01.076.White.

Zotova, Elina, Viraj Bharambe, Matthew Cheaveau, William Morgan, Clive Holmes, Scott Harris, James W. Neal, Seth Love, James A R Nicoll, and Delphine Boche. 2013. “Inflammatory Components in Human Alzheimer’s Disease and after Active Amyloid-B<inf>42</Inf> Immunization.” *Brain* 136 (9): 2677–96. doi:10.1093/brain/awt210.

6. Statement of Contributions

According to § 9 (2):

Prof. Dr. Olga Garaschuk conceived the study and designed the experiments in this dissertation together with Karin Riester and Dr. Bianca Brawek.
Experiments that involved the electroporation of microglia and the measurements of the spontaneous Ca^{2+}-signaling of microglia were performed by Dr. Bianca Brawek.
The sample collection and tissue processing for the ELISA experiments were performed by Karin Riester. The protein assays were performed together with Elizabeta Zirdum and partially by the company microBIOMix GmbH.
Sample collections and tissue processing for the immunohistochemical experiments were performed by Karin Riester. The immunohistochemical stainings of the brain slices were performed by Daria Savitska.
All remaining experiments were performed by Karin Riester. Further, she was involved in the analysis of all experiments and wrote this thesis.